SIMMER-III Code-Verification Phase I

W. Maschek (Editor)
Institut für Neutronenphysik und Reaktortechnik
Projekt Nukleare Sicherheitsforschung

SIMMER-III Code-Verification

Phase I

W. Maschek (Editor)

Institut für Neutronenphysik und Reaktortechnik
Projekt Nukleare Sicherheitsforschung

Abstract

SIMMER-III is a computer code to investigate core disruptive accidents in liquid metal fast reactors but should also be used to investigate safety related problems in other types of advanced reactors. The code is developed by PNC with cooperation of the European partners FZK, CEA and AEA-T. SIMMER-III is a two-dimensional, three-velocity-field, multiphase, multicomponent, Eulerian, fluid-dynamics code coupled with a space-, time-, and energy-dependent neutron dynamics model. In order to model complex flow situations in a postulated disrupting core, mass and energy conservation equations are solved for 27 density components and 16 energy components, respectively. Three velocity fields (two liquid and one vapor) are modeled to simulate the relative motion of different fluid components. An additional static field takes into account the structures available in a reactor (pins, hexans, vessel structures, internal structures etc.). The neutronics is based on the discrete ordinate method (S_N method) coupled into a quasistatic dynamic model.

The code assessment and verification of the fluid dynamic/thermohydraulic parts of the code is performed in several steps in a joint effort of all partners. The results of the FZK contributions to the first assessment and verification phase is reported.

SIMMER-III Code-Verifikation Phase I

Kurzfassung

SIMMER-III ist ein Computercode zur Analyse kernzerstörender Unfälle in schnellen flüssigmetallgekühlten Reaktoren. Der Code soll aber auch für Sicherheitsuntersuchungen anderer fortgeschrittener Reaktortypen eingesetzt werden. Der Code wird federführend von PNC in Kooperation mit den Europäischen Partnern FZK, CEA und AEA-T entwickelt.

SIMMER-III ist ein zweidimensionaler, 3-Geschwindigkeitsfeld-, Multiphasen, Multikomponenten, Euler-Fluiddynamikcode, der mit einem orts-, zeit- und energieabhängigen Neutronikmodell gekoppelt ist. Um die komplexen Verhältnisse bei einer postulierten Kernzerstörung modellieren zu können, werden die Konservierungsgleichungen für 27 Dichte- und 16 Energiekomponenten gelöst. Die 3 Geschwindigkeitsfelder (2 für Flüssigkeit, eines für Gas) werden benutzt, um die Relativbewegung der verschiedenen Fluid-Komponenten zu simulieren. In einem zusätzlichen Strukturfeld können die in einem Reaktor auftretenden Strukturen (Brennstäbe, Kästen, Tankstrukturen, Einbauten etc.) modelliert werden. Die Neutronik basiert auf der Diskreten Ordinaten Methode (S_N Methode), die in ein quasistatisches Dynamikmodell integriert ist. Die Code-Verifikation des Fluiddynamik/Thermohydraulikteils erfolgt in mehreren Schritten. Die Ergebnisse der FZK Beiträge zur ersten Verifikationsphase werden vorgestellt.

Contents

I.   Introduction

SIMMER-III is a two-dimensional, three-velocity-field, multiphase, multi-component, Eulerian, fluid-dynamics code coupled with a space- and energy-dependent neutron dynamics model /1/.

The development of SIMMER-III began in late 1988 at the Los Alamos National Laboratory (LANL) and Power Reactor and Nuclear Fuel Development Coopera-tion (PNC) in collaboration and under the agreement with the United States Nu-clear Regulatory Commission. Following this initial two years joint study, the whole project was transferred to PNC, and since then the development program has latterly attracted international interest, and since 1992 the European research organizations, the former Kernforschungszentrum Karlsruhe of Germany (now FZK), AEA Technology of United Kingdom (AEA-T) and the Commissariat à l'Energie Atomique of France (CEA) have been participating in the project.

The assessment of the code is a joint effort between PNC and the European part-ners. The first part of the SIMMER-III assessment performed at FZK comprises analyses of the fluiddynamics part of the code and analyses of the melt-ing/freezing and vaporization/condensation models. The applications of SIMMER-III are given in 5 independent chapters in accordance with an agreed for-mat developed by PNC, FZK, CEA and AEA-T. In the report only typical examples for each verification/assessment task are selected.

In the first chapter the sloshing motion of liquids is described including also the case when particles are embedded into the flow. The second chapter deals with shock waves in gas and two-phase media. Then follows an application of SIMMER-III on rapid fuel vaporization tests with temperature ramp rates up to 10^5K/s. In a further application the melting and freezing models are tested simu-lating the penetration of melt into tube structures. Finally the flowing and im-pact processes of liquid slugs on rigid surfaces and obstacles are tested. The SIMMER-III results are compared to experiments, analytical solutions or results from other codes developed specifically for a special category of problems (e.g. high resolution shock capturing codes). When SIMMER-III is applied for accident analyses a multiple of different phenomena and effects must be described rang-ing from shock waves and single fluid flow to multiphase conditions and phase transitions. Therefore it is required that the code can handle all the different con-ditions and requirements with good accuracy. In addition also the speed of com-

putation is of utmost importance for the code als already the much less sophisticated for-runner of SIMMER-III, the SIMMER-II code /2/ needed about 100 h of CPU time (computer generation in the 80') for a mechanistic description of a core disruption in a liquid metal reactor.

The overall conclusion from assessment and verification phase I is, that SIMMER-III can handle the different problems analyzed with good accuracy. A further speed-up of the code is of importance.

The code verification is performed in several steps with intermediate major code changes and improvements. Further versions of the code have been released since the end of verification phase I and the second step in the verification effort has been started. The results will be given in another report.

/1/ Kondo S., Tobita, Morita K., Shirakawa N.,
"SIMMER-III: An Advanced Computer Program for LMFBR Severe Accident Analysis";
ANP'92, Int. Conf. on Design and Safety of Advanced Nuclear Power Plants, Tokyo, (Japan), 1992

/2/ Bohl W.R., Luck L.B.,
SIMMER-II: A Computer Program for LMFBR Disrupted Core Analyses, LA-LA-11415-MS, 1990

II. Code Description

SIMMER-III is a two-dimensional, three-velocity-field, multiphase, multi-component, Eulerian, fluid-dynamics code coupled with a space-, time- and energy-dependent neutron dynamics model.
The scope and salient features of SIMMER-III are listed below:
-   two dimensions (r-z or x-z)
-   three velocity fields (two for liquids and one for vapor)
-   full LMR materials (fuel, steel, sodium, control and fission gas)
-   a fractional-step algorithm (a four-step method) for fluid dynamics
-   first-order donor-cell differencing and optional higher-order scheme
-   optimum pressure iteration and fluid convection consistent with a semi-implicit method
-   improved analytic EOS with best fitting
-   both pool and channel flow regimes with smooth transition
-   flexible interfacial area convection
-   momentum-exchange functions and heat-transfer coefficients consistent with flow-regime modeling
-   simplified (heat-transfer limited) heat and mass transfer modeling that treats non-equilibrium processes
-   improved can wall and crust heat-transfer modeling for better coupling with fluid fields
-   simple two-node fuel-pin model (sophistication planned in future versions of the code)
-   S_N-neutronics with space, time kinetics and a decay heating model

II.1. Code Framework

A conceptual overall framework of SIMMER-III is shown in Fig. II.1-1. The entire code consists of three elements: the fluid-dynamics model, the structure (fuel pin) model, and the neutronics model. The fluid-dynamics portion, which constitutes about two thirds of the code, is interfaced with the structure model through heat and mass transfer at structure surfaces. The neutronics portion provides nuclear heat sources based on the mass and energy distributions calculated by the other code elements.

II.2. Geometrical Model

The basic geometric structure of SIMMER-III is a two-dimensional R-Z system as shown in Fig. II.2-1, although optionally an X-Z or one-dimensional system can also be used for various fluid-dynamics calculations. The neutronics mesh is a sub-region of the fluid-dynamics computational mash.

Meshcell Geometry
- *r-z* two dimensions
- Variable staggered mesh
- Sub-region for neutronics

LS

LC

Pin

RC

RS

Vapor

Pin : *pin fuel*   P : *solid particle*
C : *cladding*   L : *real liquid*
RS : *right canwall*
RC : *right crust*
LS : *left canwall*
LC : *left crust*

z

Δz_i

r

Δr_i

Density and Energy Components
- Structure field
  Density : 12   Energy : 9
- Liquid field
  Density : 10   Energy : 6
- Vapor field
  Density : 5   Energy : 1

Basic Equations
- Mass conservation : 27
- Energy conservation : 16
- Momentum conservation : 3

Velocity Fields
- Liquid field : 2
- Vapor field : 1

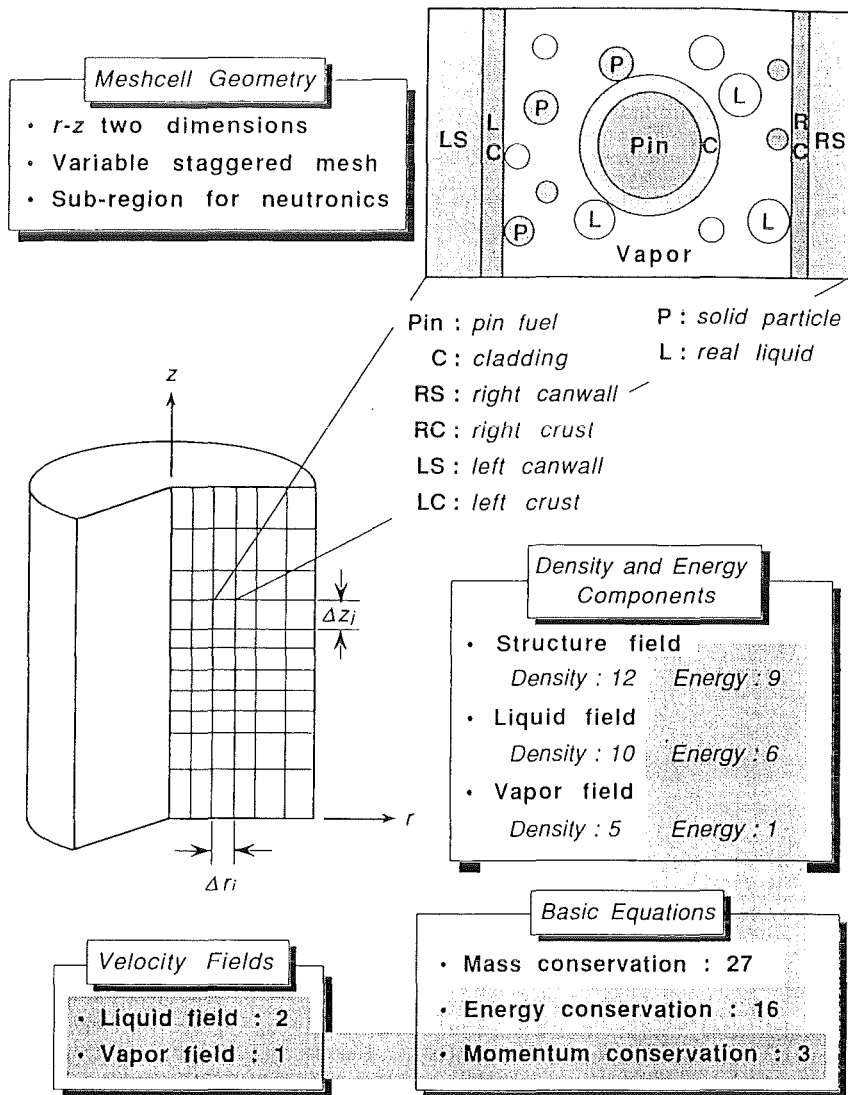Fig. II.2.1   SIMMER-III Geometric Framework

II.3. Fluid-Dynamics Model

The differential equations involving fluid mass, momentum and internal energy are shown schematically by

$$\frac{\partial \bar{\rho}_m}{\partial t} + \nabla \cdot \left(\bar{\rho}_m \, V_q \right) = - \, \Gamma_m \quad,$$

$$\frac{\partial \bar{\rho}_m V_q}{\partial t} + \sum_{m \in q} \nabla \cdot \left(\bar{\rho}_m \, V_q V_q \right) + \alpha_q \nabla p - \bar{\rho}_q g$$

$$+ K_{qS} V_q - \sum_{q'} K_{q \, q'} \left(V_{q'} - V_q \right) - VM_q$$

$$= - \sum_{q'} \Gamma_{qq'} \left[H(\Gamma_{qq'}) \, V_q + H(- \Gamma_{qq'}) \, V_q \right] \quad, \quad \text{and}$$

$$\frac{\partial \bar{\rho}_M e_M}{\partial t} + \sum_{m \in M} \nabla \cdot \left(\bar{\rho}_m e_m V_q \right) + p \left[\frac{\partial \alpha_M}{\partial t} + \nabla \cdot \left(\alpha_M \, V_q \right) \right]$$

$$- \frac{\bar{\rho}_M}{\bar{\rho}_q} \left[\sum_{q'} K_{q \, q'} \left(V_q - V_{q'} \right) \cdot \left(V_q - V_{qq'} \right) \right.$$

$$\left. + K_{qS} V_q \cdot \left(V_q - V_{qS} \right) - VM_q \cdot \left(V_q - V_{GL} \right) \right]$$

$$= Q_N + Q_{MF} \left(\Gamma_{MF} \right) + Q_{VC} \left(\Gamma_{VC} \right) + Q_{HT}(h, a, \Delta T) \quad.$$

The density components are subscripted by m, the energy components by M and the velocity components by q. Similar to the former codes, component mass and energy are represented by macroscopic density and specific internal energy in SIMMER-III.

where
symbols:
$\bar{\rho}$	;	macroscopic density,
v	;	velocity,
e	;	internal energy,
α	;	volume fraction,
p	;	pressure,
K	;	momentum-exchange coefficient,
VM	;	virtual mass,
Γ_m	;	total mass-transfer rate per unit volume from component m,
$\Gamma_{qq'}$	;	mass-transfer rate from q to q',
$H(x)$	;	Heaviside unit function,
Q_N	;	nuclear heating rate,
Q_{MF}	;	energy interchanging rate for melting or freezing,
Q_{VC}	;	energy interchanging rate for vaporization or condensation,
Γ_{MF}	;	melting or freezing rate for mass interchange,
Γ_{VC}	;	vaporization or condensation rate for mass interchange,
Q_{HT}	;	energy interchanging rate for heat-transfer,
h	;	heat-transfer coefficient,
a	;	interfacial area per unit volume,
ΔT	;	temperature difference between components,

suffix:
m	;	density component,
q, q'	;	velocity fields,
r	;	energy component,
qS	;	stands for terms existing at interfaces between velocity field q and structure,
qq'	;	stands for terms existing at interfaces between velocity field q and q',
GL	;	stands for terms existing at interfaces between vapor and an averaged liquid velocity,
$m \in q$	;	includes all density components m existing in q,
$m \in r$	;	includes all density components m existing in energy component r.

The overall fluid-dynamics solution algorithm is based on a time-factorization approach in which intra-cell interfacial area source terms, heat and mass transfer, and momentum exchange functions are determined separately from inter-cell fluid convection.

II.4. Interfacial Area Model

For the heat and momentum transport an interfacial area modelling is applied with a comprehensive representation of flow topologies. To obtain the mass, momentum, and energy transfer terms, the binary contact areas must be determined for 42 possible contact interfaces among seven fluid energy components and three structure surfaces (a fuel pin, left can wall and right can wall). Such binary contact areas are determined based on the convectible interfacial areas and flow regime which describes the geometry of the multiphase flow.

Flow regimes are modeled for both the pool flow in which the effect of the structure is negligible and the channel flow which is confined by structure.

II.5. Momentum Exchange Functions

The developed formulations are based on the analogy from the engineering correlations of steady-state two-velocity flow, since both theoretical and experimental knowledge of details is limited for a multicomponent three-velocity flow. Fluid-structure, fluid-fluid drag and liquid-vapor virtual mass effects are formulated. The momentum exchange function between velocity fields q and q', $K_{qq'}$, in the momentum equation is a function of the drag coefficient and interfacial areas.

II.6. Heat Transfer Coefficients

Heat-transfer coefficients are required to perform the heat and mass transfer calculations. Heat transfer coefficients are defined for forty-two binary contacts between the energy components and contribute to 30 vaporization/condensation (V/C) paths and 20 melting/freezing (M/F) paths. The coefficients control heat transfer between the bulk and interface temperatures for each fluid energy component. The coefficients are based on pseudo-steady state considerations.

II.7. Heat and Mass Transfer Model

After the interfacial area and heat-transfer coefficients are obtained, the conservation equations without convection are solved for intra-cell heat and mass transfer in two steps. The first step calculates the phase transition processes occurring at interfaces, described by a non-equilibrium heat-transfer-limited model. This is a non-equilibrium process because the bulk temperature does not generally satisfy the phase-transition condition when the mass transfer occurs at the interface. The second step of mass and energy transfer is through an equilibrium process occurring when the bulk temperature satisfies the phase-transition condition. At 42 possible interfaces defined in SIMMER-III, all the important non-equilibrium mass-transfer processes are modeled, including 30 vaporization/condensation (V/C) paths and 20 melting/freezing (M/F) paths. The M/F transfers include the crust formation on a can wall that furnishes thermal resistance, and steel ablation and particle formation that contribute to fluid quenching and bulk freezing.

II.8. Equations-of-State Model

An EOS model is required to close and complete the basic fluid-dynamic equations set. Moreover it is crucial from the viewpoints of numerical accuracy and stability, and computing efficiency. An improved analytic EOS model using the flexible thermodynamic functions has been developed for SIMMER-III, which treats the basic reactor-core materials: mixed-oxide fuel, steel, sodium, control (B_4C) and fission gas. These materials are assumed to be immiscible, such that a unique EOS for each material can be defined.

II.9. Fuel Pin Configuration

The fuel-pin and can wall model is another salient element of SIMMER-III by representing the stationary structure in the core as well as their time-dependent disintegration. The standard fuel-pin model of the present SIMMER-III version is rather simple with a pellet interior modeled by a single temperature node and with its breakup modeled only by a thermal (melt-fraction) criterion. However the separated treatment of a pellet surface node provides better thermal coupling with the fluid. Because of relatively large thermal inertia of the pellet interior, the fuel-pin heat-transfer calculation is performed with time steps larger

than the fluid-dynamics steps. This simplified model is considered to be sufficient e.g. for simulating the fuel-pin behavior in a voided channel typical in a loss-of-flow accident.

II.10. Can Wall Configuration

The can wall model treats separated left and right can walls assumed to be located at the mesh cell boundaries. The presence of the can wall at a cell boundary eliminates radial fluid convection. Fuel crust can grow on a can wall when the heat and mass transfer model predicts this. Inter-cell heat transfer also is calculated when one of the two can walls at a cell interface is missing. When the can wall becomes thin, then the two nodes are merged into a single interior node.

II.11. Neutronics Model

The neutronics model which has been developed for the present SIMMER-version is based on the previous SIMMER-II code. The space dependence of neutron flux is modeled by an S_n transport theory similar to TWOTRAN-II and the dynamics is treated by an improved quasi-static method. The calculation of shielded macroscopic cross section is performed within in the code. An additional feature of SIMMER-III is a simple decay heating model. At present a new development is under way at FZK to replace the TWOTRAN part of the code by more advanced techniques based on TWODANT, both to improve accuracy, flexibility and speed of the neutronics calculations.

Summary Report on an Application for the SIMMER-III Code

Assessment, Phase 1

Liquid Sloshing Motion Including Particles

by

W. Maschek, E. Hesselschwerdt, C.-D. Munz, S. Kleinheins

Forschungszentrum Karlsruhe
Postfach 3640, 76021 Karlsruhe, Germany

April 1994

Outline of Case

In the framework of the SIMMER-III code assessment liquid sloshing processes are simulated and compared with experiments. Such liquid sloshing phenomena can play an important role in core disruptive accidents. The SIMMER-III code should therefore be capable to describe sloshing processes with good accuracy. The calculations presented are compared with experiments in which particles are embedded into the flow.

Key Words

Two-dimensional two-phase flow sloshing motions, water waves, dam-break problem, water-step problem, particulate flow

1.   Objectives of the Application

Liquid sloshing motions play an important role in core disruptive accident simulations of liquid metal reactors. Under pessimistic assumptions analyses show that the reactor core melts and a large whole core liquid fuel pool confined by blockages (frozen fuel and blanket structures) can be formed in the so-called transition phase /1/. A local fuel compaction may trigger a mild nuclear excursion in this pool. The following energy deposition leads to a pressure build-up in the core center which pushes the liquid fuel towards the pool periphery. Driven by gravity the fuel sloshes back towards the pool center and piles up in a neutronically critical or even supercritical configuration. This "centralized sloshing" /2, 3, 4/ can lead to energetic nuclear power excursions and the conditions and phenomena of these processes have therefore been studied extensively.

The simulation of sloshing motions provides an excellent test for the fluid-dynamic module of codes like SIMMER-III. Such a code must be able to describe sloshing with good accuracy. During the sloshing process smooth liquid surfaces may change and will break-up and smooth wave packages transform into sharp liquid peaks. SIMMER-III is a multi-phase code with no specific tracking of the free fluid surface. SIMMER-III is based on volume and time averaged equations. By this and the inherent numerical diffusion of the code the free surface of the moving liquid is smeared out to a certain extent. This represents a general difficulty in

describing sloshing phenomena. As could be shown in /3, 5/ higher order differencing (2nd order) as generally used in SIMMER-III is a necessity when describing liquid sloshing motions. The code calculations in /3, 5/ were compared with experiments /6/ in which different types of sloshing motions were investigated. The above analyses concentrated on sloshing of pure liquids. Some experiments were also performed with particles mixed into the flow mainly to investigate their damping influence /6/. Another question was if particles of a specific density and size would be seperated from the liquid during a sloshing process.

In the following two different sets of calculations are performed. At first a water step problem is run with no particles. This example was chosen to get started with a simpler two field (liquid-gas) simulation and also because the recalculation of this case with AFDM /7/ showed some deficiencies /5/. Second a dam break problem with a ring of particles in some distance from the water column was tested /6/.

2.   Description of Experiments

Two typical sloshing problems from the experimental series in /6/ are investigated in this exercise (Tab. 2.1 and Fig.2.1):

In the first case (case SA-D1X-3 in /6/) a cylindrical container is divided into two concentric parts by a cylindrical diaphragm. The inner cylinder contains water of a certain height, the outer cylinder contains water at a lower level. An (r,z)-diagram of this situation is shown in Fig. 2.2.

In the second case (case SE-D1P-1 in /6/) no liquid was in the outer container (dam-break problem), but a ring of particles was placed around the central water column at a certain distance (see Fig 2.3). The particles (Specification: Acryl P210D) have a density of 1.13 g /cm^3. The shape of the particles is cylindrical with a diameter of 2.5 mm and a height of 3 mm.

SLOSHING TEST CLASSIFICATION: SA - Water step

Experimental series signature	Diameter of central water cylinder [cm]	Height of water [cm]		Typ of Obgstacle/ Disturbance	Slosh at outer wall		Slosh at pool center			
		inner cylinder	outer cylinder		Time max. height at wall [sec]	max.height at wall [cm]	Time of 1. Peak [sec]	Height of 1. Peak [cm]	Time of second Peak [sec]	Height of second Peak [cm]
D1X-3	11	20	5	-	0.36 ± 0.02	11.0 ± 1	0.62 ± 0.04	15.0 ± 3	1.24 ± 0.04	50 ± 5

SLOSHING TEST CLASSIFICATION: SE - Dam break

Experimental series signature	Diameter of central water cylinder [cm]	Height of water [cm]		Typ of Obgstacle/Disturbance: Particles		Slosh at outer wall			Slosh at pool center	
		inner cylinder	outer cylinder	Particle height in central cylinder [cm]	Particle height in outer cylinder [cm]	Arrival time at wall [sec]	Time of maximal height [sec]	maximal height Liquid/ Particles [cm]	Time of maximal height [sec]	Maximal height [cm]
D1P-1	11	20	-	-	1	0.28 ± 0.02	0.40 ± 0.02	10/8 ± 1	0.80 ± 0.04	25 ± 5

Tab. 2.1: Experimental results for the water step problem and for dam break problems with particles in the flow

3.   Analytical Solution

Analytical solutions are available for the outward sloshing phase when the water-depth is small (shallow water theory /8/). For the total sloshing process no analytical solutions are available.

4.   Understanding of Phenomena

4.1   The Water Step Problem

The water step problem represents an oscillating system by the interaction of the central water column with the outer water ring. Under specific mass combinations as in experiment SA-D1X-3 (M_{column}: M_{ring} = 1:3.75) /6/ the interaction of deep water waves with surface waves (layers of water which move on different time scales and in different directions) creates the complicated sloshing pattern as seen in Fig. 2.2. Generally from fluid dynamics theory /8/ one can infer that most of the damping in this oscillating system is related to surface waves. The kinetic energy is mostly stored in these wave packages. In the water step system with deep water areas the damping is much less than in a system with shallow water and several oscillating sloshing cycles can be observed. In the experiments the water of the central water column was colored dark to observe the detailed liquid motion. After release of the water column a surface wave and a deep water wave are created which move outwards. The deep water wave moves faster and pushes the clear water ring upwards at the container walls. The clear water of the outer ring is pushed upwards at the outer container walls. The dark water does not reach the outer container and stays at the pool bottom. In sloshing back the clear water compresses the dark water and pushes it upwards in the pool center. A dark water hump is formed. The dark water hump collapses in a broad roll and triggers an outward motion in the deep water but also a surface wave travels outward. The clear water is again pushed upwards the outer container walls and again compresses the central dark water which has spread out below the surface. The high sloshing peak thus appears in the second sloshing cycle /6/. Both the water hump and the high water peak consist of the dark water.

4.2 The Dam Break Problem with a Particle Ring

The influence of particles on the sloshing process was investigated in a series of experiments /6/. The main interest was in the damping effect of these particles on the sloshing motion. Another issue to investigate was if particles of a specific size and density have a trend to seperate from the liquid or stay intimately mixed. If a separation would take place the assumptions of SIMMER-III to put the heavy particles into the same velocity field as the liquid fuel would be questionable.

For the experiments a special size and particle density was chosen. The particles had an approx. 10% higher density than the liquid. This density increase would be similar for solid fuel particles in accident simulations. In the first experiment the particles were positioned in a ring around the central water column. The particle ring started at a radius of R = 14.5 cm in experiment SE-D1P-1 (Fig. 2.3). The particle bed height was 1 cm.

As can be seen from the experiment the liquid piles up when it hits the particle area and pushes them upwards the container walls while some mixing with the flow takes place. The pure water slightly passes the particles at the wall but generally the particles remain mixed into the flow which can be clearly seen in the centralized back-slosh. Due to the particles in the flow no symmetric and straight sloshing peak can be built up, but a cloud of liquid/gas/particles emerges. The coherence of liquid motion is destroyed by the particles and the central sloshing peak is damped.

5.   SIMMER-III Representation

Two cases are given, a water-step problem and a dam-break problem including particles in the flow.

5.1 Geometry, Initial and Boundary Conditions

The essential values to be compared with the experiment are the sloshing heights and arrival times of the liquid at the outer container wall and the liquid peak after convergence of the water at the center. For the simulation of the water-step problem with SIMMER-III, a 2-D mesh of 24 x 30 mesh points was chosen. The higher order differencing option was used. All other input values (e. g. momentum exchange coefficients) were chosen as the defaulted ones in SIMMER-

III. As we have an isothermal problem no heat and mass transfer takes place. The fluiddynamics parts of the code, the interfacial area model and the momentum exchange model are tested in these calculations. For the dam-break problem including particles a mesh of 25x30 cells has been used.

To test the SIMMER-III assumption concerning the distribution of particles on the momentums field for heavy and light components the solid particles where put into the liquid fuel field. This would also be the case with fuel particles in accident simulations.

For the SIMMER-III simulation (case D1P1) the choice of the mesh leads to some problems. For a good simulation with low numerical damping a rather fine mesh is optimal. On the other side the size of the particles (max. dimension = 3 mm) defines a lower limit for the mesh size as an ensemble of particles should exist in a mesh. For the present calculation the smallest dimension of the axial mesh is chosen as 5 mm.

In the input the maximum packing fraction for defining the particle viscosity was defined as 0.7 and the multiplier of the drag coefficient CCD was set to 1.0 /9/. Again, no friction of the fluid and the particles at the pool bottom is modelled within the code framework.

5.2   Code Version and Computer Used

The calculations are based on SIMMER-III Version 1.B. The computations were performed on a mainframe IBM3670.

5.3   Code Modifications

No code modifications have been performed.

5.4   Parametric Cases

-----

6. Results

6.1 Water-step Problem

In Fig. 6.1 and Table 6.1 the results of the SIMMER-III calculation (case D1X3) are displayed. The comparison between the experimental values and the calculations shows good agreement in the phase when the central water column collapses up to the time when the maximum water height is reached at the outer wall. First the outgoing wave typical for the two-dimensional waterstep problem is nicely simulated. In the experiment a first central slosh results in a water-hump at the center without any sharp liquid peak. In the SIMMER-III simulation the water hump is also visible but an additional water peak exists above the hump. The maximum height of this narrow liquid peak is given in Tab. 6.1.

SA D1X-3	Slosh at outer wall		Slosh at pool center			
	Time max. height at wall [sec]	max. height at wall [cm]	Time of first Peak [sec]	Height of first Peak [cm]	Time of second Peak [sec]	Height of second Peak [cm]
Experiment	0.36±0.02	11.0±1	0.62±0.04	15.0±3	1.24±0.04	50±5
Calculation	0.35	12.0	0.58	21.0	1.24	36

Tab. 6.1   comparison of experimental and calculational results for the water-step problem D1X-3

In the experiment no central spike occurs in the first in-slosh for the specific mass ratio of 1:3.75 (SA-D1X-3) for the water column to the outer pool. In experiments with other mass ratios a central spike however emerges /6/. This shows that a delicate balance of moving masses and forces creates the hump - a feature which is not covered by the code simulation. The difference between experiment and simulation may result from a lack of modelling features. From the experiment with differently coloured water it can be seen that the different fluids from the central column and the surrounding pool move as independent layers with partial surface mixing. Most important, in SIMMER-III there does not exist a model for momentum exchange between the calculational cells. The lack of such a model influences the results of this sloshing calculation. Additionally no friction at the pool bottom is simulated. After a second outward slosh a narrow peak emerges in the experiment which reaches a large height of 50 cm. Though, the overall timing in the calculation is quite good the central peak is only 36 cm high and underestimates the experimental value. It is important to note that the essential mass distributions as a function of time are calculated with sufficient accuracy. Based on the calculations performed one can deduce that SIMMER-III simulates the water-step problem with reasonable accuracy when the essential mass distributions and the timing of motion are regarded. The details of the simulation could however be improved by introducing models for intercell momentum exchange and friction at the bottom walls.

6.2   Dam-Break Problem with a Particle Ring

As can be seen in Tab. 6.2 and Fig. 6.2 in the calculations the outward moving liquid pushes the particle ring towards the outer container wall. The particle bed at the bottom is penetrated partly by the fluid. When the liquid sloshes up the container walls, the particles are in front of the water wave.The main liquid mass remains however below the liquid particle accumulation.A thin particle layer is pushed much further up than in the experiment. After flow reversal the liquid and particles are fully mixed and reassemble at the center of the container.

SD D1P-1	Slosh at outer wall			Slosh at pool center	
	Arrival time at wall [sec]	Time of maximal height [sec]	maximal Height Liquid/ Particles cm]	Time of maximal height [sec]	Maximal Height [cm]
Experiment	0.28±0.02	0.40±0.02	10/8±1	0.80±0.04	25±5
Calculation	0.25	0.40	10/17	0.80	27.0

Tab. 6.2   Comparison of experimental and calculational results for the dam break problem with Particles D1P-1

From the simulation and the experiments it can be observed that the liquid mixes with the particle bed and the particles of the specific size also remain intimately mixed in the flow. Thus the assumption of putting fuel particles into the liquid fuel field is a reasonable choice. The simulation of sloshing with a particle ring is quite satisfactory. The impact of the liquid on the particle bed, its acceleration, and the mixing of the liquid and the particles is simulated adequately. The calculated main mass distribution of the liquid agrees with the experiment. The sloshing height at the wall is overestimated for the particles. Again, no bottom friction of the particle field is simulated by SIMMER-III. The central inward slosh is overestimated in its size compared to the experiment in which the central slosh produces a broad liquid peak which is broken up in drops and particles. This is not surprising as in the twodimensional code framework the symmetry of the converging waves is preserved and the emerging instabilities are not simulated. Thus in the simulation a high central sloshing peak emerges. In comparison to the sloshing motion without particles the damping effect of particles is clearly visible in the sloshing heights achieved.

For completeness a SIMMER-III simulation (case D1) of the experiment has been performed using first order donor cell differencing for the momentum equations. The results are displayed in Fig. 6.3. As can be clearly seen the mass distributions are not adequately calculated. A strong smearing of the wave packages can be observed. The use of the first order donor cell differencing leads to incorrect results.

7. Conclusions

In summary the following conclusions can be drawn from the recalculation of the sloshing experiments with and without particles in the flow:

1) The essential features of the sloshing process are well captured by the SIMMER-III code. The essential mass distributions and velocities of the water waves are recalculated by the code.

2) The calculation of some details of the sloshing process when liquid shear flows occur in the liquid pool and dominate the behaviour are beyond the capability of the code.

   The main reasons for this are:
   - no intercell momentum exchange is simulated
   - no friction at the pool bottom is simulated

3) The instabilities of the converging water waves during the in-slosh cannot be simulated within the twodimensional framework of the SIMMER-III code. A tendency exists to overestimate central sloshing heights and the central mass accumulation.

4) The interaction of the liquid and particles can be calculated with good accuracy in the sloshing simulations. Both the particle mass distributions and the intermixing of liquid and particles can be represented by the code. The assumption of putting the solid fuel particles into the liquid fuel field seems to be justified on the basis of the experiments performed.

5) Comparative calculations show that application of second order differencing is essential for simulating the sloshing processes (with and without particles). Excessive numerical damping and diffusion discredit the first order donor cell differencing approach.

8. Recommendations

The inclusion of friction at the bottom cells and intercell momentum exchange would further improve the capability of the code.

9. References

/1/ W. Maschek, E. A. Fischer and M. W. Asprey,
"Transition Phase and Recriticality Analyses for a SNR-Type Homogeneous Core with the SIMMER-II Code,"
Proc. Int. Topl. Mtg. Liquid Metal Fast Breeder Reactor Safety and Related Design and Operational Aspects, Lyons, France, July 19-23, 1982, Vol. III, p. 357, European Nuclear Society (1982).

/2/ W. Maschek, C. D. Munz and L. Meyer
"An Assessment of Liquid Sloshing Phenomena in Pools Based on AFDM/SIMMER Code Calculations and Experiments",
Proc. 1990 Int. Fast Reactor Safety Mtg., Snowbird, Utah, August 12-16, 1990, Vol. IV, p. 395, American Nuclear Society (1990).

/3/ W. Maschek, C. D. Munz, L. Meyer
Investigations of Sloshing Fluid Motions in Pools related to Recriticalities in Liquid-Metal Fast Breeder Reactor Core Meltdown Accidents
Nucl. Techn. 98, 27 (1992)

/4/ Sa. Kondo, Y. Tobita, K. Morita, N. Shirakawa
SIMMER-III: An Advanced Computer Program for LMFBR Severe Accident Analysis, ANP'92, Vol. IV, 40-5, Oct. 1992, Tokyo

/5/ C. D. Munz, W. Maschek
Comparison of Results of Two-Phase Fluid Dynamics Codes on Sloshing Experiments
KfK 5091 (1992)

/6/ W. Maschek, A. Roth, M. Kirstahler, L. Meyer
Simulation Experiments for Centralized Liquid Sloshing Motions
KfK 5090 (1992)

/7/ W. R. Bohl, D. Wilhelm, J. Berthier and F. R. Parker,
"The AFDM Program: Scope and Significance",
Proc. 1990 Int. Fast Reactor Safety Mtg., Snowbird, Utah, August 12-16, 1990, Vol. II, p. 155, American Nuclear Society (1990)

/8/ J. J. Stoker:
Water waves
Interscience Publishers, New York 1957

/9/ M. Ishii, K. Mishima
Study of Two-Fluid Model and Interfacial Area
NUREG/CR - 1873 (1980)
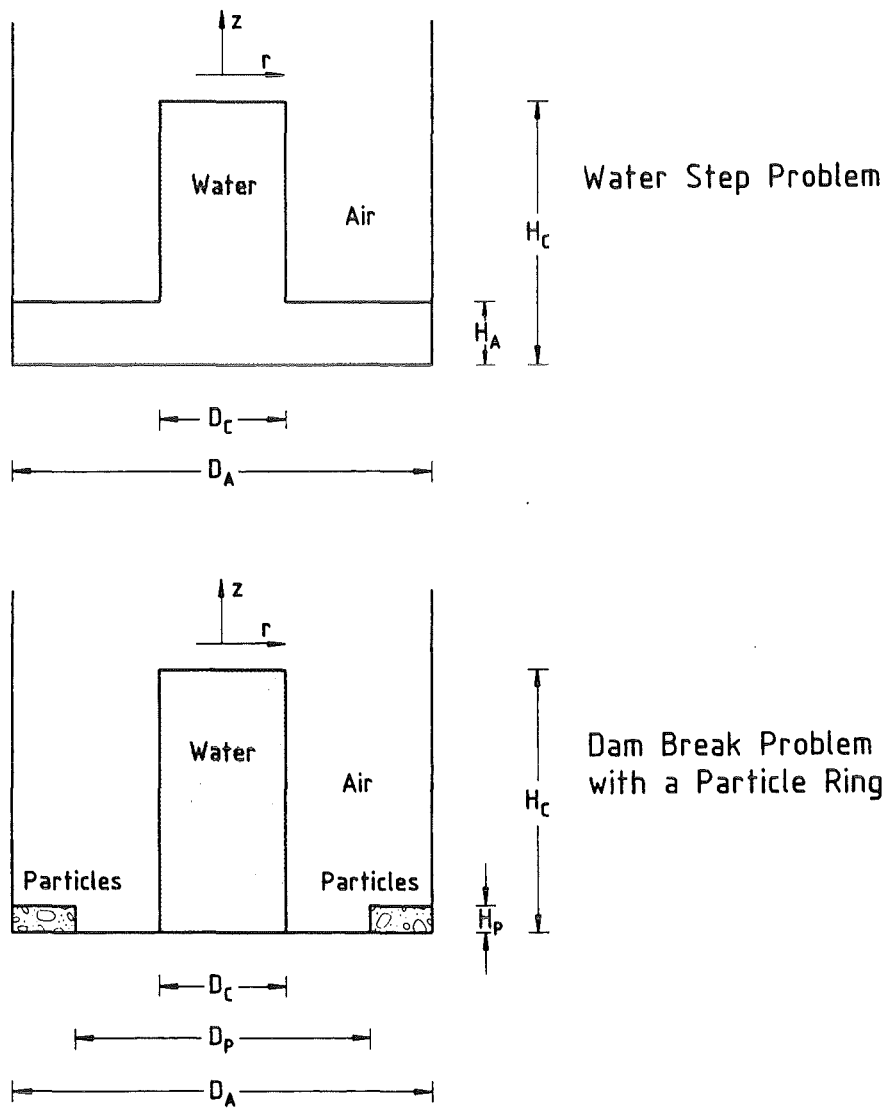
Fig. 2.1.: The two sloshing problems investigated
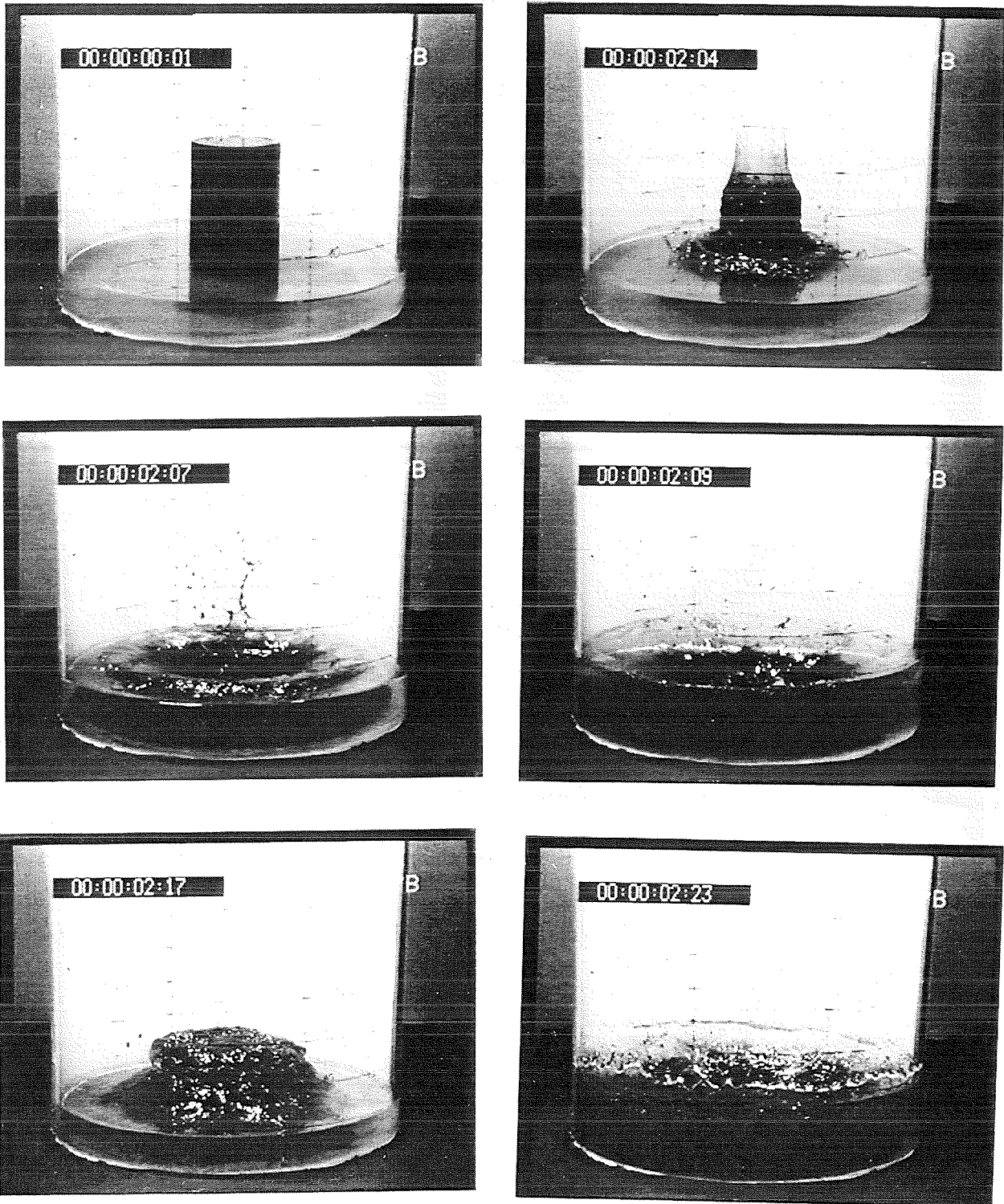
Fig. 3.1: Sloshing motions seen in a typical water step problem

Note: The numbers in the left upper window refer to video frames
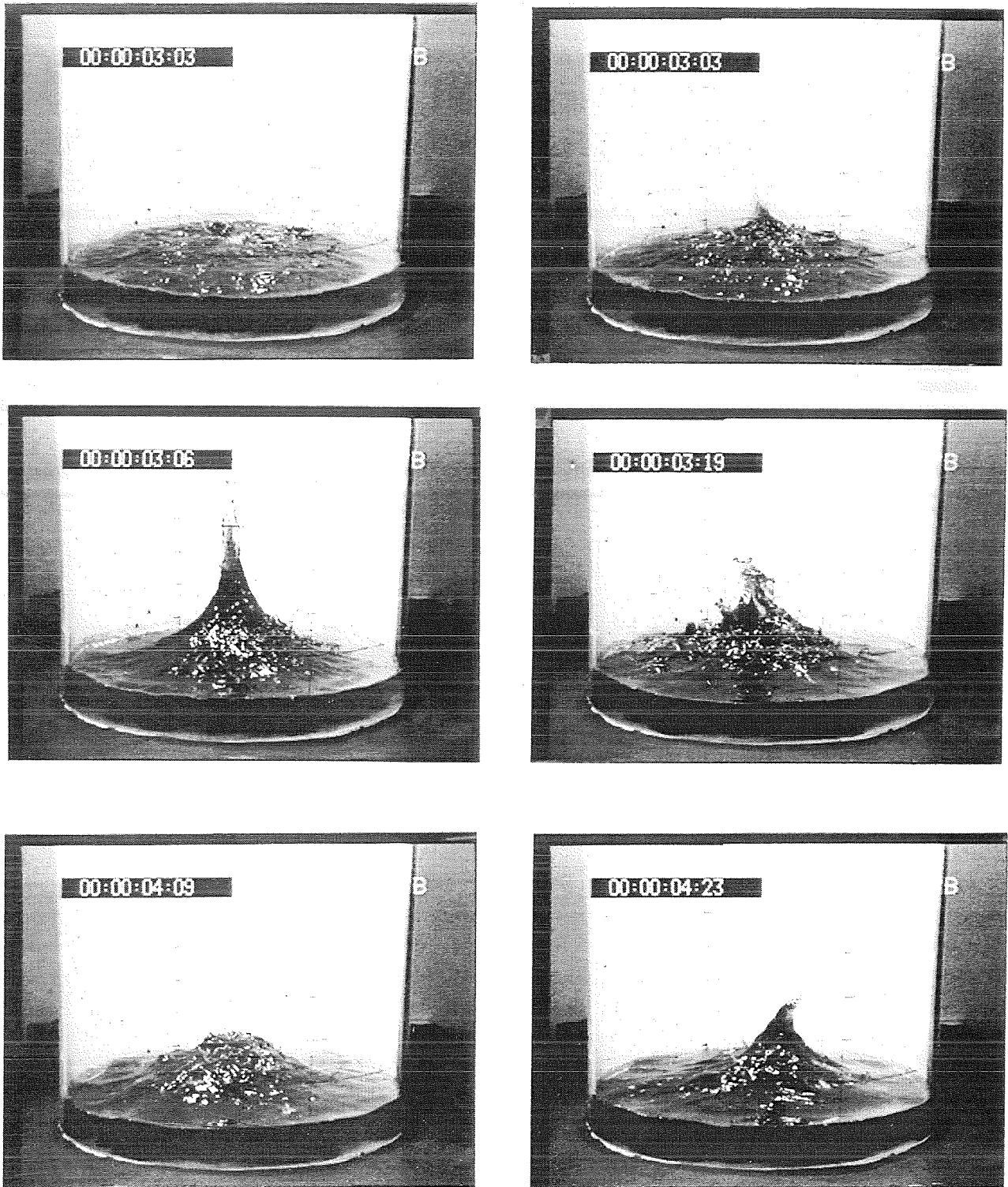
Fig. 2.2: Sloshing motions seen in a typical water step problem
(continued)
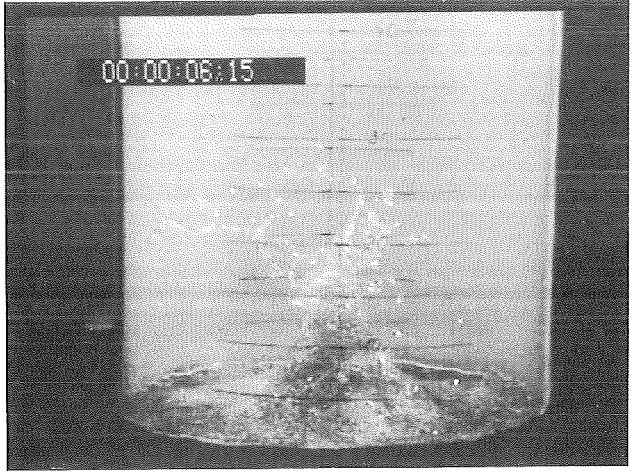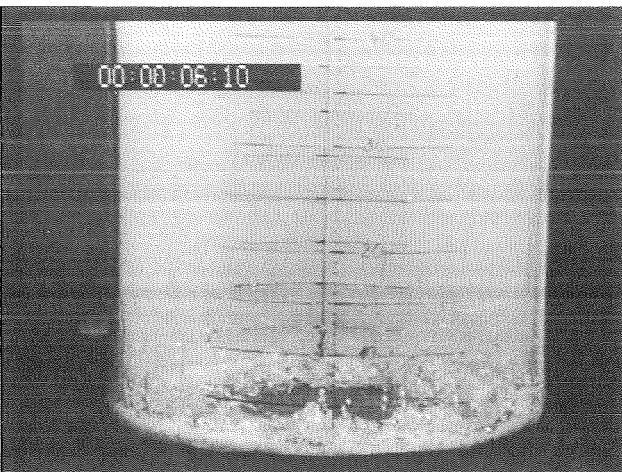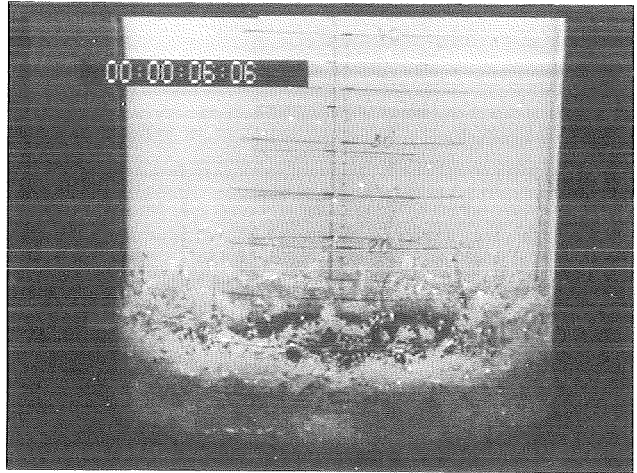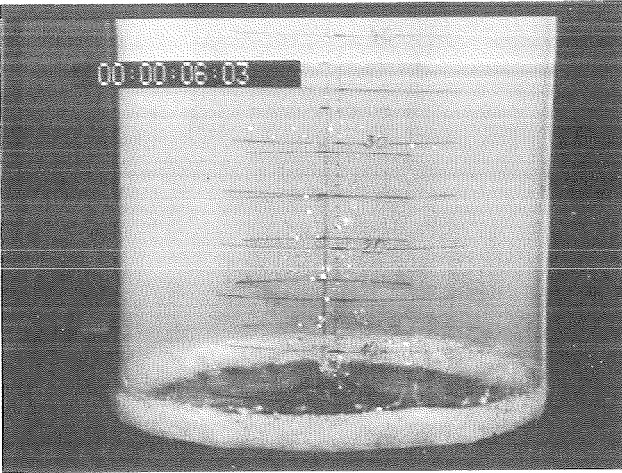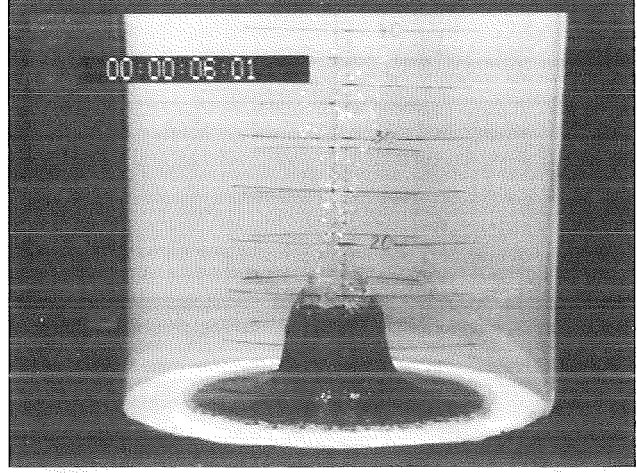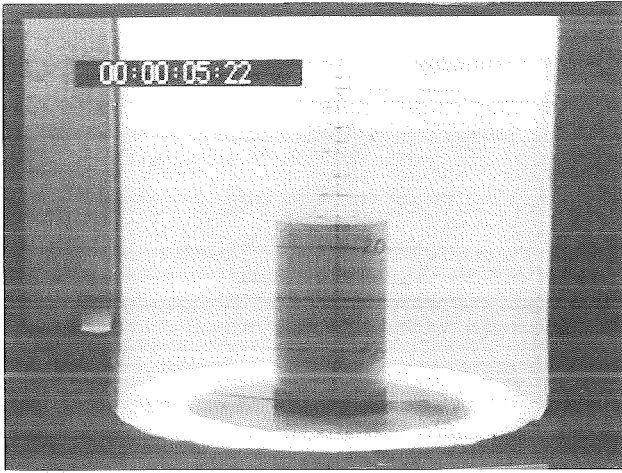
Figure 2.3: Dam break problem SE-D1P-1 with particles in the flow
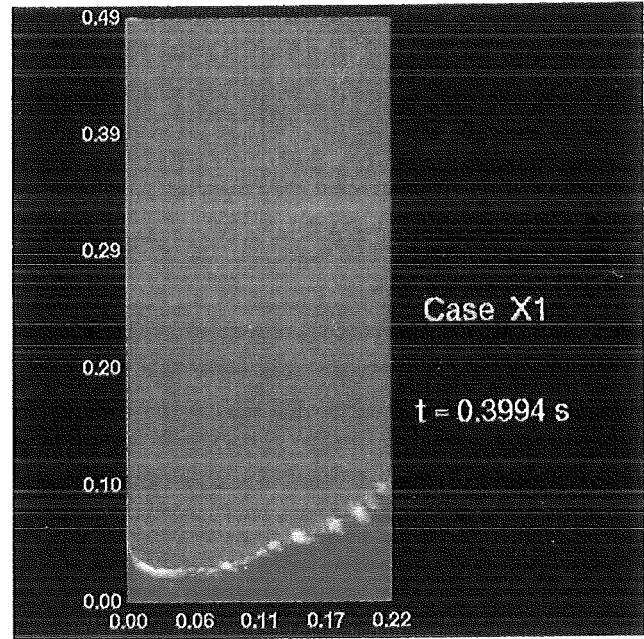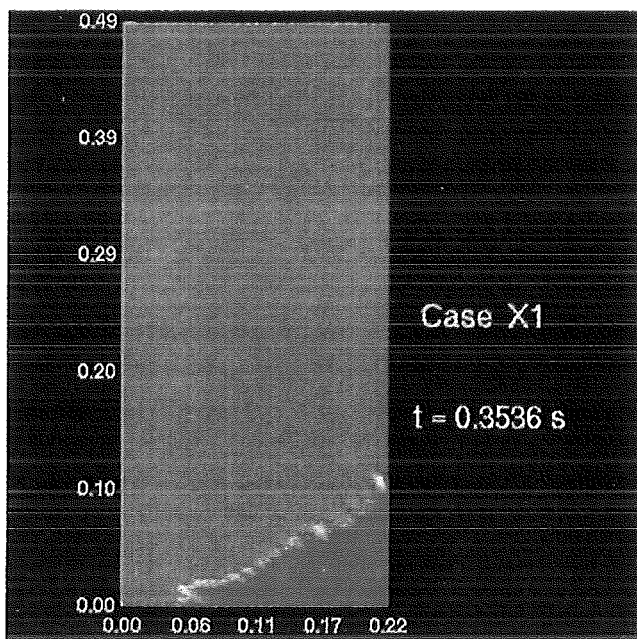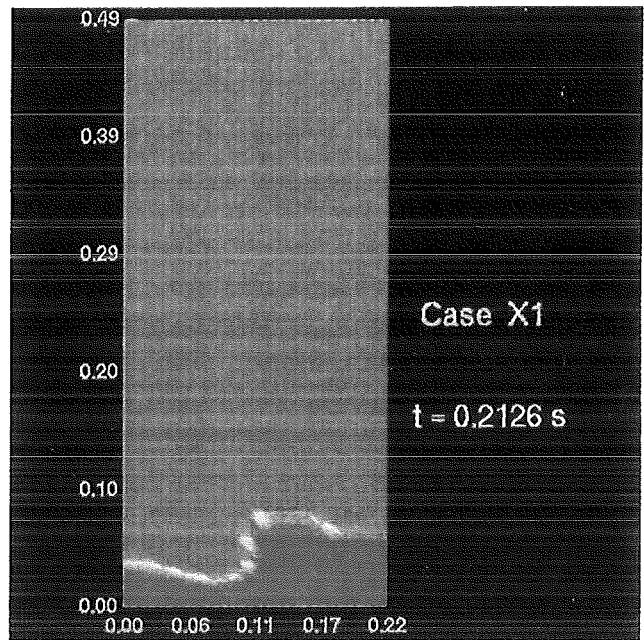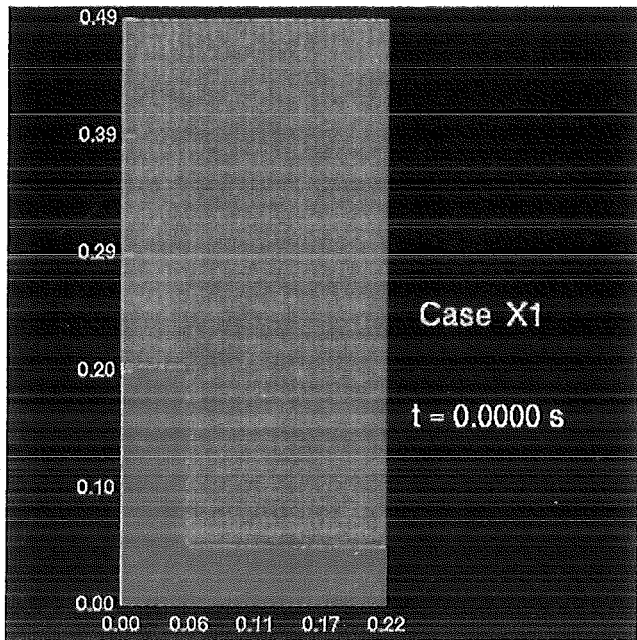
Fig. 6.1   Simulation of the water-step problem with SIMMER-III
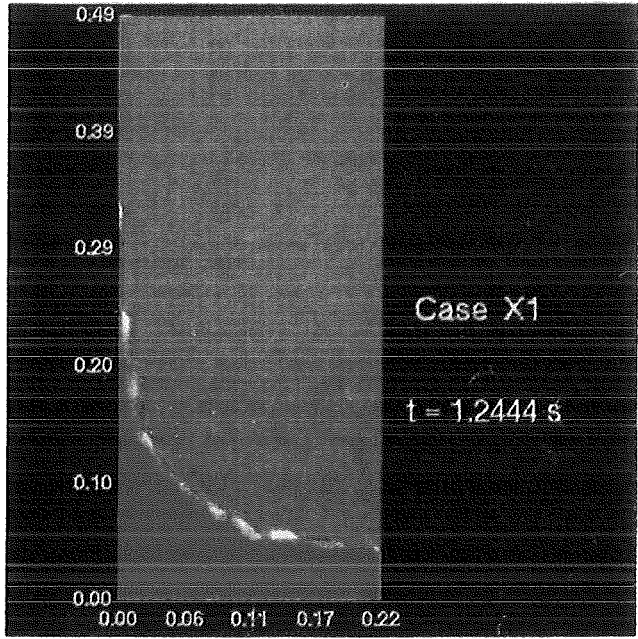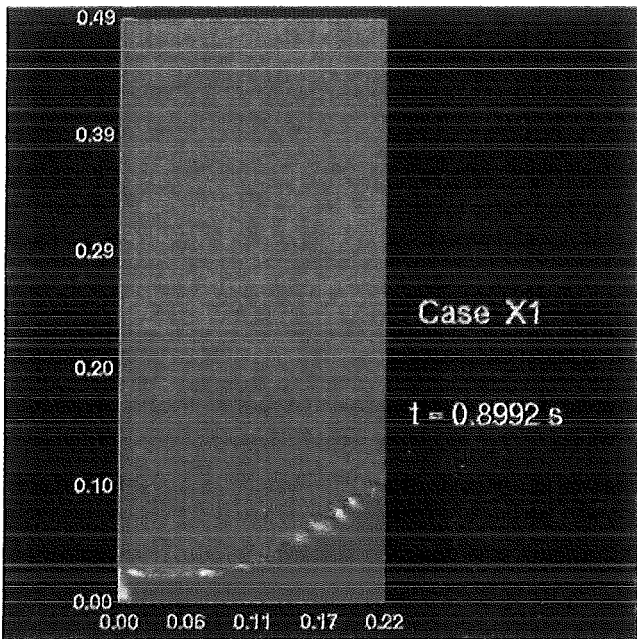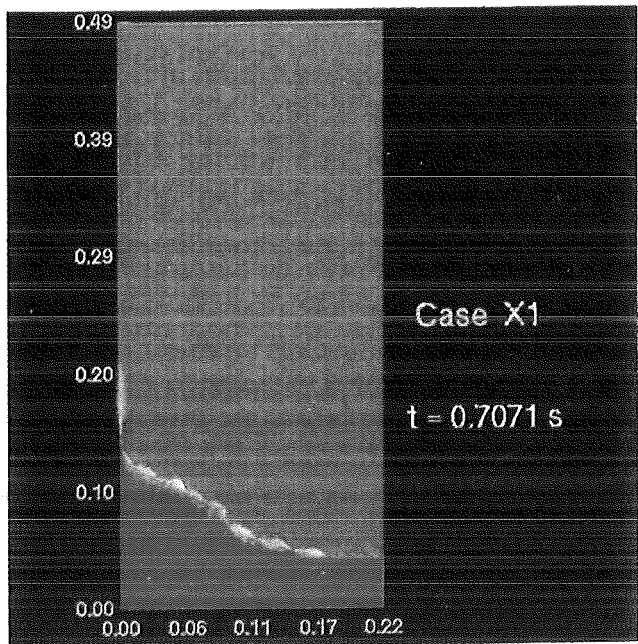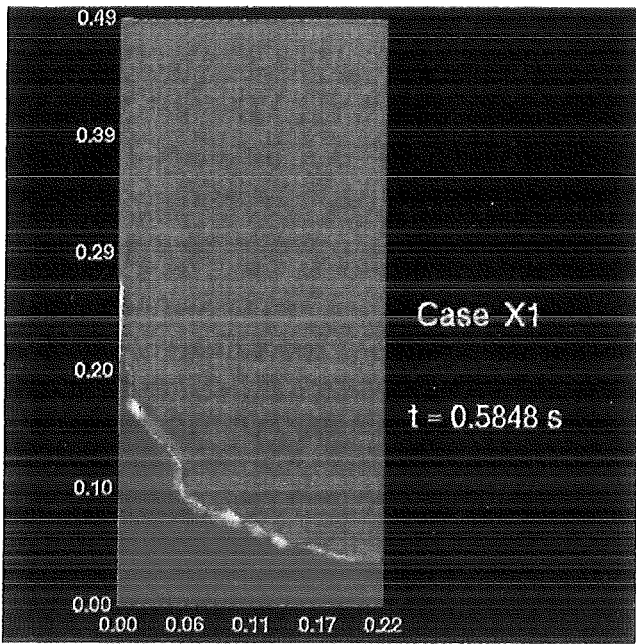
Fig. 6.1   Simulation of the water-step problem with SIMMER-III
(continued)
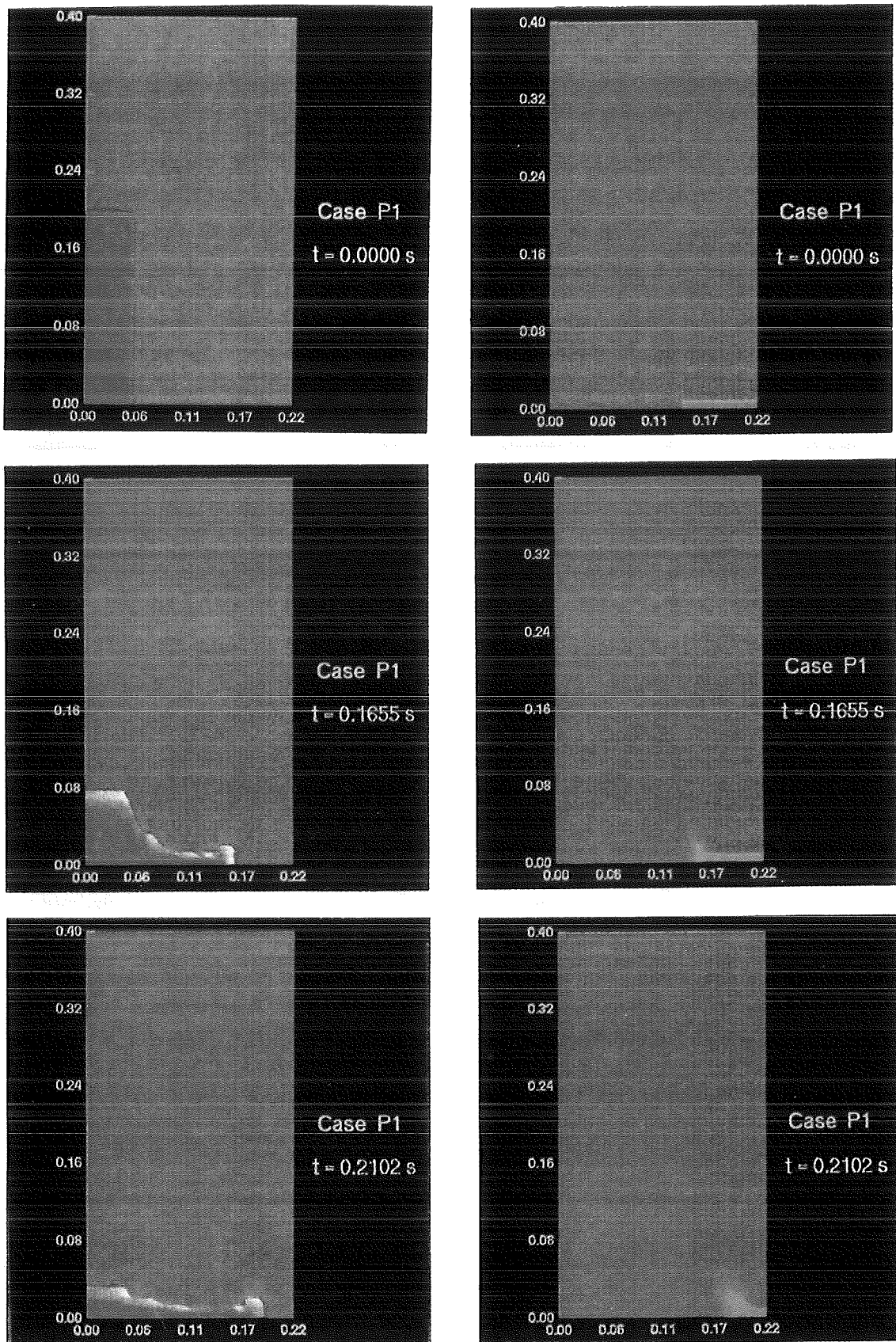
Fig. 6.2   Numerical simulation of the dam break problem SE-D1P-1
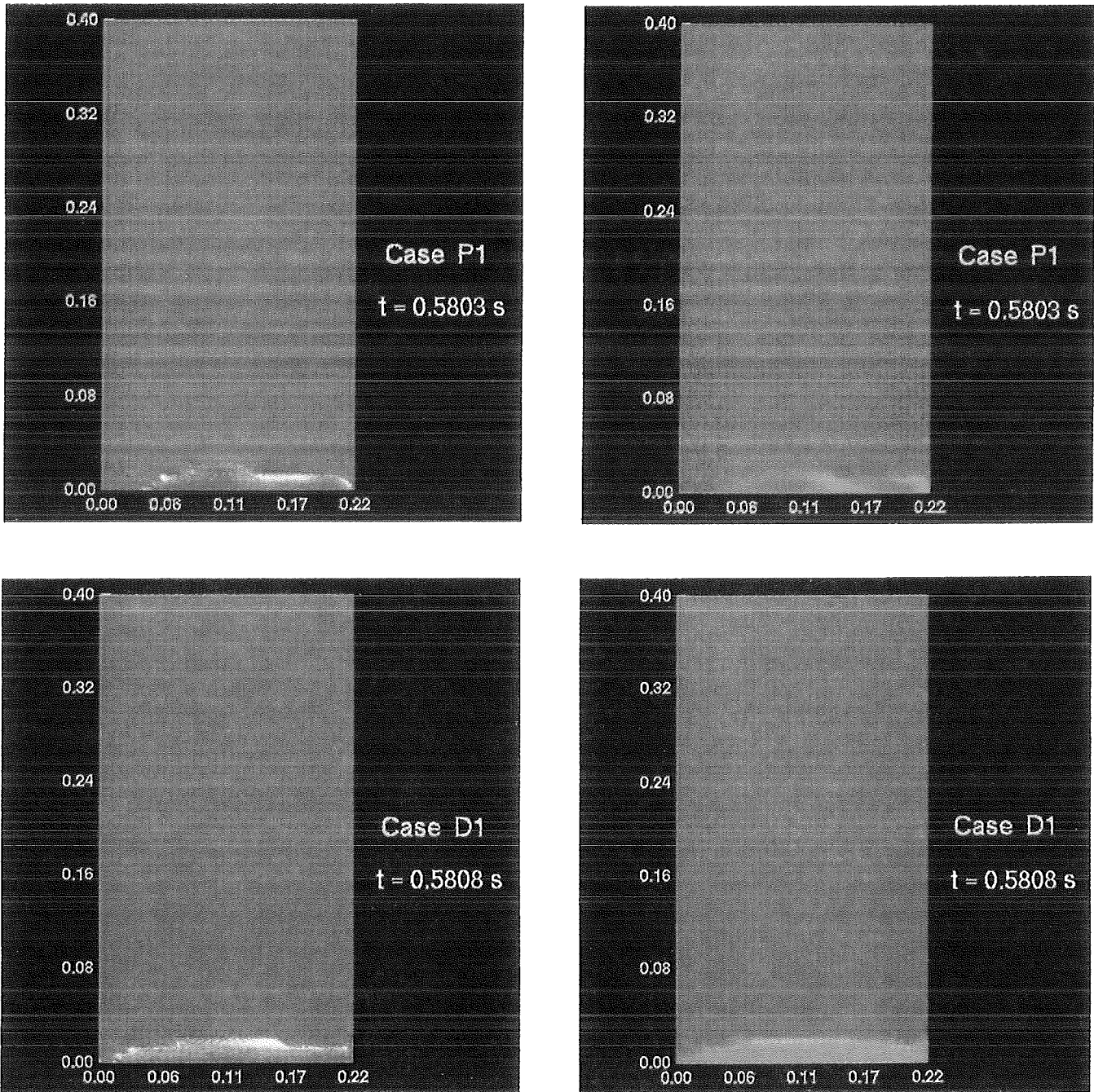with SIMMER-III (second order differencing option)
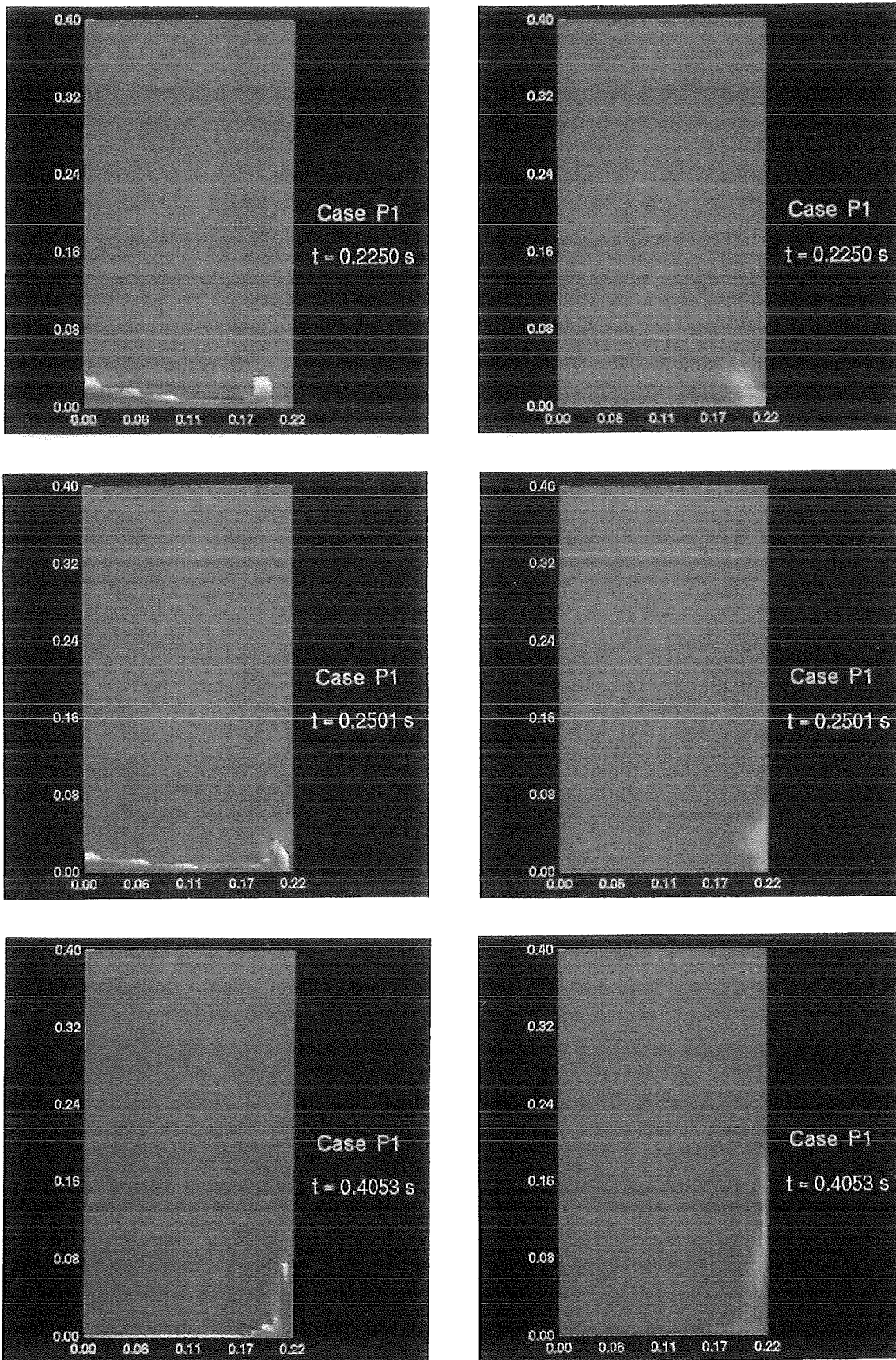
Fig. 6.2   Numerical simulation of the dam break problem SE-D1P-1
with SIMMER-III (second order differencing option)
(continued)
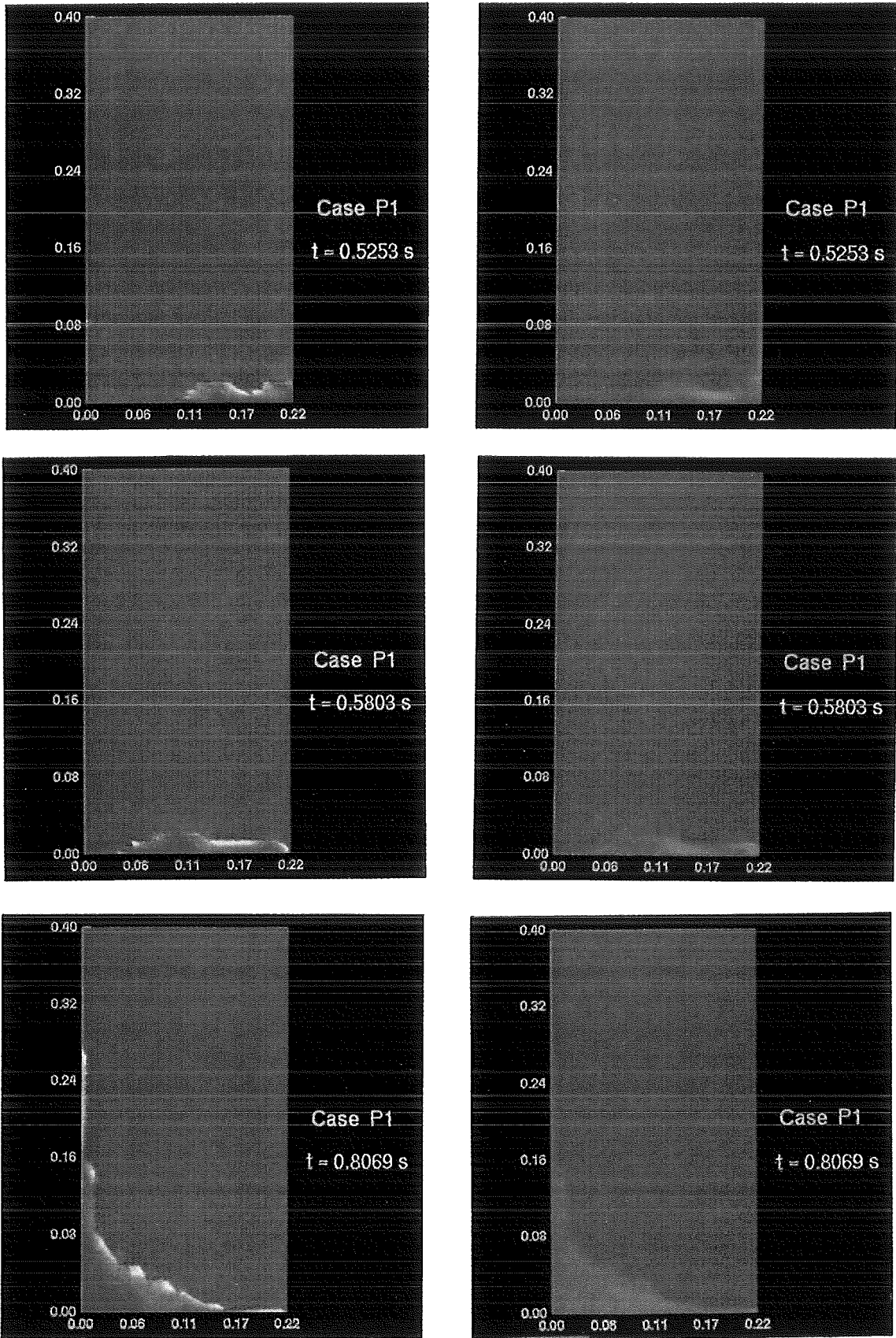
Fig. 6.2   Numerical simulation of the dam break problem SE-D1P-1
            with SIMMER-III (second order differencing option)
            (continued)

Fig. 6.3   Comparison of the wave package smearing in the numerical simula-
tions of the dam break problem SE-D1P-1 with SIMMER-III
Second order differencing option (above - case P1)
First order differencing option (below - case D1)
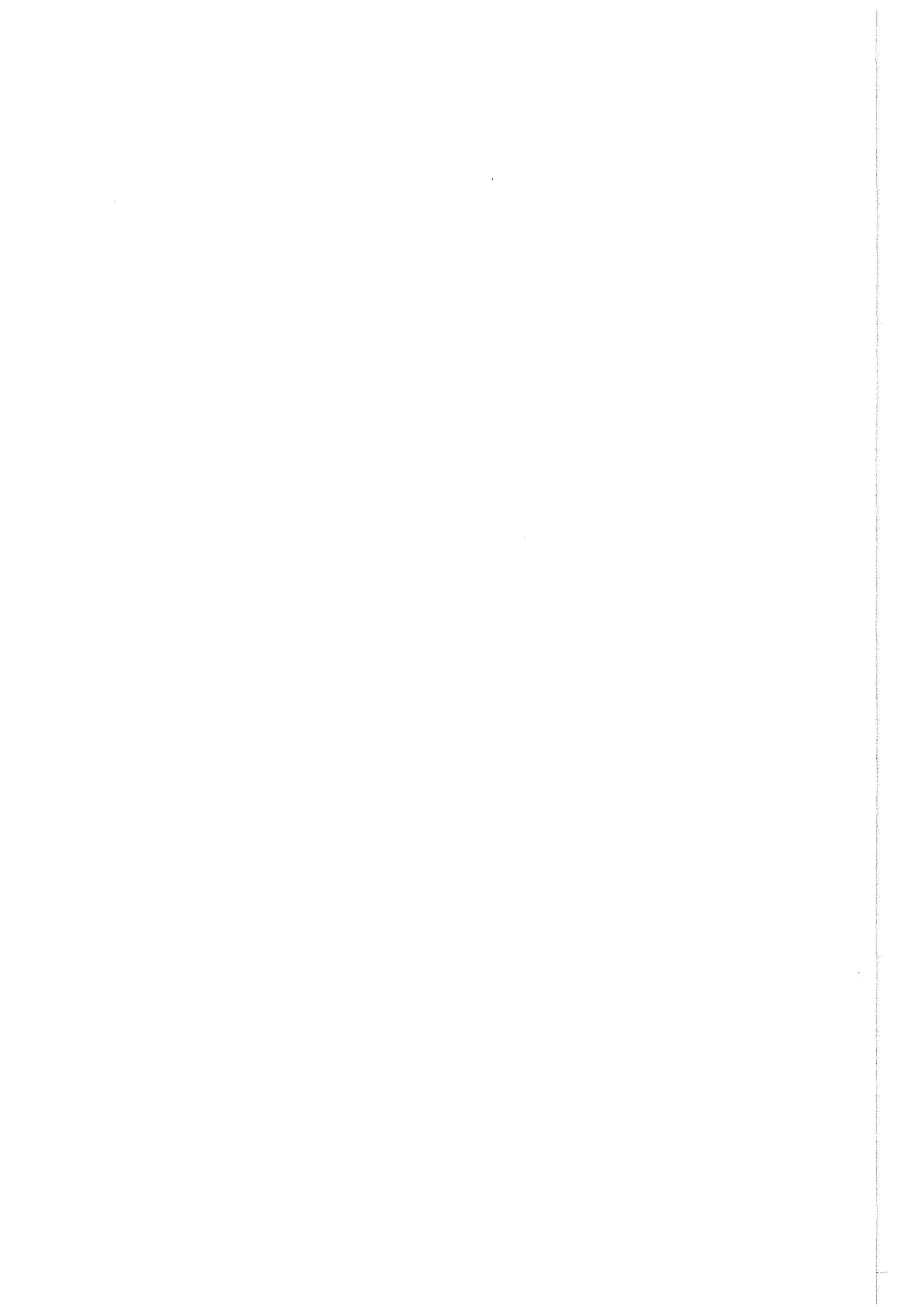
Summary Report on an Application for the SIMMER-III Code Assessment, Phase 1

Two-Phase Shock Tubes

by

C.-D. Munz, W. Maschek, M. Göz, H. Jacobs, B. Stehle

Forschungszentrum Karlsruhe
Postfach 3640, D-76021 Karlsruhe, Germany

September 1994

Outline of Case

A straight closed duct of uniform cross-section is divided into two equal parts by a diaphragm. On the left of the diaphragm, the duct contains compressed air; on the right, it contains atmospheric-pressure air, mingled with finely-divided liquid water. If the two-phase mixture is approximated by a single fluid and the gas-water mixture is considered to be homogeneous and to satisfy the equation of state of a perfect gas, an analytical solution of this shock-tube problem exists.

Key Words

Two-phase shock tube, shock waves, two phases shock waves.

1.   Objectives of the Application

This application concentrates on a verification of SIMMER-III applied to the simulation two-phase problems with strong pressure gradients.

2.   Description of Experiments

A two-phase shock tube problem has been proposed by D.L. Youngs in [1] as a numerical benchmark test for multiphase hydro-codes. The problem description is as follows: A straight closed duct of uniform cross-section is divided into two equal parts by a diaphragm. On the left of the diaphragm, the duct contains compressed air; on the right, it contains atmospheric-pressure air, mingled with finely-divided liquid water. The purpose of this problem is to test numerical methods for highly transient multicomponent compressible flow, predicting what happens when the diaphragm breaks.

Air	Air 99 %
	Water 1 %
high pressure: $p_l = 3 \cdot 10^5$ Pa	normal pressure $p_r = 10^5$ Pa
normal density: $\rho_l = 1$ kg/m^3	normal mixture density:
	$\rho_{water} = 1000$ kg/m^3

rigid wall (left) ... rigid wall (right)

| 1 m | 1 m |

Table 2.1: Two-phase shock tube problem

The overall length of the tube is 2 m, consisting of two 1 m long regions separated by a diaphragm. As boundary conditions impermeable walls are to be specified at both ends of the tube. Due to the left high pressure chamber of the shock tube, a shock wave to the right into the gas water mixture is generated, if the diaphragm breaks. The values of the physical variables are given in Table 2.1.

3.   Analytical Solution

Under the assumption of no slip between water and gas, D.L. Youngs presented in [1] values for an approximate exact solution. He did not describe this approximation in detail. He only states that under the condition of no slip he solves the equations by the method of characteristics. The values of this approximation for the initial speed of the shock wave moving into the low pressure chamber and the conditions behind the shock wave have been listed in [1] and are given in Table 3.1.

shock speed:	v_s	= 172.1 m/s
velocity behind shock:	v_2	= 80,2 m/s
pressure behind shock:	p_2	= 2.517 $\cdot 10^5$ Pa
gas density behind shock:	ρ_2	= 1.874 kg/m^3
water volume fraction behind shock:	r_2	= 0.01874

Table 3.1: Values of an approximate exact solution as given in [1]

D.L. Young proposed to compare the numerical results of the codes with these approximate analytical results at time t = 3.0, 6.0, 9.0 and 12.0 ms.

In [1], D.L. Young wrote that the method of characteristics may be used to find analytic solutions under the no slip condition. But, he did not explain this approximation and the method of solution. For such a shock tube problem usually the method of characteristics refuses to work without the introduction of additional information, e.g., the propagation rate of the shock wave. Then this shock wave can be tracked and the state before and behind the shock wave can be calculated by the characteristic theory. In the following we try to get insight into the qualitative structure of the solution by considering the shock tube problem of a single fluid approximation.

Because of the relatively low mass fraction of water in the right part of the shock tube, the basic structure of the solution should be at least similar to the solution of a single fluid shock tube problem. We introduce such an approximation unter the assumption that no interaction between water and gas takes place and the multiphase flow is replaced by the flow of a homogeneous mixture. The structure of the solution of such a problem is the following: It consists of four constant states separated by three elementary waves. A shock wave travels to the right from the high into the low pressure region. A contact discontinuity follows the shock wave and moves with the fluid velocity. Here the density jumps, while the velocity and the pressure are constant across this line of discontinuity. Into the left high pressure region moves a rarefaction wave. This structure of the solution is sketched in Figure 3.1.

If we use such a single fluid approximation to get an analytic solution we have to consider the following shock tube problem: Both parts of the shock tube are filled with gas. The water inside the right part of the shock tube yields an increase of the density only; i.e. the gas/water mixture is considered to be a homogeneous perfect gas. We assume that the equation of state is overall that of a perfect gas

(3.1)
$$p = (\gamma - 1)\,\rho\,\varepsilon$$

where ε is the specific internal energy and γ the constant adiabatic exponent (air: 1.4). The right and left values of the primitive variables are given in Table 3.2. In order to match the large density difference, the ideal gas approximation introduces a large difference in temperatures. The temperature of the left chamber of the shock tube is 1045 K, while in the right one it is T = 31.7 K.

The structure of the exact solution of this problem corresponds to that sketched in Figure 3.1. This problem is the usual Riemann problem of gas dynamics and can be solved exactly in terms of the solution of a fixed point problem (see [2]). A fast iterative procedure for this Riemann problem has been proposed by Halter [3]. This iterative procedure has been used in our calculations.

Air	Air
$p_l = 3 \cdot 10^5$ Pa	$p_r = 10^5$ Pa
$\rho_l = 1$ kg/m^3	$\rho_r = 10.99$ kg/m^3
$v_l = 0.0$ m/sec	$v_r = 0.0$ m/sec

Table 3.2: Single fluid shock tube problem

Using this approximation we obtained the values in Table 3.3.

shock speed:	v_s	= 172,2 m/s
velocity behind shock:	v_2	= 80,57 m/s
pressure behind shock:	p_2	= 2,515 $\cdot 10^5$ Pa
gas density behind shock:	ρ_2	= 1,84 kg/m^3
water volume fraction behind shock:	r_2	= 0,0189

Table 3.3: Values of single fluid shock tube approximation with $\gamma = 1.4$

The values agree very well with the those of Young (Table 3.1). The computation times t = 3.0, 6.0, 9.0, and 12.0 ms as proposed by Youngs seem to be too large, if we consider these calculations. The velocity of the left boundary of the rarefaction wave is given by the sound velocity in the undisturbed state p_l, v_l, p_l. This sound velocity is given by

(3.2) $$c_l = \sqrt{\gamma\, p_l/\rho_l}$$

and has the value $c_l \approx 650$ m/sec. Hence after the time t = 1.5 ms the rarefaction fan will reach the left wall. Here, the rarefaction wave is reflected, generating a wave which travels to the right and may disturb after some time the right going waves. Furthermore, after 6 ms the shock wave reaches the right wall and is re-

flected there. According to this simplified analytical solution a comparison between numerical results and this analytical solution should be performed within the time intervall [0.0, 1.5] ms.

We solved the gas dynamic problem numerically with walls at both ends. We used here a so called high resolution scheme (see [4]). The numerical results are shown in Figures 3.2, 3.3, and 3.4. These results at t = 1.5 ms coincide very well with the exact solutions of the Riemann problems. But at times t = 3.0 ms and t = 4.5 ms we see a strong influence on the pressure and velocity by the rarefaction wave reflected at the left wall. The total density of the mixture is only changed slightly. These results clearly show that the rarefaction wave reflected at the left wall influences the right going waves after some time. Hence the times for comparison proposed by Youngs should be reduced.

The solutions of these single fluid gas dynamical shock tube problems, of course, neglect any two phase effects and may give good approximations in special cases only. They can only show the following: If the two-phase solution has a structure as given in Figure 3.1, then the single fluid approximation should give an estimation the right wave velocities. This is due to the fact that the propagation speed, e. g., of the shock wave, is determined by the integral conservation of mass, momentum and energy. If the two-phase mixture is homogeneous and the two-phase effects do not generate another structure of the solutions, then the one-fluid model will be a good approximation. If the two phase effects or effects generated by non-homogeneity of the mixture become relevant, these approximate solutions can only give an estimation of the average velocity but can not show details of the wave structure.

Additionally, we looked at another shock tube problem: the limit case of the two phase shock tube problem when the volume fraction of water tends to zero. The gas dynamic Riemann problem, considered here, is sketched in table 2.3. The values of density and pressure coincide with the values of the two phase shock tube problem when the volume fraction of water tends to zero. The solution of this Riemann problem is sketched in figure 3.1. A shock wave travels to the right, followed by a contact surface, while a rarefaction wave moves into the high pressure region. The value of physical quantities obtained from the solution of this Riemann problem are given in table 3.4. The solution at time t = 1.5 msec is given in Figure 3.5.

Air	Air
$p = 3 \cdot 10^5$ Pa	$p = 10^5$ Pa
$\rho = 1$ Kg /m^3	$\rho = 1$ Kg /m^3
v = 0.0 m/sec	v = 0.0 m/sec

Table 3.4:   Gas dynamic shock tube problem

shock speed:	$v_s =$	453.9 m/s
velocity behind shock:	$v_2 =$	201.44 m/s
pressure behind shock:	$p_2 =$	$1.91 \cdot 10^5$ Pa
density behind shock:	$\sigma_2 =$	1.798 kg/m^3

Table 3.5: Results of the gas dynamic shock tube approximation.

4.   Understanding of Phenomena

The solution of the Rieman problems for homogeneous gas is well understood. But, the main question is, how accurate is that approximate model for the situation with real interphase exchange. The results in Chapter 6 show that the analytical solutions are rather poor for comparisons.

5.   SIMMER-III Representation

5.1   Geometry, Initial and Boundary Conditions for a Reference Case

A 1-D mesh into the z-direction was used with a uniform grid of 100 zones in the space interval [0.0, 2.0]. The boundary conditions of a perfect were specified.

5.2   Code Version and Computer Used

Calculations are based on SIMMER-III Version 1.G. The computer used was the Fujitsu VP400EX.

5.3 Code Modification

no

6. Results

We started our comparison of the numerical results of SIMMER-III in the case of the pure gas dynamic shock tube problem. The space interval [0.0, 2.0] is discretized using 100 grid zones. In the two-dimensional SIMMER-III-Code we set IBM = 1 and JBM = 100. The constant of gravity is set to zero. In the exact solution, the maximum of the wave speed is at about 810 m/s. According to the CFL-condition an appropriate time step for an explicit numerical scheme is then given by

$$(6.1) \qquad \Delta t = 0.3 \, \Delta x / 810 = 0.741 \cdot 10^{-5} \, .$$

The SIMMER-III-Code is a semi-implicit numerical scheme and hence the time step may be chosen larger than that given by (6.1). But the CFL-condition is a quite natural condition, if shock waves will be captured with a good resolution. It states that within one time step a wave can cross one-grid zone only and the numerical smearing introduced within on time step is limited by this spatial resolution. If the time step is increased, more dissipation will be introduced. Hence, to test the capability of the SIMMER-III-Code to resolve shock waves, the time step should be restricted by the CFL-condition. This is done in our calculation by setting DTMIN = DTMAX = $0.741 \cdot 10^{-5}$.

Figure 6.1 and 6.2 show the results of SIMMER III for void fraction, pressure, velocity, and temperature at time 1.5 ms. The small circles indicate the values of the numerical solution, while the solid line gives the exact solution. The results given by the first picture are produced using the usual time step calculation based on the velocity CFL-condition, but starting with the small value $\Delta t = 0.741 \cdot 10^{-5}$ to give the calculation the chance of a good initial resolution for the break-up of the discontinuity into the different waves. The results in figure 6.1 indicate a good approximation of the shock wave with some small wiggles behind it. The shock wave is captured within six grid zones. A relatively strong dissipation is observed at the left going rarefaction wave. This numerical smearing is strong and not expected for a second order accurate scheme. The small contact discontinuity is cap-

tured well within five grid zones as clearly visible at the temperature distribution. Only the small hump at the velocity distribution disturbs this impression.

If the time step is decreased to get a better resolution of the shock wave a lot of spurious oscillations are generated. This fact is clearly indicated in Figure 6.2. The time step within the whole calculation has been fixed to $0.741 \cdot 10^{-5}$. Strong wiggles in the velocity and pressure distribution are shown in figure 6.2 behind the shock wave, which have been moved to the left up to the rarefaction wave.

The results for the two phase shock tube problem where the initial values are as given in table 1.1 are shown in the Figures 6.3 and 6.4. The first Figure shows those of the usual time step calculation, starting with the small time step $0.741 \cdot 10^{-5}$. The Figure 6.4 shows results with the time step being fixed at this small value within the whole calculation. The differences between these pictures are relatively small. Inreasing the time step does not influence the results very much. One difference appears in the pressure plot. With small time steps, a steeper rise of the pressure in front of the compression wave becomes visible which may be interpreted as a shock wave running ahead. The Figures indicate a large difference between the numerical solutions and the single-fluid approximations. There are of course two possibilities: the numerical results are bad or the single fluid approximations fail in this case.

We believe in the latter of these possibilities, which is motivated be the following considerations. Especially, figure 6.4 indicates that the fastest wave to the right is a shock wave propagating into the low pressure region. If we compare the velocity of this wave with the gas dynamic shock tube problem where the water volume fraction is set to zero (table 3.5), we find that it is similar to that of the shock wave occuring in this problem. That means, within the two-phase shock tube problem the wave structure becomes more complicated: the single shock wave decouples into a pre-shock which moves with nearly the same velocity as in the pure gas. It becomes visible in figure 6.4 and is smeared out in the large time step calculation given in Figure 6.3. Behind this pre-shock two-phase effects become important and smooth out the profile. The gas velocity of the two phase shock tube calculations are much higher than within the single fluid approximation and lie between this and the pure gas case. For comparison we plot in Figure 6.5 the numerical results of SIMMER III together with these two approximations.

The results given in the paper of Youngs (in [1]) are performed for different constants of a quadratic interphase friction law. For the values of this constant corresponding to low and intermediate interphase friction his results are much more similar to the single fluid approximation. This may be due to the fact, thatin these cases the interphase-friction law is not realistic. Unfortunately he does not show results for a value giving large velocity separation. Figure 6.6 shows the numerical results of SIMMER-III for the fluid and the gas velocity, which indicates that the velocity separation is large. This means, that the one-fluid approximation should not be a good candidate for comparison in this case. We remark that Kondo et al. [5] performed calculation with the interphase friction law of Youngs and obtained a good agreement with the results of codes, presented in [1].

To get more clarity we applied another multifluid code to the two phase shock tube problem. At Kernforschungszentrum Karlsruhe (KfK), the IVA-KA code is being developed (in a first step) for describing premixing of corium melt relocating downwards into a water pool. It is a finite difference code and based on the code IVA3 that has originally been developed by Kolev [6]. In its present state, IVA-KA describes the individual but coupled motions of three fluids, i.e. a gas phase, liquid water, and some other material, i.e. corium. The coupling between the fluids is due to assuming the same pressure in all three fields locally and due to exchange of momentum, energy, and mass. Thermal equilibrium between water and vapor is not assumed but is always being approached due to heat and mass transfer. The corium can be liquid initially and freeze during the process (as particles) or it can consist of solid particles from the beginning.

Besides the usual conservation equations of mass, momentum, and energy (or entropy in the case of IVA-KA), IVA-KA solves additional conservation equations for the concentrations of "inert" components in all three fluids (e.g. noncondensable gas in the gas phase) and the particle number densities from which the sizes of discontinuous structures (bubbles, drops, and particles) can be determined in connection with the corresponding volume fractions. Therefore such sizes depend on the history of the process. They are very important in calculating the exchange terms. The proper types of exchange terms are chosen on the basis of flow regimes assigned to each mesh cell and of the temperature conditions.

IVA-KA describes transient two or threedimensional flow in cylindrical or in Cartesian coordinates. Complicated geometries can be simulated by a "porous body" approach, i.e. by excluding arbitrary volume fractions in any mesh cell from access

by the fluid mixture and by assigning limited (possibly zero) permeabilities to cell boundaries. When IVA-KA is started with the same discretization parameters, it produces quite similar results as the SIMMER III Code. IVA-KA uses first order donor-cell differencing but the numerical dissipation is not much stronger. The wave into the mixture is slower, but the overall structure of the numerical solutions is the same.The results are plotted in Fig. 6.6 and Fig. 6.7 in comparison with the single fluid approximations and the SIMMER III results, respectively.

7.   Conclusions

The numerical results of SIMMER III for the pure gas dynamical shock tube problems are good except for spurious oscillations occuring at small time steps. The results for SIMMER III for the two-phase shock tube problem agree very well with those of the multifluid code IVA-KA, but disagree with results of Young [1], which is thought to be due to the use of different friction laws.The numerical results and our considerations indicate that there is no reliable exact, numerical or experimental solution for the two-phase shock tube problem of Youngs [1] under realistic conditions. Hence, we will look in the future for experimental results of two-phase shock tubes problems. For experiments the Youngs problem seems not to be a very favourable shock tube problem, because it is very difficult to get such a high volume fraction of water in experiments. To obtain the exact solution of the Riemann problem for a two-phase shock tube seems to be very complicated, which is due to the non-conservative form of the equations and the source terms. Numerical results with a one-dimensional high resolution scheme for the multiphase flow equations including realistic interphase exchange terms would be very valuable, because they would allow to analyze the influences of the different terms and their numerical modelling.

8. References

[1] G.F. Hewitt, J.M. Delhaye and N. Zuber: Multiphase Science and Technology, Volume 6, Hemisphere Publishing Corporation, New York 1992

[2] T. Chang and L. Hsiao: The Riemann problem and Interaction of Waves in Gas Dynamics, Pitman monographs, United Kingdom 1989

[3] E. Halter: A fast solver for Riemann problems, Math. Meth. in the Appl. Science 7 (1983), 101 - 107

[4] C.D. Munz and S. Hirmer: HYDSOL Version 2.0: Ein Programm zur numerischen Lösung zweidimensionaler kompressibler Strömungen, internal report, KfK 1992

[5] Sa. Kondo, Y. Tobita, K. Morita und N. Shirakawa: SIMMER III: An advanced computer program for LMFBR severe accident analysis, Int. Conf. on Design and Safety of Advanced Nuclear Power Plants, Tokyo 1992

[6] N.I. Kolev: IVA3: A transient 3d, three phase three-component flow analyzer, Proc. Int. Mtg. on Safety of Thermal Reactors, Portland, OR, 1991, 171 - 180
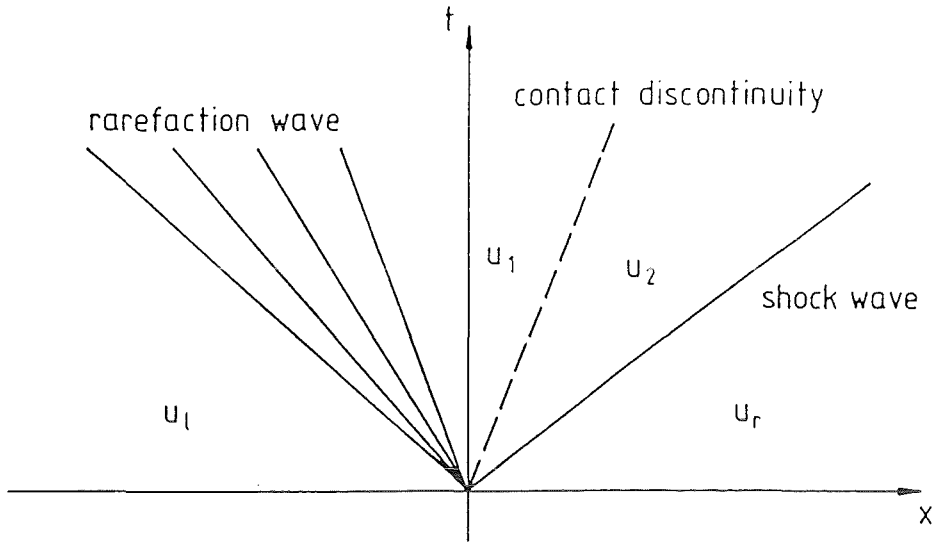
<u>Figure 3.1:</u>   Single fluid shock tube solution in the (x, t)-plane
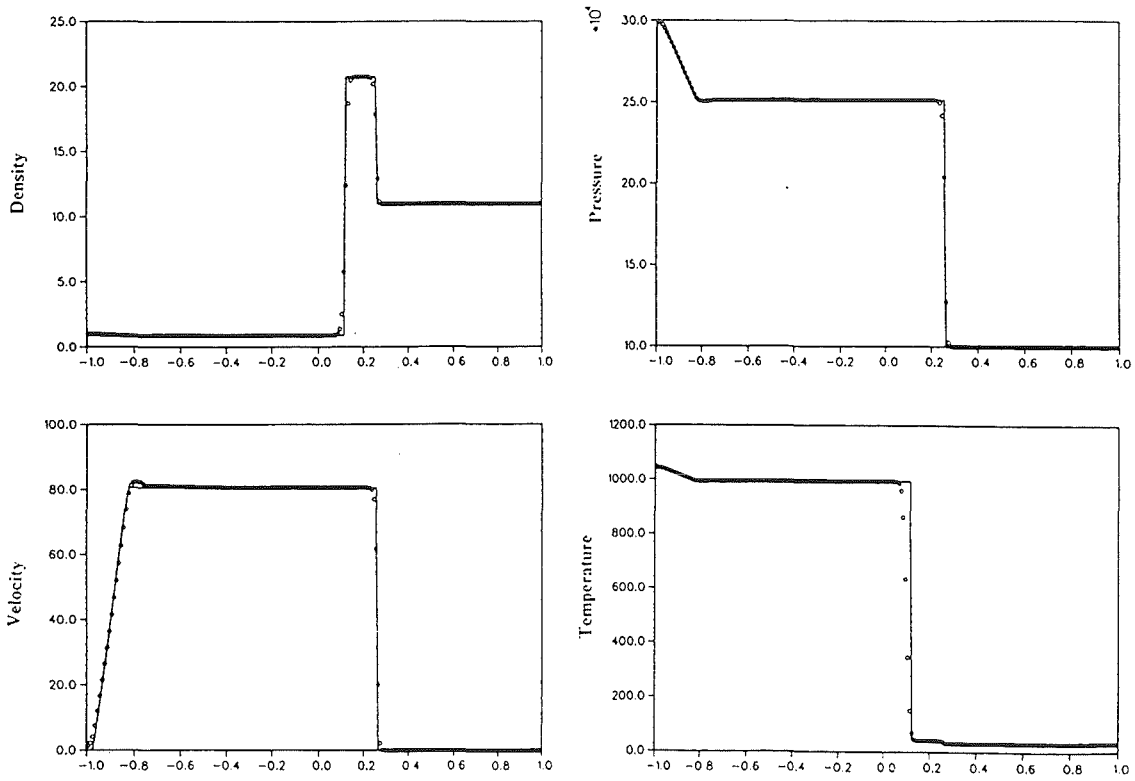
<u>Figure 3.2:</u>   Numerical solution with constant γ at t = 1.5 ms
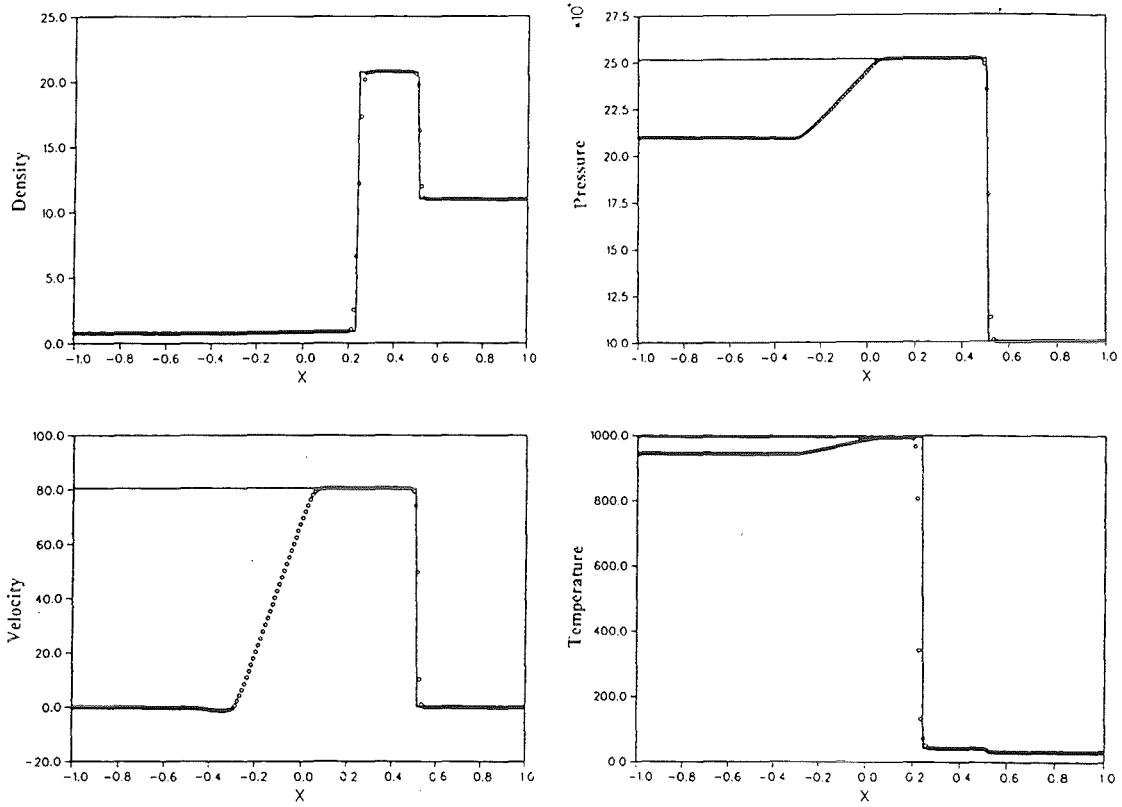
Figure 3.3: Numerical solution with constant γ at t = 3.0 ms
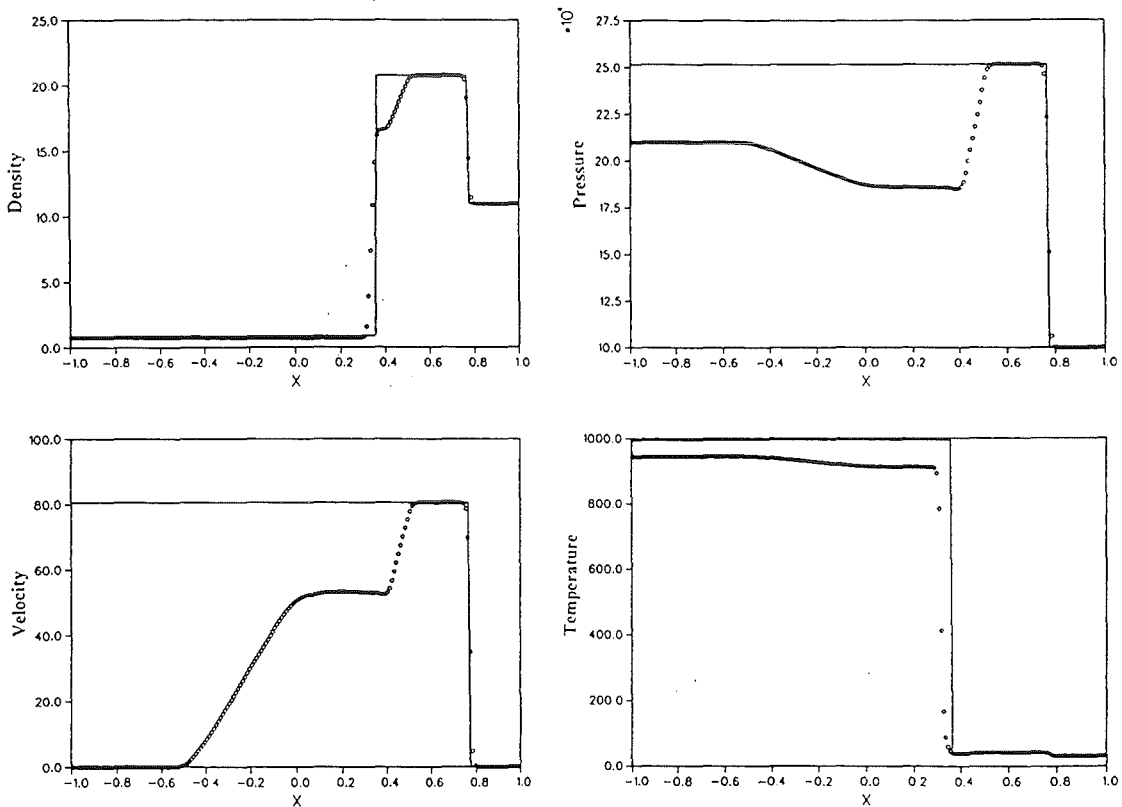
Figure 3.4: Numerical solution with constant γ at t = 4.5 ms
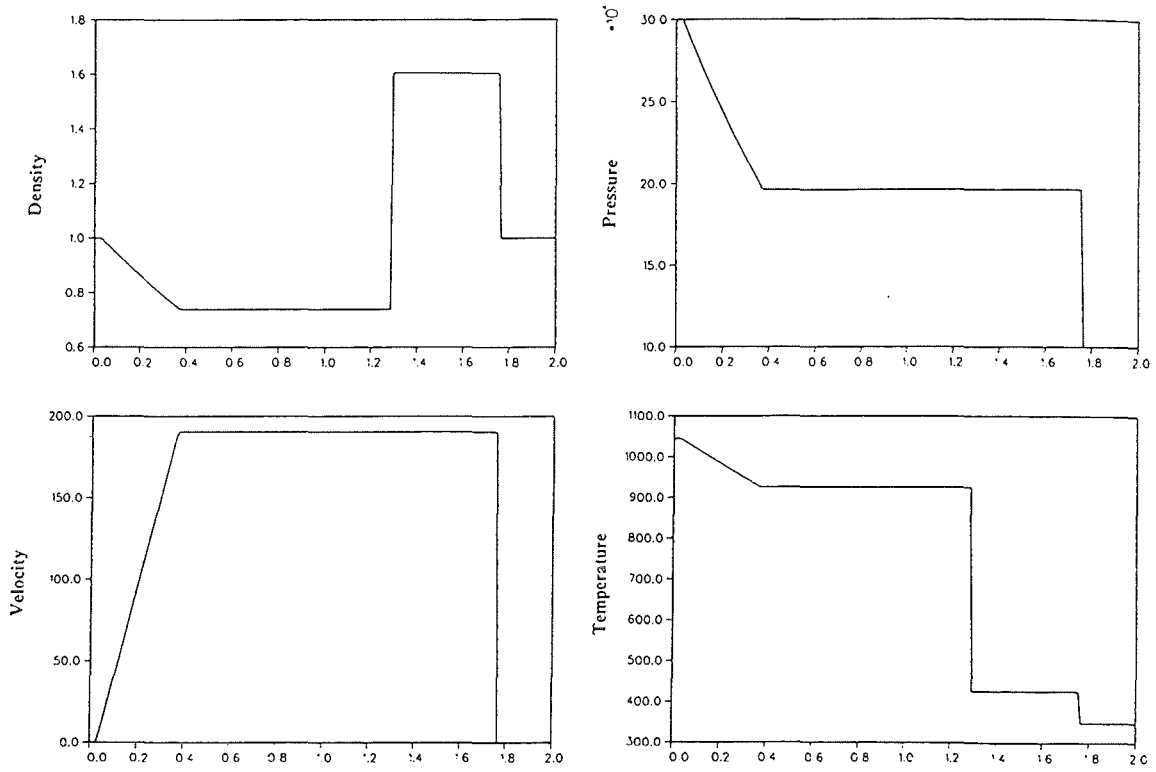
Figure 3.5: Exact solution of the gas dynamic shock tube problem at t = 1.5 ms
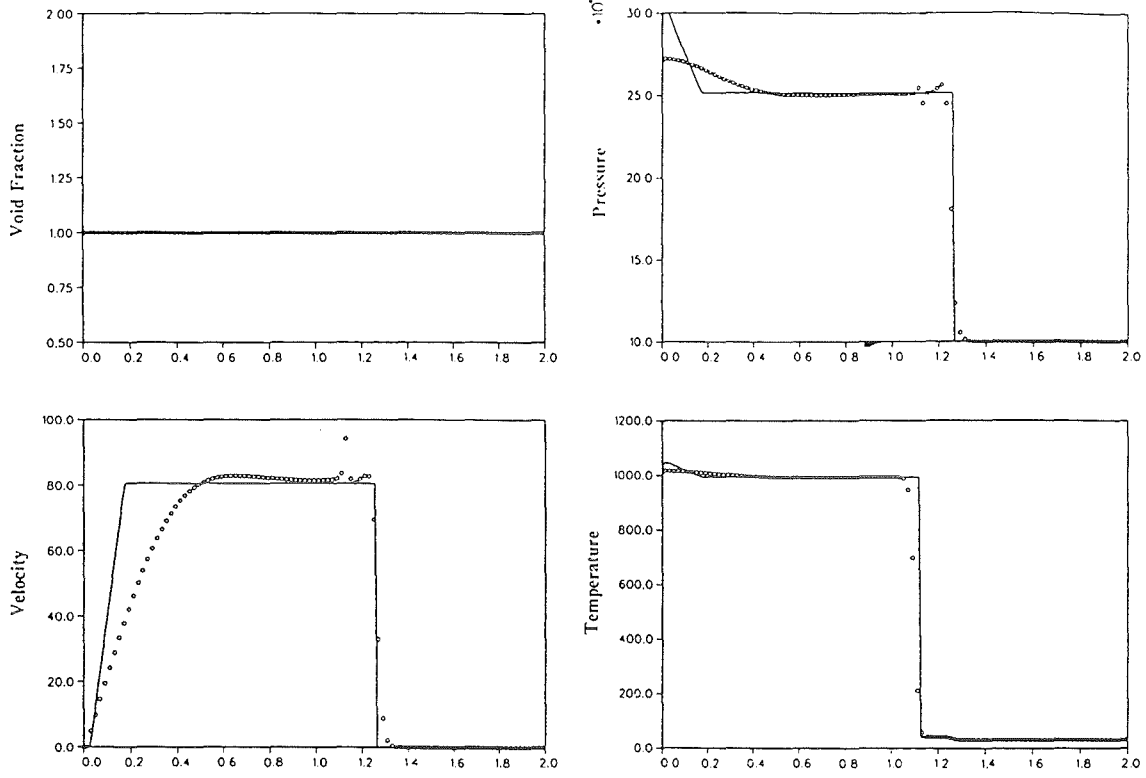
Figure 6.1:   SIMMER III results for single fluid approximation
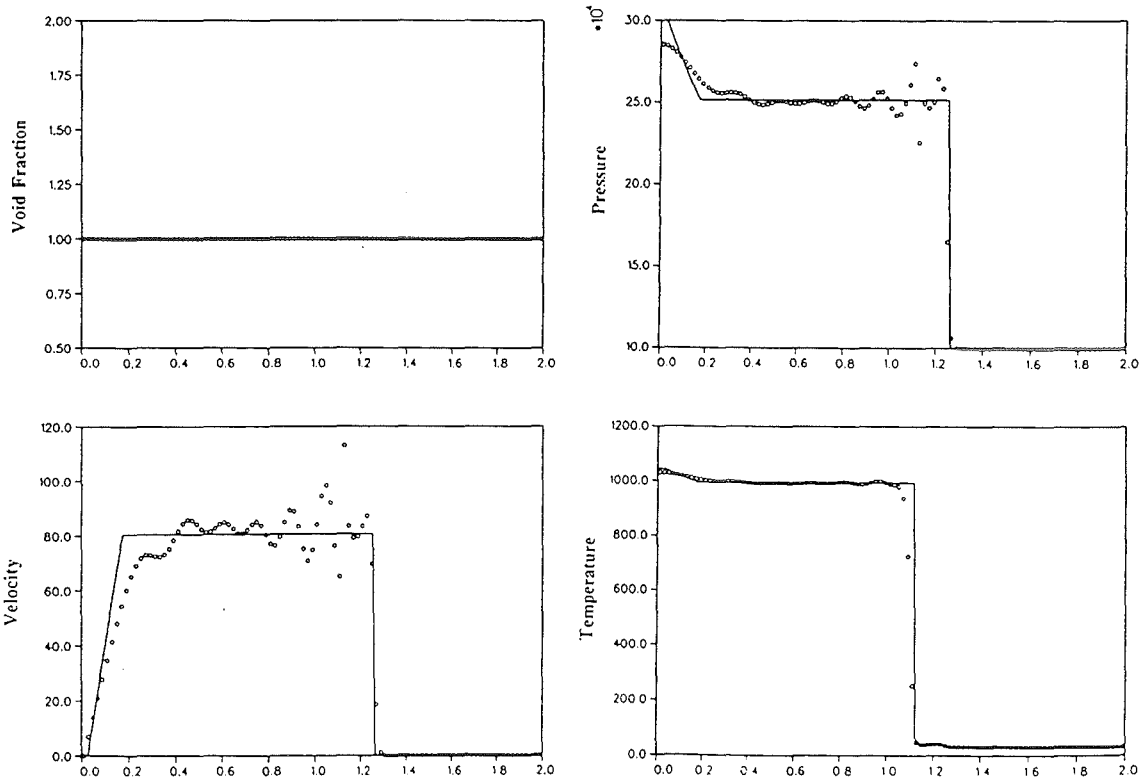
Figure 6.2:   SIMMER III results for single fluid approximation; small time steps
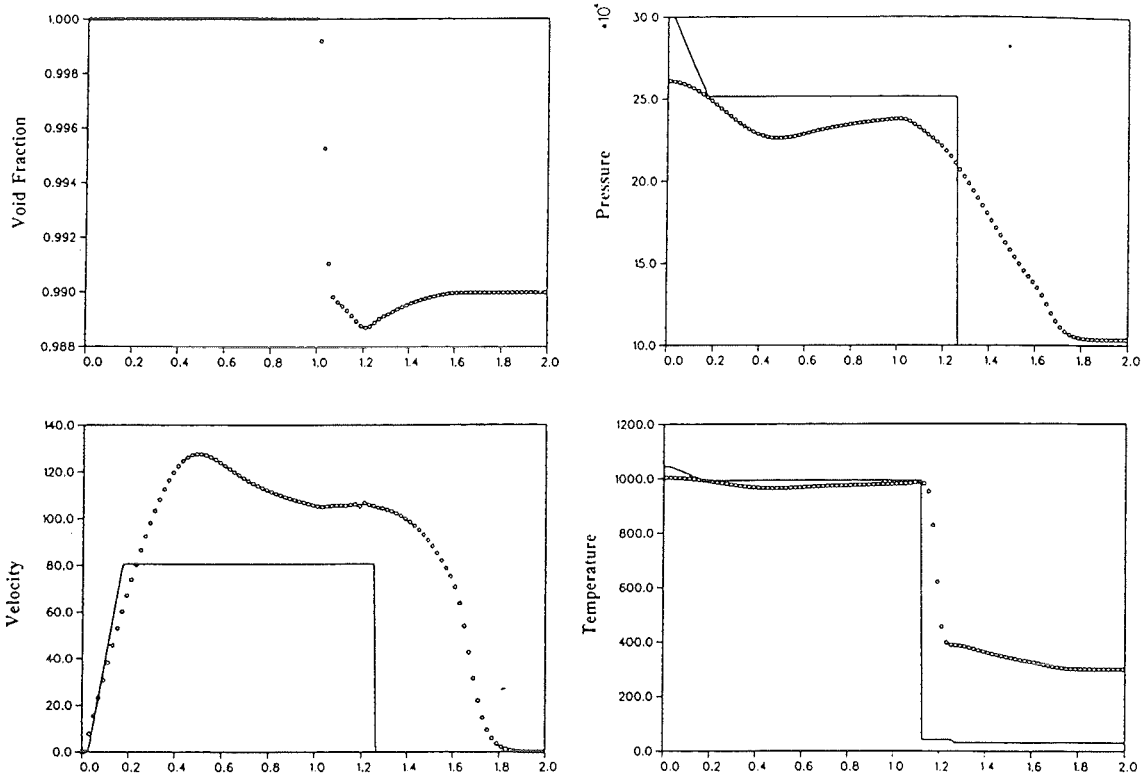
Figure 6.3: SIMMER III results for two phase shock tube problem in comparison with single fluid approximation at time 1.5 ms.
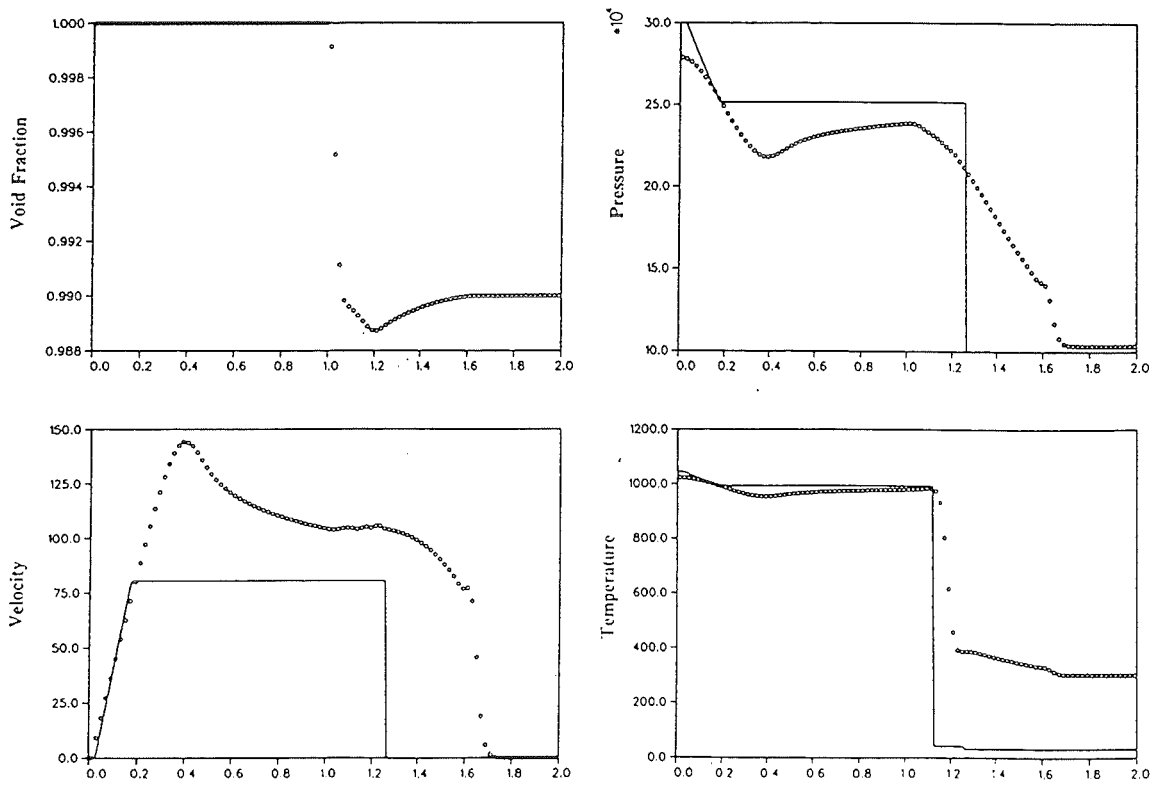
Figure 6.4: SIMMER III results for twp phase shock tube problem in comparison with single fluid approximation at time 1.5 ms, small time steps
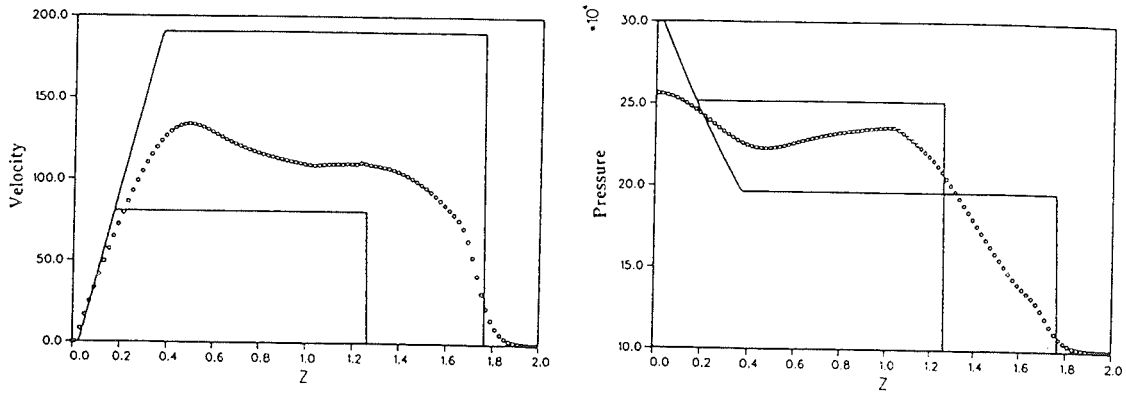
Figure 6.5:   Comparison of SIMMER III-Results (ooo) with single-fluid approxima-
tion (———) and pure gas solution (———) at time t = 1.5 ms
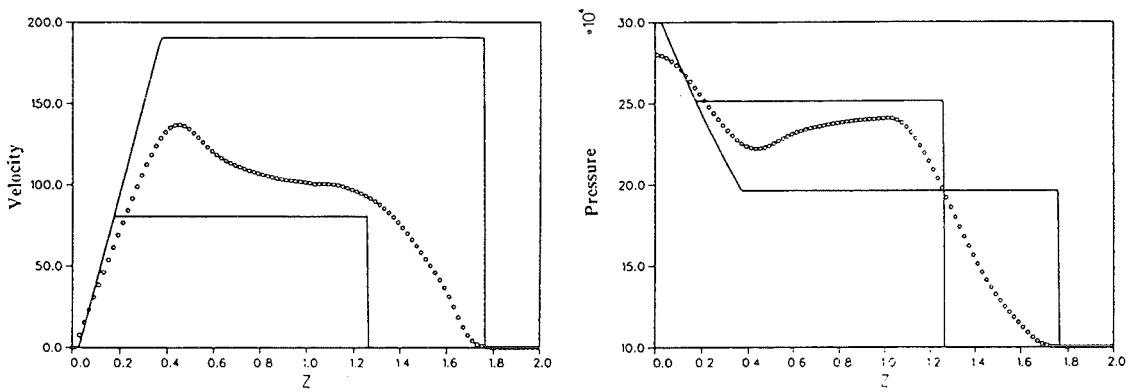
Figure 6.6:   IVA-KA results for the two phase shock tube problem in comparison
with single fluid approximations at time 1.5 ms.
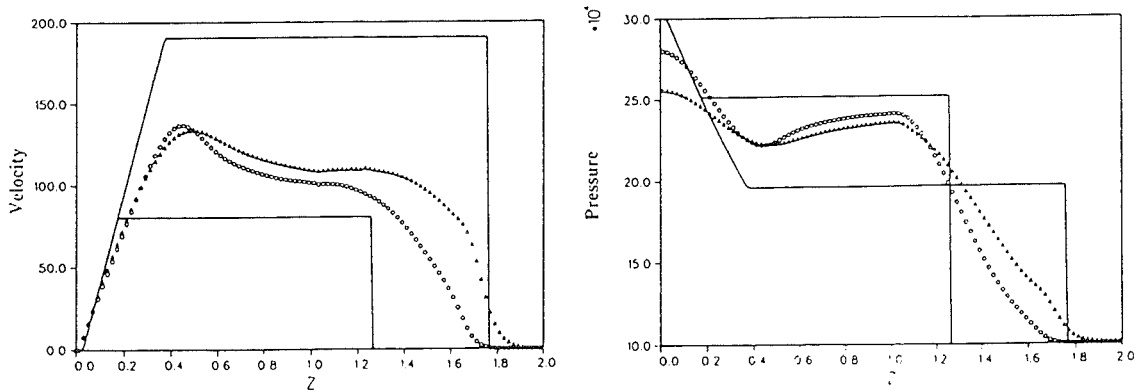
Figure 6.7:   Comparison of IVA-KA (■ ■ ■) and SIMMER III (ΔΔΔ) results.

Summary Report on an Application for the SIMMER-III Code Assessment, Phase 1

Rapid Fuel Vaporization

by

W. Maschek, S. Kleinheins, C.D. Munz, E. Hesselschwerdt

Forschungszentrum Karlsruhe
Postfach 3640, 76021 Karlsruhe, Germany

April 1994

Outline of Case

During superprompt critical nuclear excursions the fuel is rapidly heated above its boiling point and vaporizes. The vapor pressure build-up leads to a material disassembly and to nuclear shutdown. If a significant superheating of the fuel could take place this shutdown could be delayed and the energy yield would be increased. Another mechanism which can lead to rapid material disassembly is the build-up of single phase pressures when the heated material expands and the void regions are eliminated.

The SIMMER-III Code is tested if it is capable to describe such rapid heating processes with material expansion and pressure build-up. Both theoretical considerations and experimental results from rapid vaporization tests (EEOS-12) serve as a basis for comparison.

Key Words

Rapid vaporization, superheat,

1. Objectives of the Application

During superprompt critical nuclear excursions (e. g. caused by a recritica-lity) the fuel of an assembly is rapidly heated above its boiling point and vaporizes. The heating rates during such an excursion go up to a few 10^5 K/s. The vapor pressure build-up leads to an acceleration of the material and the material disassembly results into a rapid nuclear shutdown. If a significant transient superheating of the fuel could take place, the pressure build-up and the nuclear shutdown could be delayed and the energy yield of the excursion would increase. Another important mechanism which can lead to rapid material disassembly and nuclear shutdown during a nuclear excursion is the build-up of single phase pressures. Under the rapid heating the fuel expands and any void region in the material-configuration is eliminated. The SIMMER-III Code /1/ is tested if it is able to describe such rapid heating processes with pressure build-up. Both theoretical considerations /2/ and experimental results from rapid vaporization tests (equation of state experiment: EEOS-12) /3, 4/ serve as a basis for comparison.

2.   Description of Experiments

In the case of a significant transient superheat the fuel vapor pressure build-up would be delayed leading also to a delay in the material disassembly process. This problem was addressed in a paper by Fischer and Maschek /2/. In this investigation a bubble dynamics model was used to estimate the fuel superheat during an excursion for a heating rate of 400 K/ms. The results lead to the conclusion that superheat in the order of 20 K is to be expected, which is negligible in an excursion analysis. In-pile experiments by Reil and Breitung /3, 4/ showed no indication of any significant superheat and thus confirm in a broad sense the results of /2/. A somewhat different situation arises when fission gas release builds up a significant pressure before the fuel vaporizes. This case occurs with irradiated fuel, and was studied in the "effective equation of state" (EEOS) series of in-pile experiments by Breitung and Wright /5/. The fission gas pressure is typically 2 to 3 MPa when the fuel reaches the liquidus point. A model for the interpretation of the EEOS experiments with irradiated fuel was developed by Fischer /6/; it is in part based on the bubble dynamics model of /2/. The results of both theory and experiment are that in the initial part of the transient, the pressure is essentially determined by the fission gases. However, when the fuel reaches the boiling temperature determined by the inert gas pressure, rapid vaporization occurs, and the pressure then follows the fuel vapor pressure curve. It is, however, not the sum of inert gas and fuel vapor pressure.

3.   Analytical Solution

-----

4.   Understanding of Phenomena

Based on the experiments /5/ and the analytical investigations /2/ the phenomena are understood.

5.   SIMMER-III Representation

Two types of SIMMER calculations were performed. In a first series of calculations vaporization into the vacuum was simulated. In a second series the evaporation into a gas atmosphere of 20 and 35 bar was simulated. In SIMMER-III the thermal expansion of fuel is treated. Thus any void space in a material probe with fixed boundaries is eliminated when the temperature increases and single phase pressures are built up. In the case of evaporating into a gas atmosphere the gas is additionally compressed during the heat-up process.

5.1   Geometry, Initial and Boundary Conditions

For the calculations a two cell geometry with rigid boundaries has been chosen with the initial liquid fuel temperature of 3100K. The power of $8 \cdot 10^8$W is deposited in a step like fashion during a time window of $\sim$ 22 ms, a heating rate of 400 K/ms and 650 K/ms is reached in the fuel sample depending on the mass of the sample.

5.2   Code Version and Computer Used

The calculations are based on SIMMER-III Version 1B. The computations were performed on a mainframe IBM 3670.

5.3   Code Modification

No code modifications have been performed.

5.4 Parametric Cases

------

6. Results

6.1 Evaporation into Vacuum

By the calculations of evaporation into the vacuum the vapor equation of state should be checked and especially the resulting superheat during evaporation should be calculated.

In SIMMER-III the predicted superheat depends on the available void fraction as the available space determines the amount of fuel vapor needed to build up a certain pressure. With a higher initial void fraction the superheat should therefore increase. In the calculations the initial void fraction is transiently reduced during the heat-up by fuel expansion.

For the current calculations two different fuel samples of the same size but with different void fractions of ~ 30% and 55% were assumed. The power input resulted in heating rates of ~ 420 K/ms and 650 K/ms, respectively.

The results of the evaporation calculations are displayed in Fig. 6.1 (pressure), Fig. 6.2 (fuel temperature), Fig. 6.3 (single phase pressure build-up) and Fig. 6.4 (super-heat).

The calculations were performed with the default values of the interfacial area model, especially to mention the input quantities:

	NMAX	=	10^{11}	(Maximum nucleation site density)
	TAUNUC	=	10^{-4}	(Nucleation time constant)
and	CTHETA	=	10^{5}	(Coefficient in the exponent of nucleation site density equation)

Those quantities could have a direct influence on the vaporization process.

In the Figs. 6.1 and 6.2 the pressure and temperature traces during the fuel heat-up are given for both void fraction cases. With the lower void fraction the thermal expansion of the fuel leads to a rapid pressure increase by the build-up of single phase pressures after $\sim$ 11 msec (Fig. 6.3). For the higher void fraction no single phase conditions are reached under the given conditions. The superheat developed during the excursion is displayed in Fig. 6.4 for the higher void case and shows that a superheat of approximately 30 K is calculated. The superheat is rather constant over the temperature range. This value is in quite good agreement with the predictions given by /2/ where for a 400 K/s temperature ramp a superheat of 20 K is given. When calculating the saturation temperature $T_{sat} = T_{sat} (P_{sat})$ and when comparing with the relation $P_{sat} = P_{sat} (T_{sat})$ it was noted that the fit of the T_{sat} curve shows some deviations when comparing with the P_{sat} curve of up to 2%. This translates into a temperature deviation of 10 - 15 K. The above results concerning the superheat must be seen under this uncertainty range.

To check the sensitivity of the evaporation model with relation to the parameters NMAX, TAUNUC and CTHETA the parameters were chosen as NMAX $= 10^{12}$, TAUNUC $= 10^{-6}$ and CTHETA $= 5000$. The calculations revealed that only a negligible influence is exerted by these parameters in the tested range. In an additional calculation the maximum bubble size was reduced from 10^{-3} to 10^{-6} m thus directly increasing the surface area. As expected in this case the superheat was reduced to approximately 2 K.

In conclusion one can state that the superheat is calculated in good agreement with the theoretical results of Fischer and Maschek /2/ and also with the experimental evidence.

When heating up the fuel the liquid expands as is shown in Fig. 5. The extrapolation of the Drotning /7/ data was suggested in /9/:

$$\rho (T) = 8860 - 0.916 (T - 3120)$$

This relation is formulated in SIMMER-III in terms of the specific volume.

6.2 Evaporation into an Inert Gas Atmosphere

In these calculations the fuel cells were pressurized with an inert gas with $20 \cdot 10^5$ Pa and $35 \cdot 10^5$ Pa at the liquidus point. Again the default values in the IFA (Interfacial area) model were used for the calculations. With respect to the initial conditions and the heating rate, the calculations performed can be compared to the experiment EEOS-12 with irradiated fuel [8, 6]. The measured pressure trace and the analysis from [6] (shaded area) are shown in Fig. 6.6. The important result is that the pressure build-up in the early part of the transient is essentially (but not completely) determined by the fission gas pressure, until the fuel starts boiling. Then, the pressure follows the vapor pressure curve of the fresh fuel.

Thus under the rapid heating conditions of the experiment, the total pressure over irradiated (U, Pu) oxide is controlled by a suppression mechanism. At any given temperature, the fission gas components suppress fuel boiling if their pressure p_{gas} is higher than the fresh fuel saturation vapor pressure p_{sat} of unirradiated fuel. If p_{sat} exceeds p_{gas}, the total pressure is, to a first approximation, equal to p_{sat}. Under the millisecond heating in the experiment, the total pressure from irradiated fuel may be taken as $p_{tot} = \max (p_{gas}, p_{sat})$. In the EEOS-12 experiment the boiling point was reached at approximately 5150 K. The pressure then follows the vapor pressure curve.

The SIMMER-III calculated pressure-temperature dependency is plotted into the experimental pressure trace of Fig. 6.6. As can be seen the exact experimental pressure development is not fully reproduced by SIMMER-III. In the early part of the transient up to the boiling point, SIMMER-III can partly calculate the pressure increase with its thermal expansion model. When boiling is reached at 5150 K the calculated pressure is higher by approx. 40 % compared to the experimental value. The difference in the pressure development between evaporation into vacuum and against a pressurized gas, as calculated by SIMMER-III can be seen in Fig. 6.7. The pressure is higher when fill gas is available because SIMMER-III considers the gas pressure and the fuel vapor pressure as partial pressures and adds them. In Fig. 6.8 and Fig. 6.9 the pressure and temperature traces are given for the evaporation into a pressurized gas atmosphere. The pressure increases slowly at the start of the power transient which is caused by a compression of the inert gas.

That the SIMMER-III results do not fully agree with the experimental results is not surprising, as the SIMMER-III code has not a detailed bubble dynamics model. In SIMMER-III the gas and vapors present in a cell are in the same bubble population, and the pressure is the sum of the partial pressures. In the early part of the transient the gas temperature in the calculations lags considerably behind the liquid fuel temperature (~ 300 K) because the large bubbles in the liquid are at rest. The heat transfer area is small and therefore the thermodynamic pressure increase due to temperature rise is not well predicted. In addition SIMMER-III produces very little vapor below the boiling point. According to the bubble dynamics and mass transfer model in /2/ nearly half of the pressure in the gas bubbles at the boiling point is due to fuel vapor.

Finally the influence of the time step size was investigated. For the calculation with 20 bars of fission gas pressure the timestep was reduced by a factor of 10. As can be seen in Fig 6.10 the influence of time step size is marginal.

Thus, one can conclude that SIMMER-III simulation shows some deviations in the early part of the transient, but they can be explained by the limitations of SIMMER-III modeling. In the later part, SIMMER-III agrees well with the experiment.

7. Conclusions

The SIMMER-III code describes rapid vaporization processes with sufficient accuracy. The superheat which drives the evaporation process is calculated in good agreement with theory and experiment.

8. Recommendations

When recalculating the EEOS12 experiment (evaporation against a fission gas pressure) the early pressure increase up to fuel boiling cannot be recalculated fully satisfactorily. A more detailed bubble dynamics model e. g. discerning between gas and vapor bubbles would be necessary to match the detailed features of the EEOS12 experiment. Such a model is however beyond the scope of the code and might not be of importance when using the code for accident simulations.

9. References

/1/ Sa. Kondo, Y. Tobita, K. Morita, N. Shirakawa
SIMMER-III: An Advanced Computer Program for LMFBR Severe Accident
Analysis;
ANP'92, Vol. IV, 40-5, Oct. 1992, Tokyo

/2/ E. A. Fischer and W. Maschek
The Role of Vapor Bubble Dynamics during Energetic Power Excursions in Fast
Reactor Core Disruptive Accidents;
Nucl. Technol. 71, 173 - 186 (1985)

/3/ W. Breitung, K. O. Reil
Vapor Pressure Measurements on Liquid Uranium Oxide and (U, Pu)-mixed Oxide;
Nucl. Sci. Eng. 101, 26 (1989)

/4/ W. Breitung, K. O. Reil
The Density and Compressibility of Liquid (U, Pu) - mixed oxide;
Nucl. Sci. Eng. 105, 205 (1990)

/5/ W. Breitung, S. A. Wright
Measurements of the Total Pressure from Irradiated (U, Pu) - mixed Oxide;
Nucl. Sci. Eng. 105, 303 (1990)

/6/ E. A. Fischer
A Model for an Effective Equation of State for Irradiated Fast Reactor Fuel;
Nucl. Technol. 98, 100 (1992)

/7/ W. D. Drotning
Thermal Expansion of Molten Uranium Dioxide
Proc. 8th Symp. Thermophysical Properties Gaithersburg, Maryland;
June 15 - 18, 1981; National Bureau of Standards (1981)

/8/   W. Breitung
      Analysis of Measured Total Pressures from Irradiated Solid and Liquid
      (U, Pu) - mixed Oxide;
      Nucl. Sci. Eng. 105, 1 (1991)

/9/   E.A. Fischer
      A New Evaluation of the Urania Equation of State Based on Recent Vapor
      Pressure Measurements;
      Nucl. Sci. Eng. 101,97 (1989)
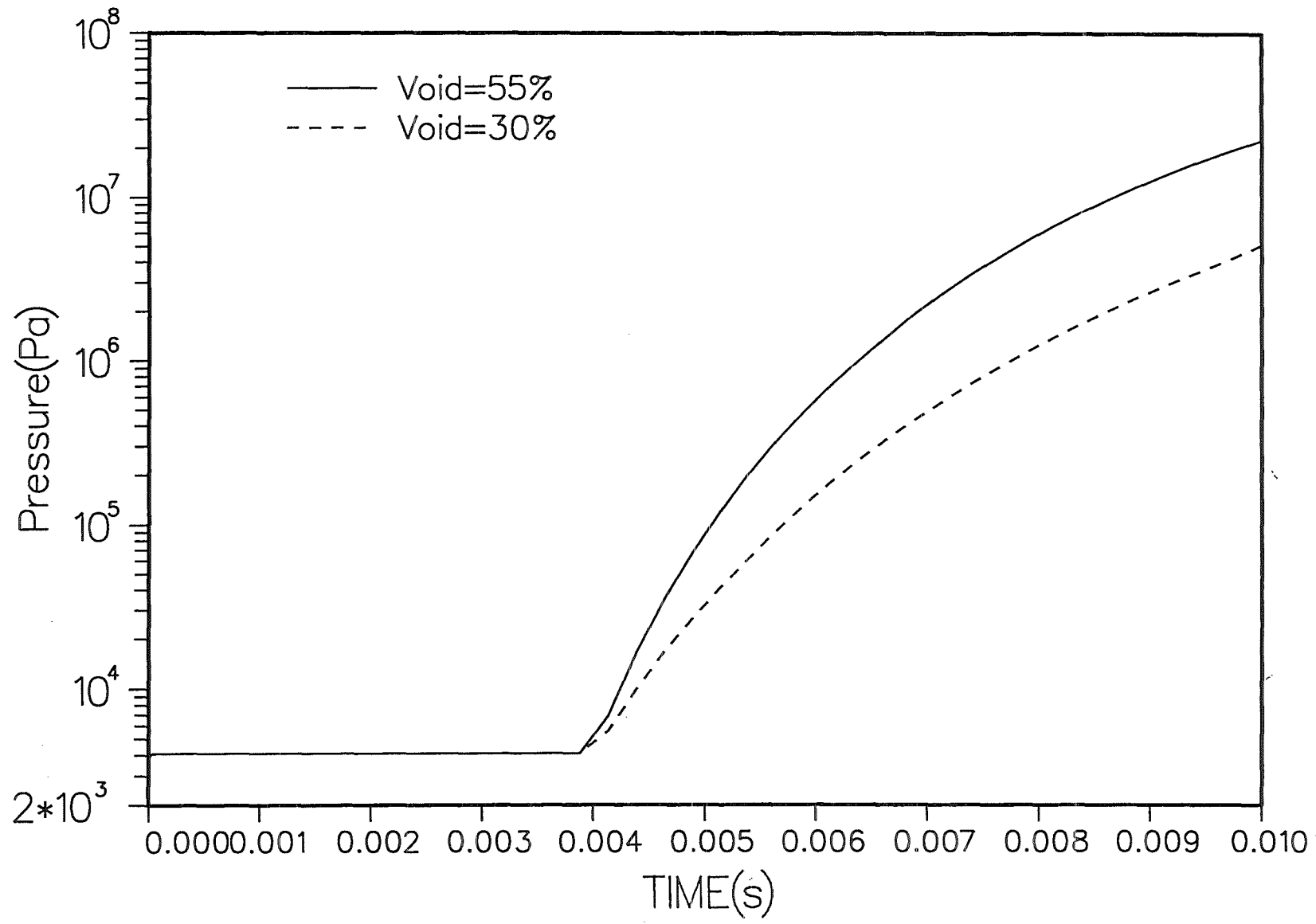
Fig: 6.1   Pressure development of the rapid vaporization test into vacuum for material void fractions of 30 % and 55 %
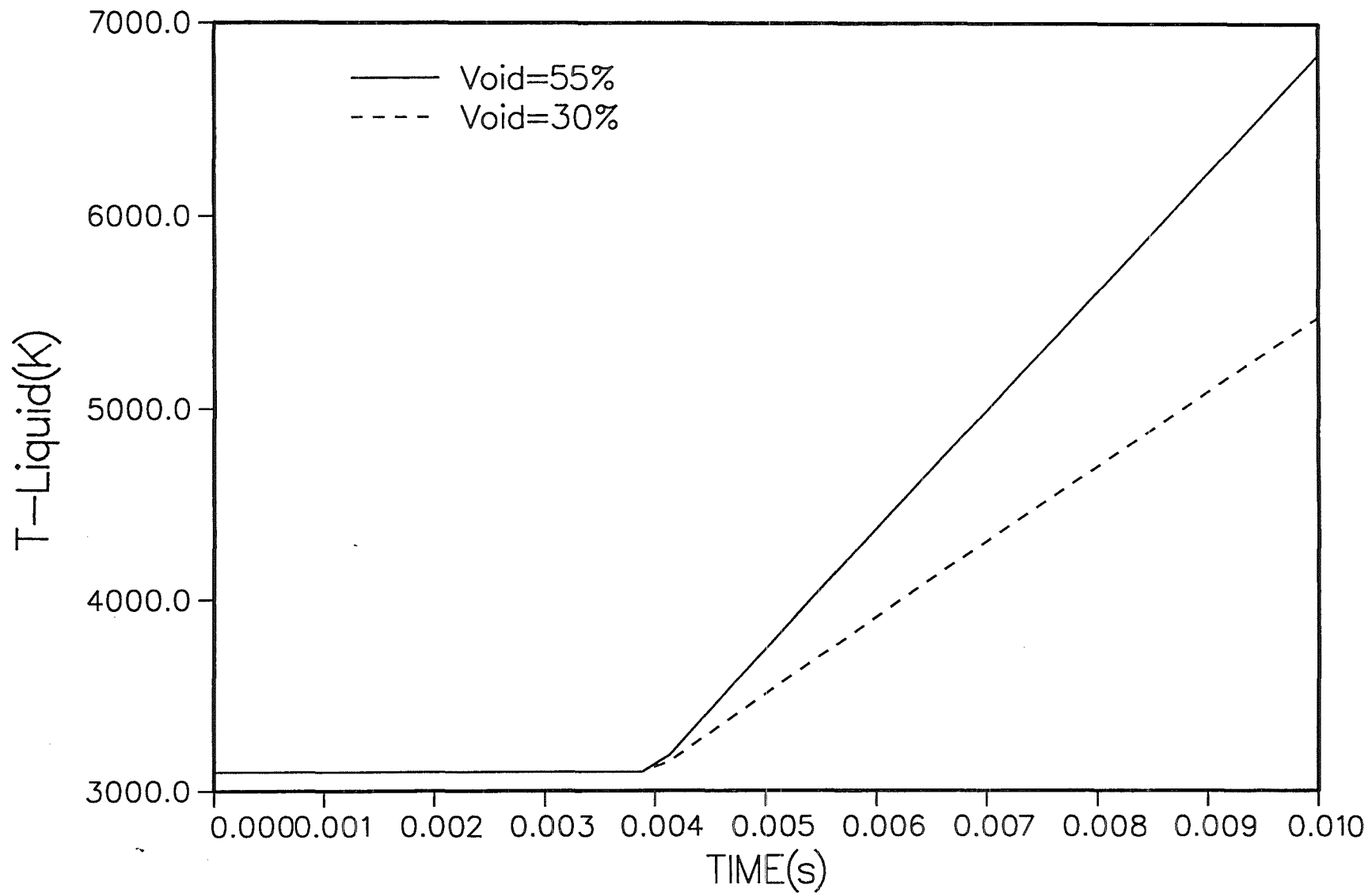
Fig: 6.2   Fuel Temperature development of the rapid vaporization test into vacuum for material void fractions of 30 % and 55 %
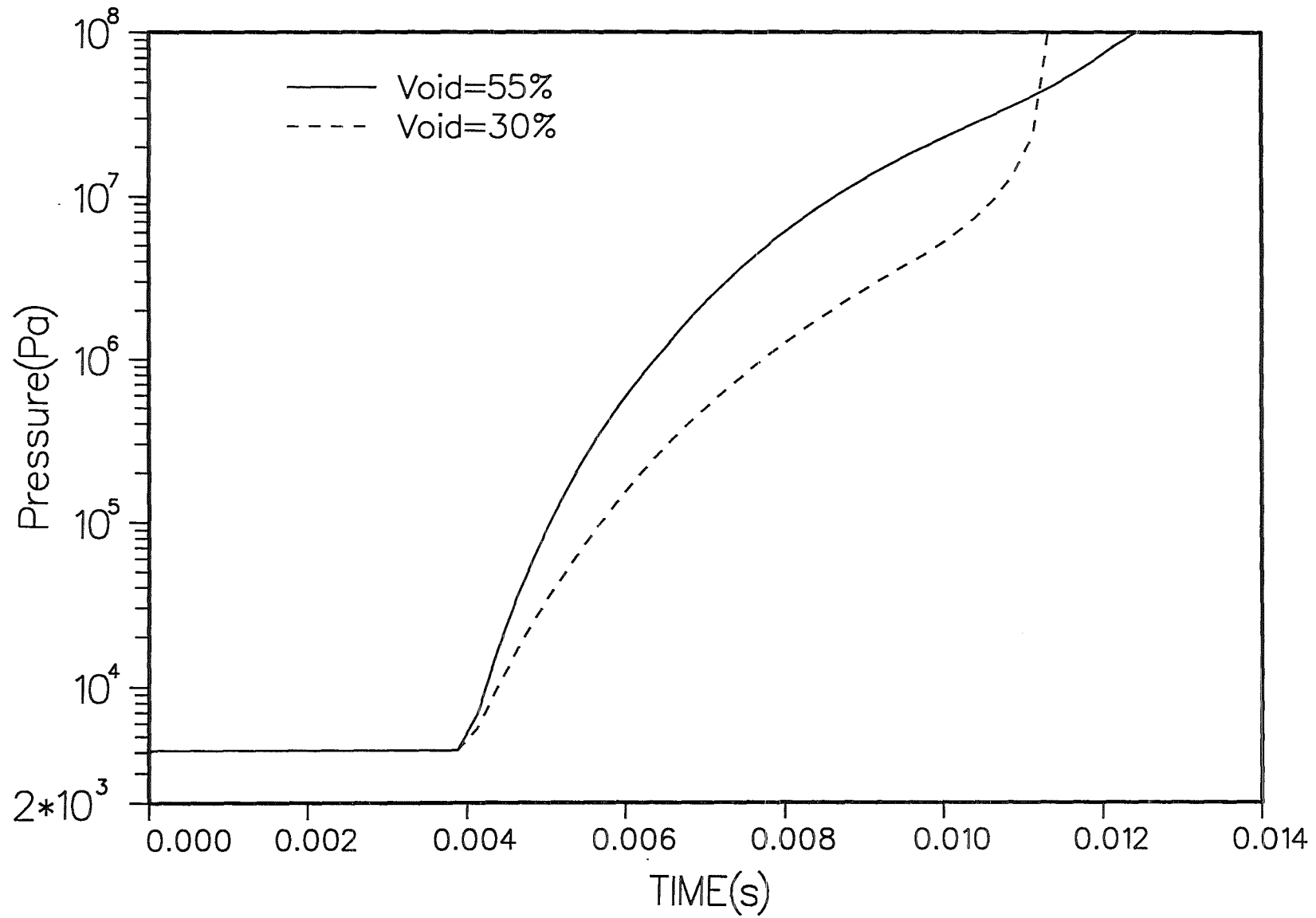
Fig: 6.3   Build-up of single phase pressures in the 30% void fraction case
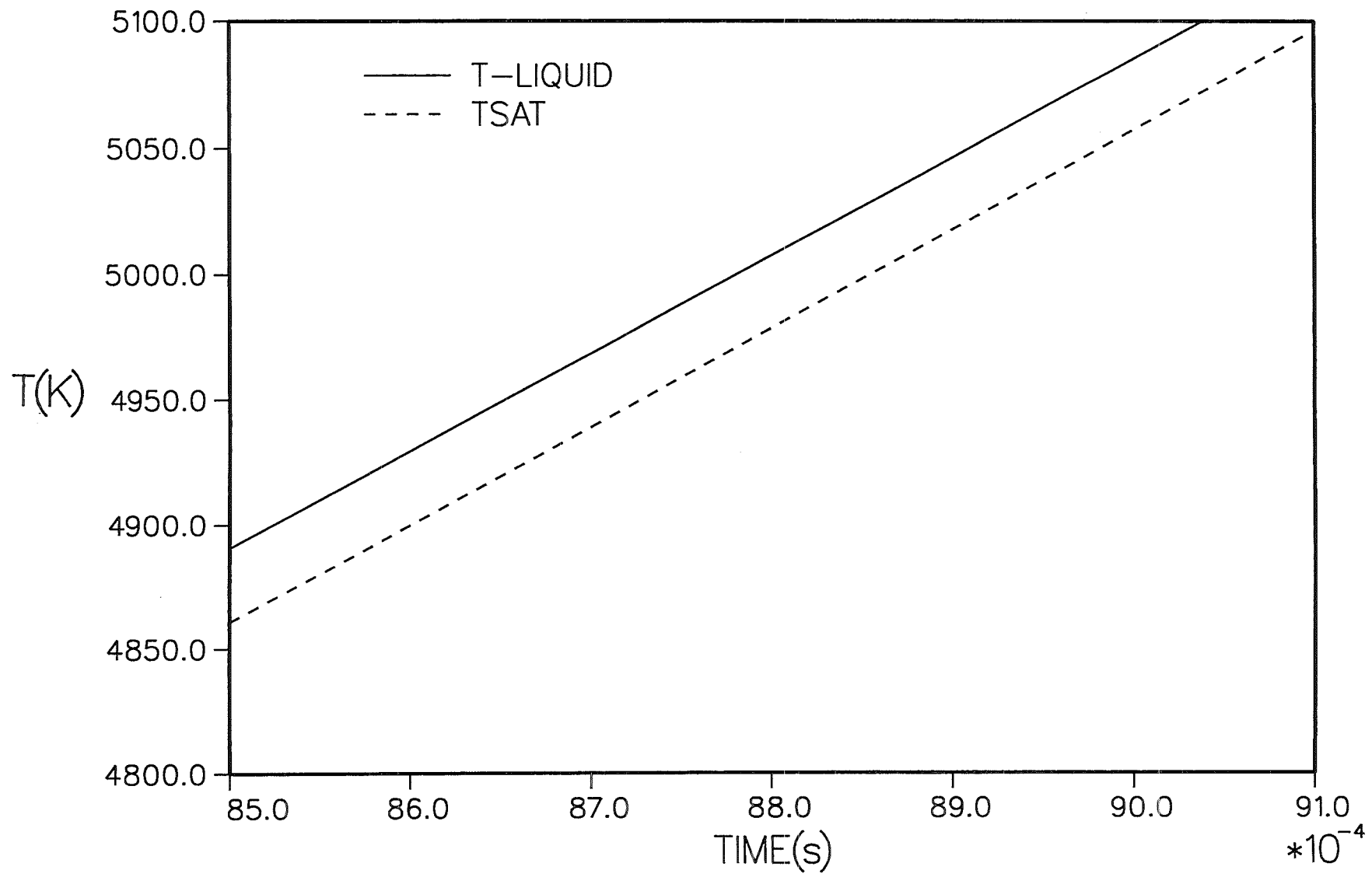
Fig: 6.4   Superheat: Liquid fuel temperature and saturation temperature development of the rapid vaporization test for material void fraction of 55 %
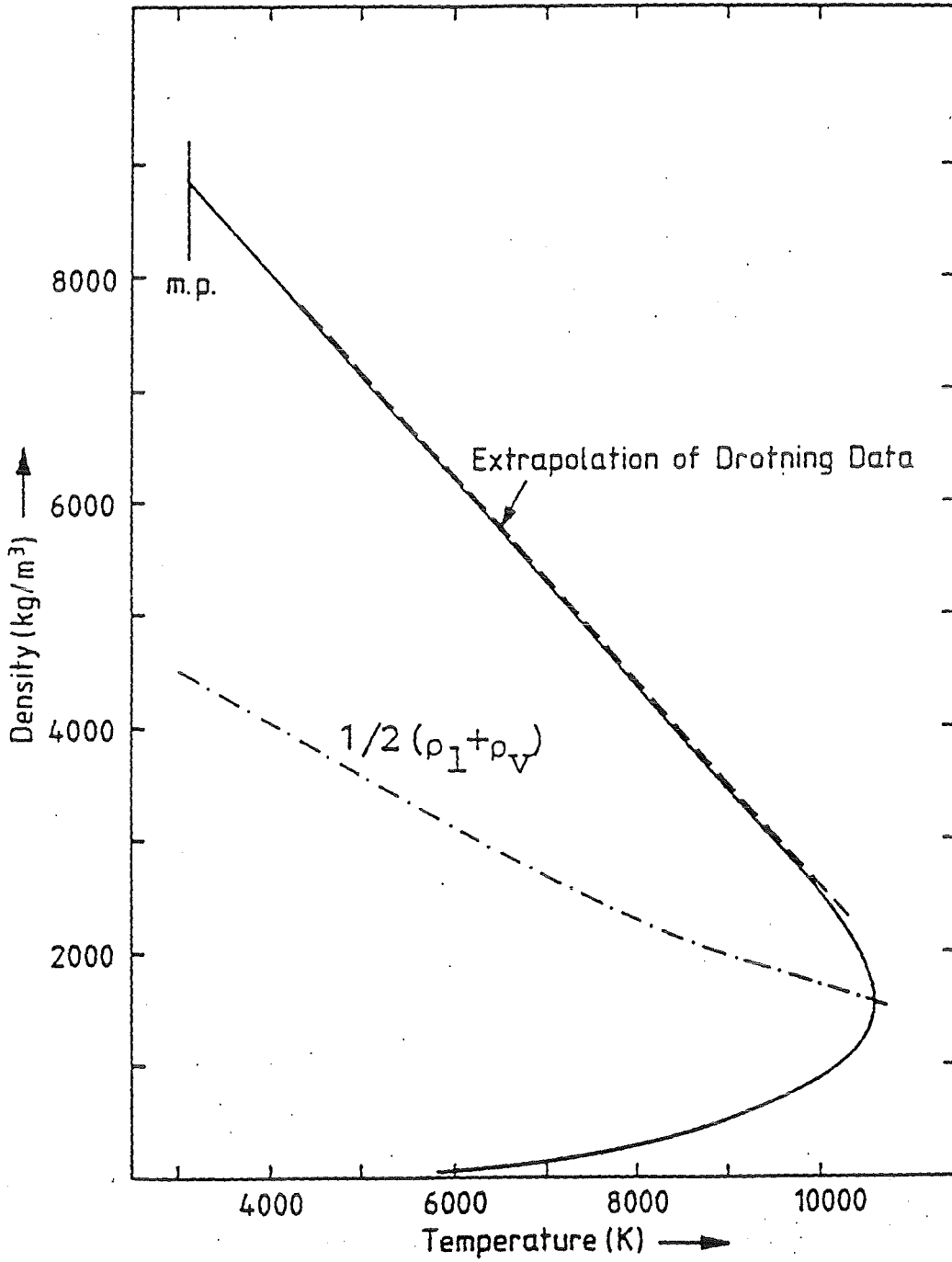
Fig: 6.5   Density of the saturated liquid and vapor
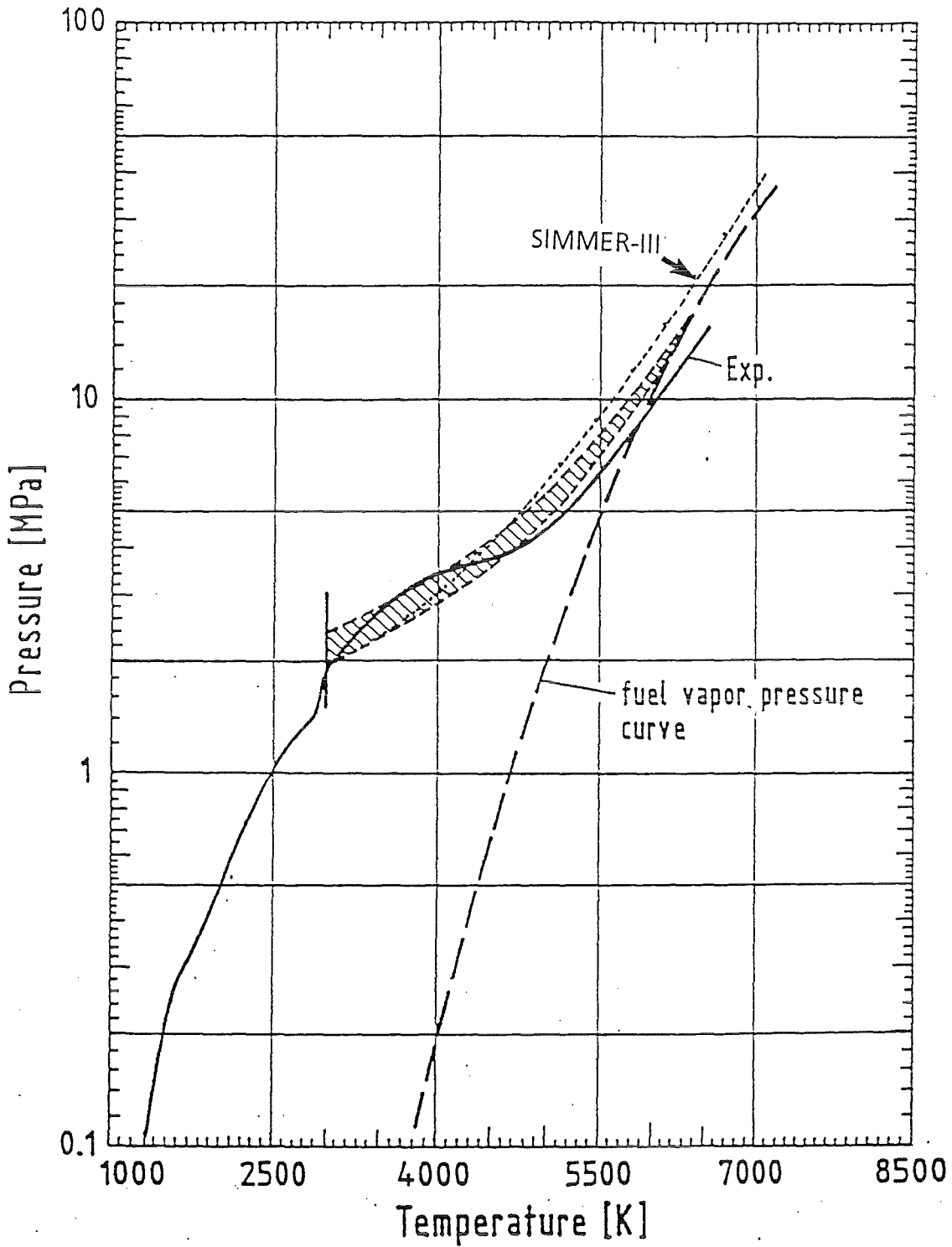
Calculated and Measured Pressure,
EEOS-12

Fig: 6.6   Calculated and measured pressure of the EEOS-12 experiment
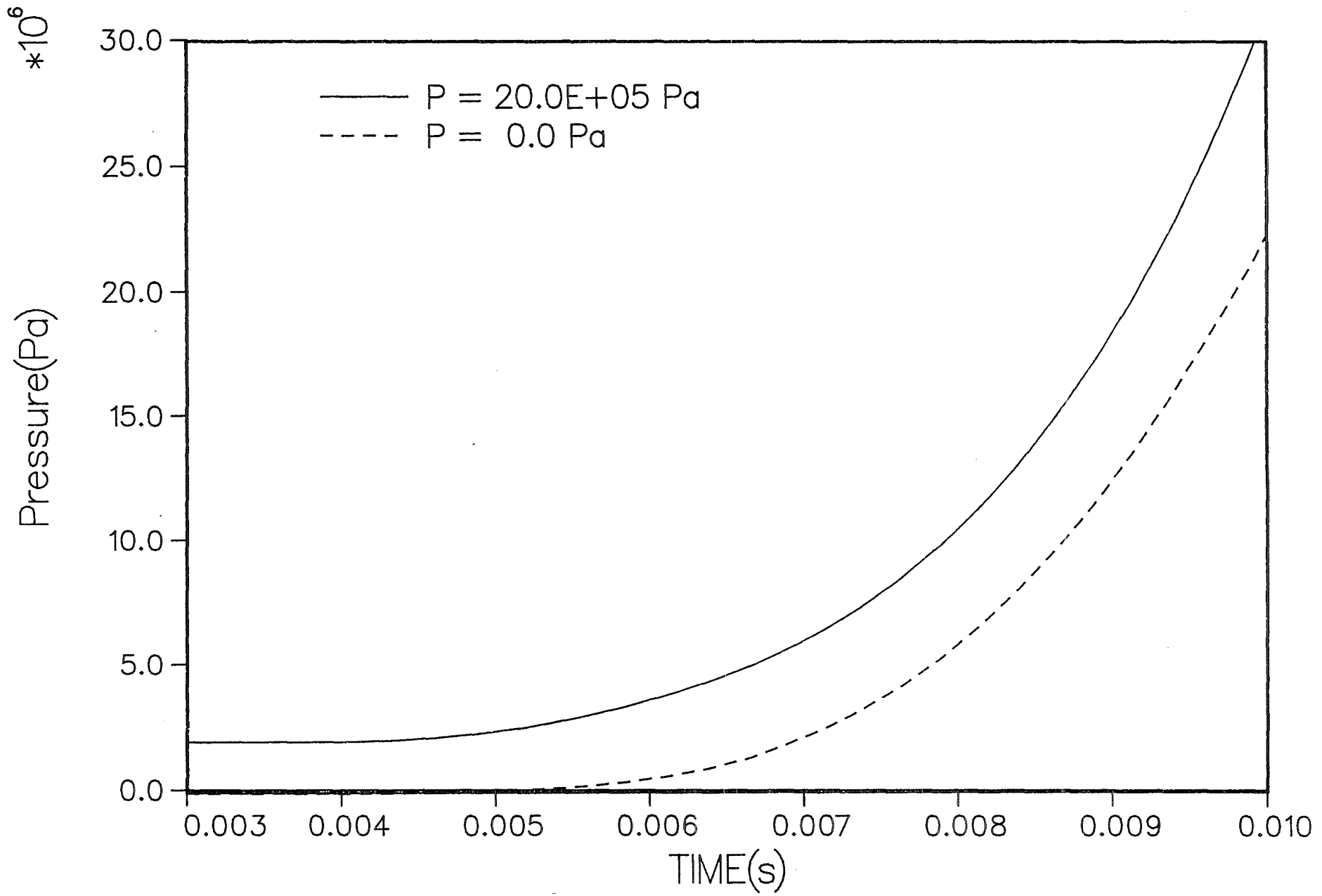
Fig: 6.7   Difference in pressure development between evaporation into
vacuum and against a pressurized gas
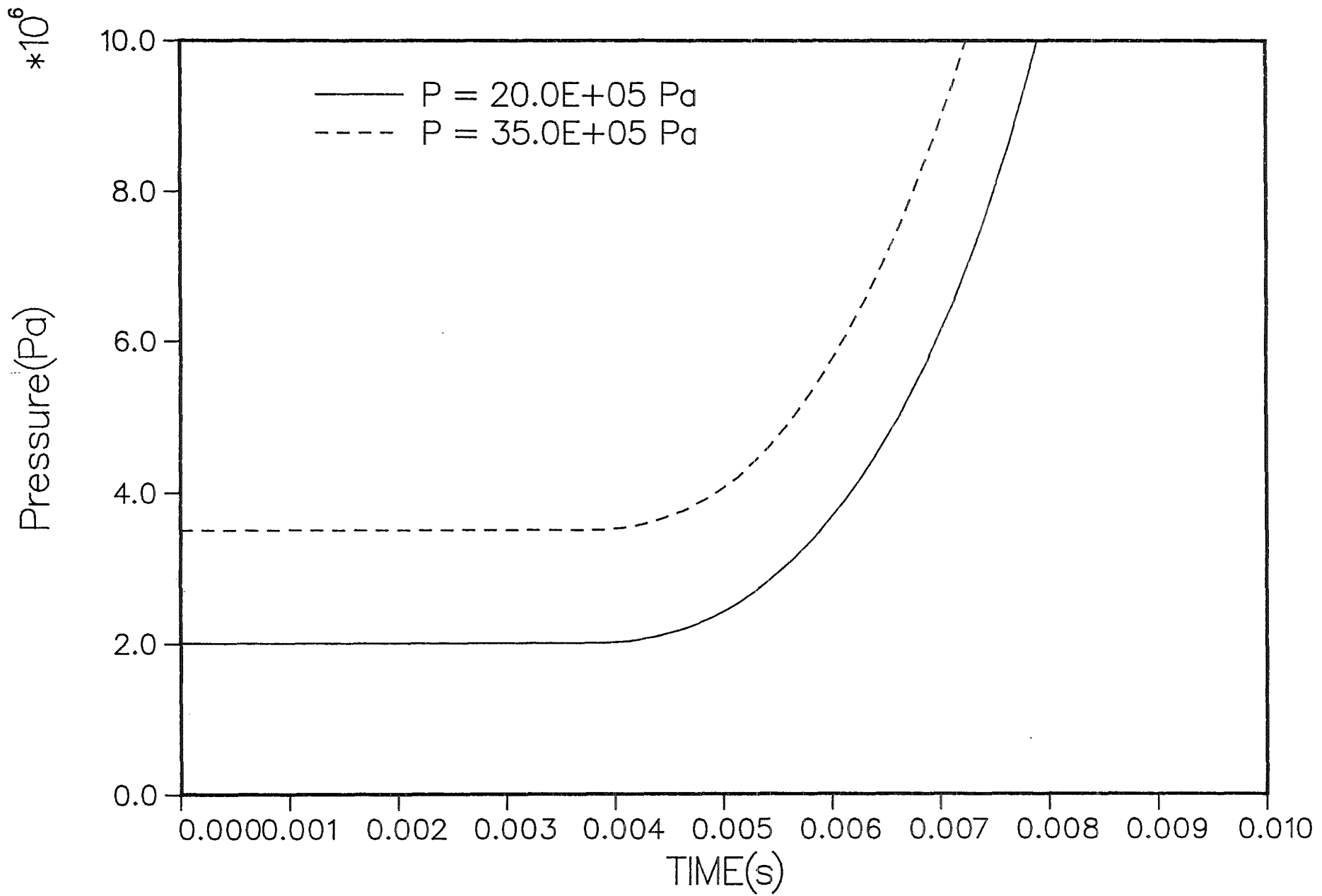
Fig: 6.8   Pressure development of the rapid vaporization test against a
pressurized gas (2 and 3.5 MPa initial fission gas pressure)
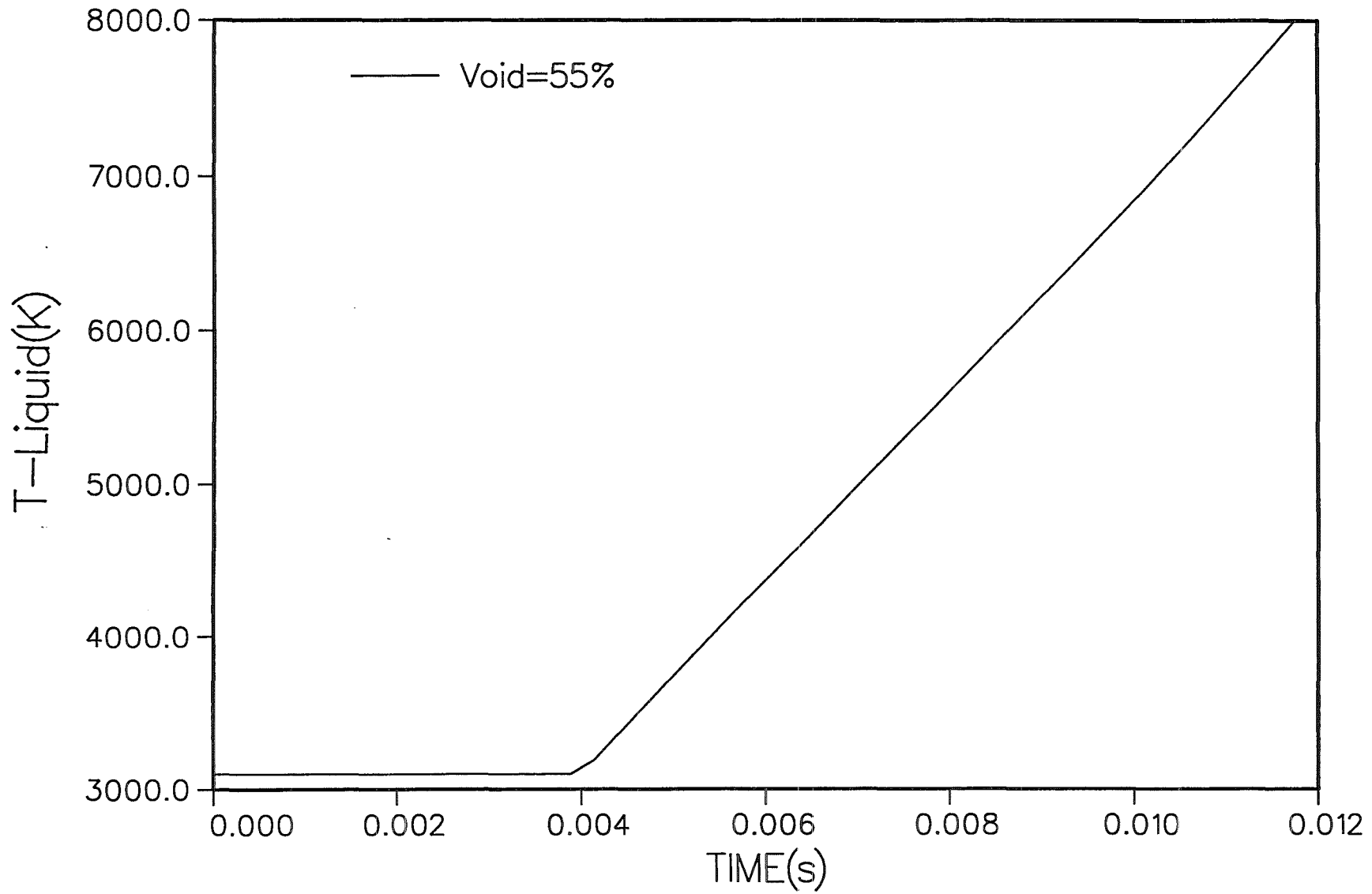
Fig: 6.9   Temperature development of the rapid vaporization test against a
pressurized gas (2 and 3.5 MPa initial fission gas pressure)
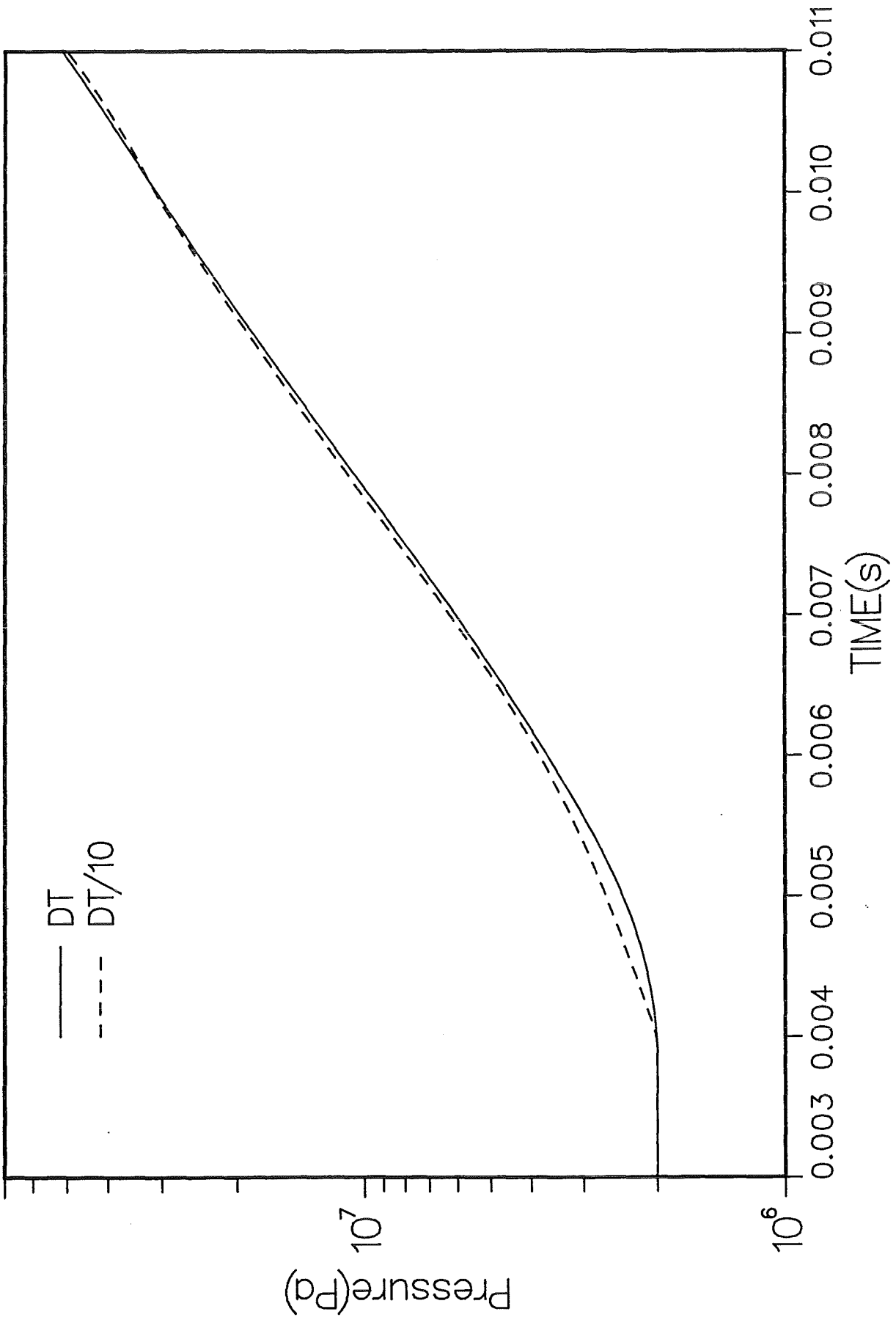
Fig: 6.10   Influence of time step size on the evaporation calculation

Summary Report on an Application for the SIMMER-III Code Assessment, Phase 1

Penetration and Freezing of Hot Melts Into Vertical Tube Structures

by

M. Flad*, W. Maschek, S. Kleinheins

Forschungszentrum Karlsruhe
Postfach 3640, 76021 Karlsruhe, Germany

*D.T.I. GmbH Karlsruhe

September 1995

Outline of the Case

In the framework of the SIMMER-III code assessment the freezing models and pressure losses at area changes are investigated by simulating a THEFIS experiment /1/. In the THEFIS experiments a hot Al_2O_3 thermite melt penetrates into cold tube structures leading to an increasing crust build-up at the tube walls until the cross section is blocked completely. The maximum penetration length, the penetration vs time dependence and the crust formation are compared to the data derived from the experiments.

Key Words

Freezing/Melting; Conduction limited freezing behaviour; Pressure losses at area changes.

1. Objectives of the Application

By the simulation of a hot melt penetrating a cold tube structure the heat and mass transfer models should be assessed. The penetration of the melt passing through cold tubes represents an integral test of heat transfer coefficients, melting and freezing models and pressure loss calculations at changing area cross sections.

2. Description of the Experiment

In the THEFIS experiment series performed at FZK the freezing behaviour of a thermite melt inside cold steel/quartz tubes is investigated. At the beginning of the test the tube holds room temperature and is lowered into a crucible containing Al_2O_3 at 2300 K. Shortly after immersing into the melt a driving pressure is imposed which injects the melt up into the tube.
The mass of Al_2O_3 supplied in the crucible exceeds by far the amount of material necessary to fill the structure. The Al_2O_3 crust build-up at the colder walls gradually reduces the flow area and the flow velocity until the melt comes to a halt. For the test analysed the substrate tube consisted of quartz.

The maximum penetration length and the penetration vs time dependence is recorded. Also a post-experiment analysis of the crust is performed. The results show a deep penetration of the Al_2O_3 melt consistent with a conduction freezing behaviour /2/.

3. Analytical Solution

No analytical solution available.

4. Understanding of Phenomena

The large penetration length of the Al_2O_3 melt is characteristic for a conduction limited freezing behaviour. The crust growth finally leads to a closure of the flow path and a stoppage

of the flow. The maximum crust thickness and closure is reached downstream of the flow entrance when a superheated melt is regarded.

The Al_2O_3 results from a thermite reaction which does not proceed completely. Post-experiment investigations of the crust revealed some impurities originating from the basic material and the crucible. Therefore, the thermophysical properties of the Al_2O_3 melt applied differ somewhat from the values available for pure material. Previous simulations with SIMMER-II showed a distinct influence of the viscosity on the maximum penetration length /3/.

At the beginning of the test the driving pressure increases due to the opening characteristic of the solenoid valve. After 0.4 sec the final pressure difference is achieved. As no information about the pressure transient characteristic of the valve was available a standard correlation has been applied for the simulation. Analyses with SIMMER-II /3/ demonstrated the influence of the initial pressure increase on the penetration velocity. The same holds for SIMMER-III.

5. SIMMER-III Representation

The THEFIS test facility consisting of the quartz tube and the feeding reservoir is modelled as a one-dimensional system. One hundred axial cells are provided and split up into 10 cells for the reservoir and 90 cells for the quartz tube (Fig. 1). A higher order differencing scheme is used.

For the Al_2O_3 equation-of-state the values from the THINA simulation /4/ with AFDM are applied and transformed to SIMMER-III input data with the SAEOS data converter.

5.1 Geometry, Initial and Boundary Conditions for a Reference Case

According to the experiment a vertical quartz tube with 6 mm inner diameter and 1 mm wall thickness is modeled. The tube length is 1.8 m. The reservoir is attached at the lower inlet of the tube and consists of a bottomless tank with 8 mm diameter and 0.2 m height. At the beginning of the simulation the tube structure holds 300 K. At the upper end of the tube a pressure of 0.1 MPa is imposed.

The reservoir contains Al_2O_3 at 2300 K (solidus temperature 2100 K). The pressure at the reservoir inlet rises within 0.4 sec from 0.1 MPa to the final value of 0.2 MPa (driving pressure difference 0.1 MPa). The pressure increase at the beginning follows an exponential law and is supposed to come close to the opening characteristic of a solenoid valve used in the experiment.

5.2 Code Version and Computer Used

The simulations have been performed using SIMMER-III version 2.G on an IBM 3090 mainframe. The calculation consumed 25 hours CPU time approximately.

5.3 Code Modifications

This simulation is within the scope of the SIMMER-III application range. No modification of models has been required. However, some modifications had to be done to cope for floating divides which occured. In SP VITER and VITERP the determinant of the S-matrix for velocities happens to become smaller than permissible. In SP IFASRC and HTC one field element of the thermal conductivity KPLM resp. KR was found to become zero occasionally probably resulting from an allocation error. The modifications worked well for this special 1d-case but are not meant to be a general remedy.

5.4 Parametric Cases

A parametric case with a non-superheated melt was run giving a reduction in penetration distance in accordance with /5/. In this case, the maximum crust growth occurs at the tube inlet.

6. Results (and Discussion)

The results from the simulation show a good agreement with the data derived from the experiment. The maximum penetration length is underestimated by about 10 % (Fig. 2). Approaching the maximum penetration value the cross section is blocked to about 90 % ($\alpha_{tube} + \alpha_{crust}$) by crust formation (Fig. 3, 4).

The velocity (~ mass flow) through the inlet area is substantially decreased (about 1/80 of the maximum value), but not completely stopped (Fig. 5). As heat losses of the tube to the environment can not be considered and heat conduction in axial direction is not modeled the cooling down of the melt is delayed.

The penetration transient stays somewhat behind the values recorded in the THEFIS experiment. This was also noted in previous calculations with SIMMER-II. These calculations showed /3/ that with a different pressure characteristic for the solenoid valve (higher $\frac{dp}{dt}$) the results are improved.

Some problems arise at the very beginning of the calculation when large pressure spikes from the leading edge arrive at the reservoir and disturb the acceleration of the melt (Fig. 5). Using default input values for the momentum exchange functions the penetrating melt comes to a premature standstill. The cooling down of the melt generates particles at the leading edge causing an artificial stoppage of the flow. The low particle fraction should not be able to obstruct the flow path.

The SIMMER-III 2.G default values for the momentum exchange functions had to be changed. Thus, the maximum packing fraction for solid particles, ALPMP, was raised from 0.7 to 0.9; and the maximum discontinuous fraction in a fluid mixture, ALPDM, was changed from 0.7 to 0.9. These changes were necessary to enable a further penetration of the melt into the tube. With these modifications the crust formation at the final state shows ist characteristic conduction limited freezing behaviour.

In SIMMER-III correct pressure losses are obtained for the flow through an area restriction (orifice) only if the orifice region is represented by at least two meshes. In this application, area changes produced by crust formation do not differ widely from one cell to another, so that the pressure loss calculation leads to satisfactory results. The analyses of pressure losses at area changes showed that SIMMER-III gives good results for a flow through a sudden expansion. For a flow through a sudden restriction with an area change more than 50 %, deviations from the handbook /6/ pressure losses are calculated.

7. Conclusions

The simulation agreed well with the data derived from the experiment. The experience from former simulations with SIMMER-II was a good support /3/. The integral assessment proved the heat transfer coefficients and the melting/freezing models to be adequate for simulating a melt penetration with a conduction limited freezing behaviour. The dafault values for the momentum exchange functions should be raised.

8. Recommendations for Model Improvements

The acceleration of the penetrating melt is affected adversely by high pressure spikes propagating from the leading edge of the melt down to the reservoir. These spikes resulting from 'packing' problems should be smoothed.

It is desirable to remove the floating divides that occured throughout the simulation. These errors probably result from numerical rounding errors not taken into account and from an allocation error.

Concerning numerics some improvements are also desired to reduce the large CPU time necessary. The consumed CPU time of about 25 h appears to be much too high for the problem concerned.

9. References

1.   G. Fieg, M. Möschke, I. Schub, H. Werle
        Penetration and Freezing Phenomena of Ceramic Melts into Pin Bundles
        The 1990 Int. Conf. on Fast Reactor Safety Snowbird, Utah, USA, Vol. II,
        387, August 12 - 16 (1990)

2.   M. Epstein
        Transient Freezing of a Flowing Ceramic Fuel in a Steel Channel
        Nucl. Sci. Eng. 61, 310 (1976)

3.   W. Maschek, G. Fieg, M. Flad
        Experimental Investigations of Freezing Phenomena of Liquid/Particle Mixtures in the
        THEFIS Facility and Their Theoretical Interpretation
        The 1990 Int. Conf. on Fast Reactor Safety Snowbird, Utah, USA, Vol. I,
        519, August 12 - 16 (1990)

4.   D. Wilhelm, personal communication

5.   S. J. Hakim
        Analyses of a Prototypic and a Simulant Experiment Related to Freezing in Flow
        Channels
        LA-7938-C (1979)

6.   I. E. Idelchik
        Handbook of Hydrodynamik Resistance
        Berlin, Springer Verlag (1986)
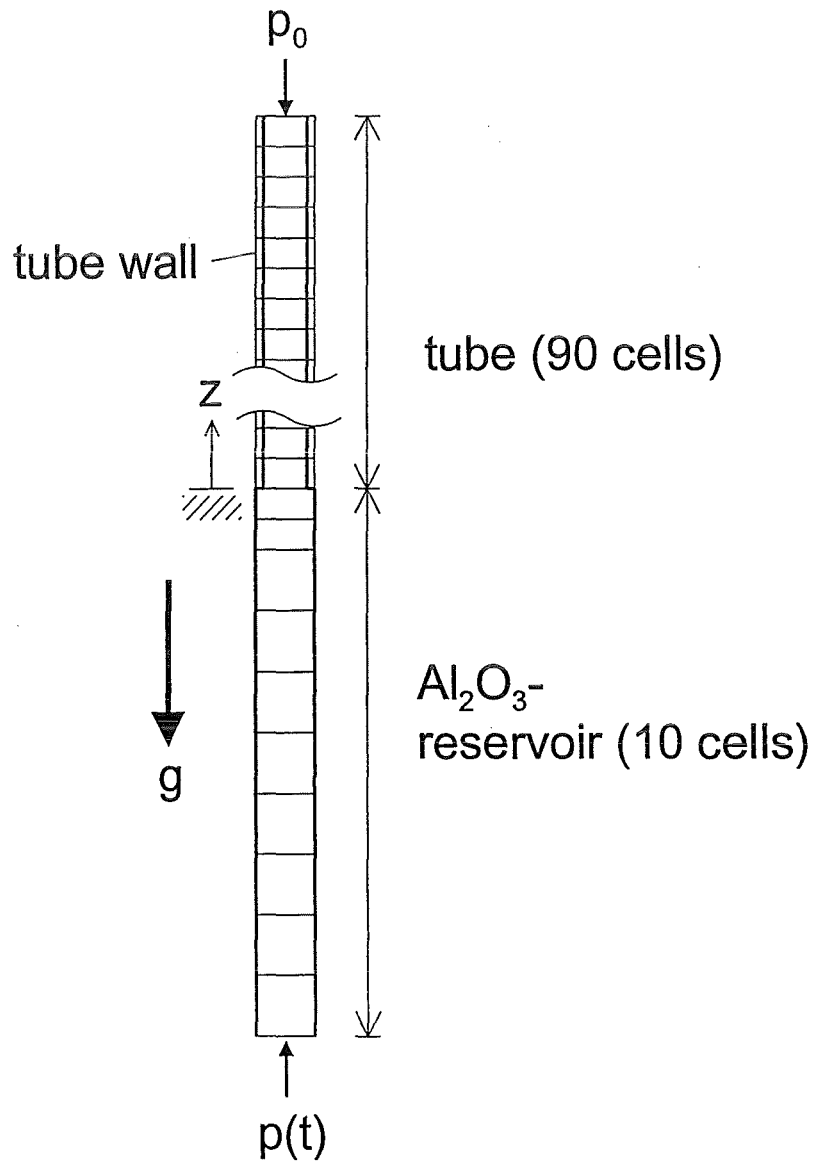
Fig. 1: SIMMER-III Representation

6
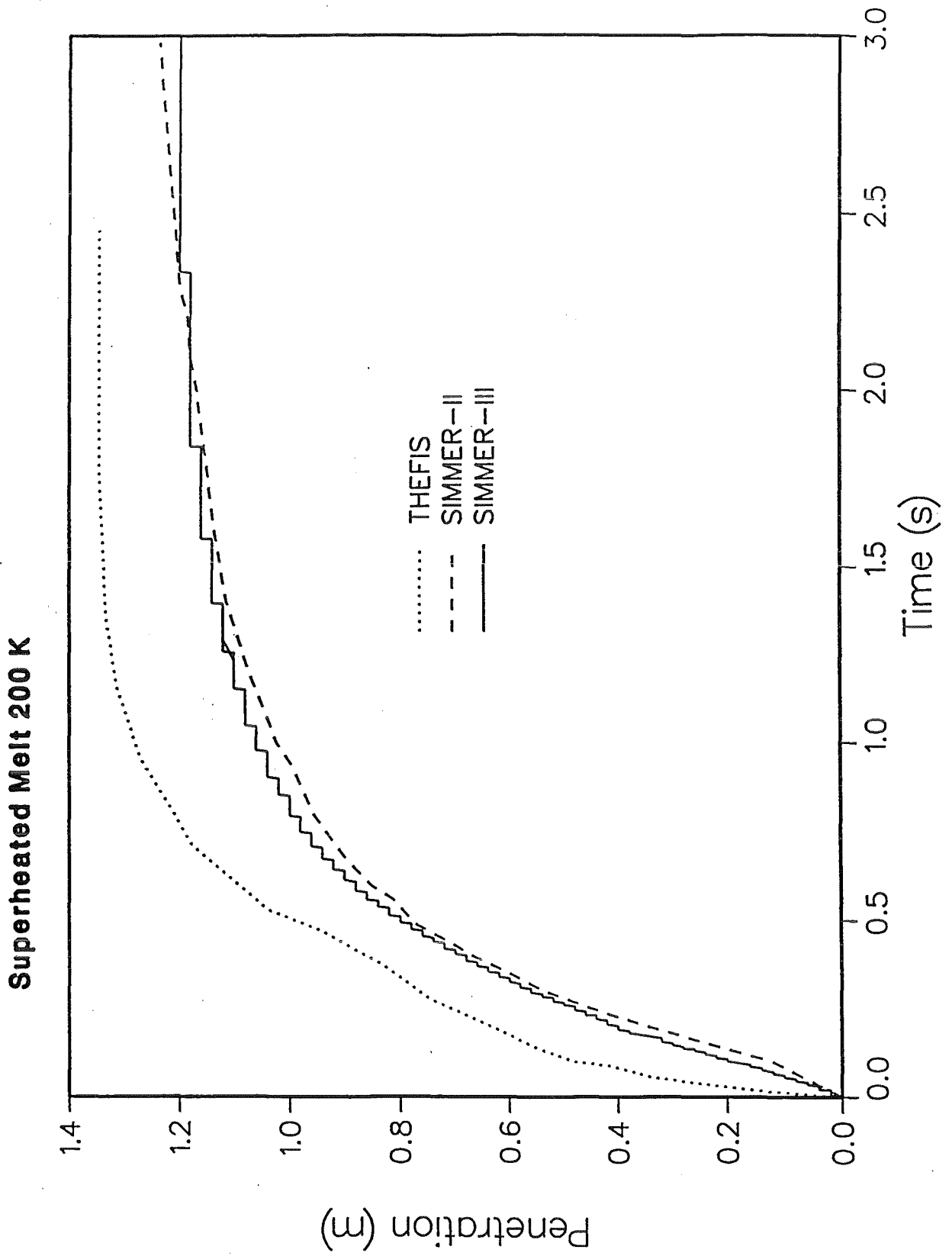
Fig. 2:   Penetration Length versus Time
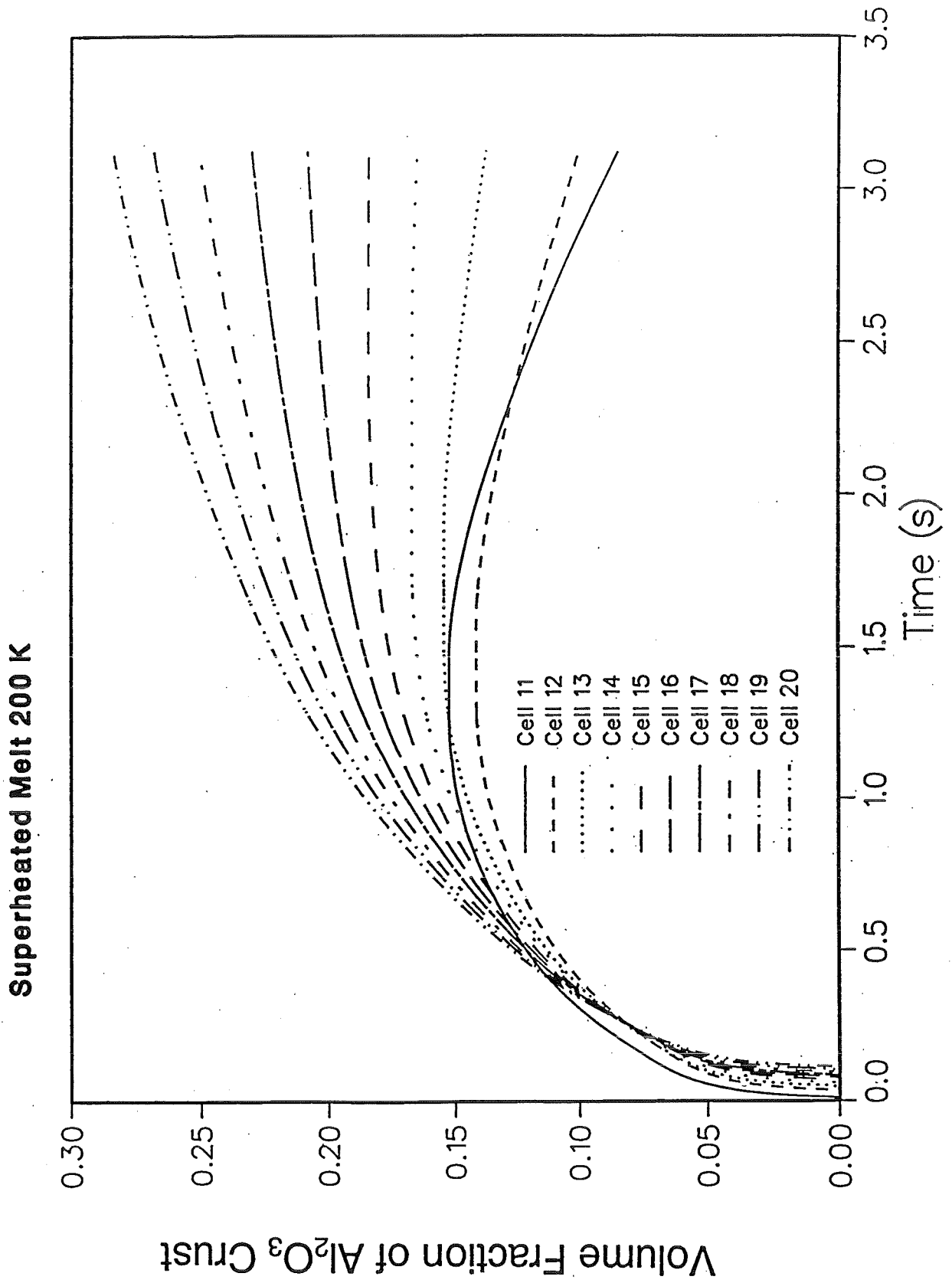
Fig. 3: Crust Formation (Cells 11 to 20)
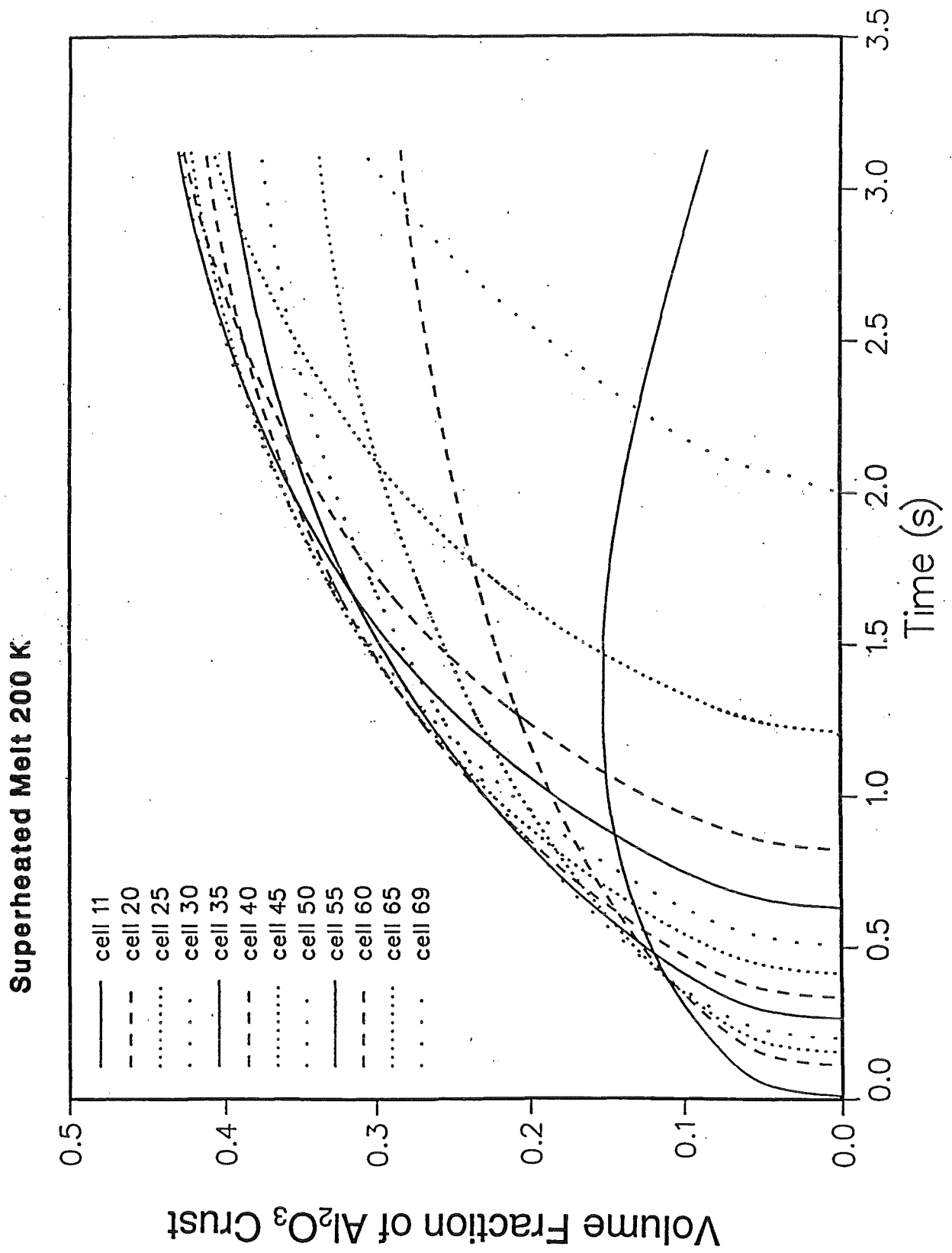
Fig. 4: Crust Formation (Cells 20 to 69)
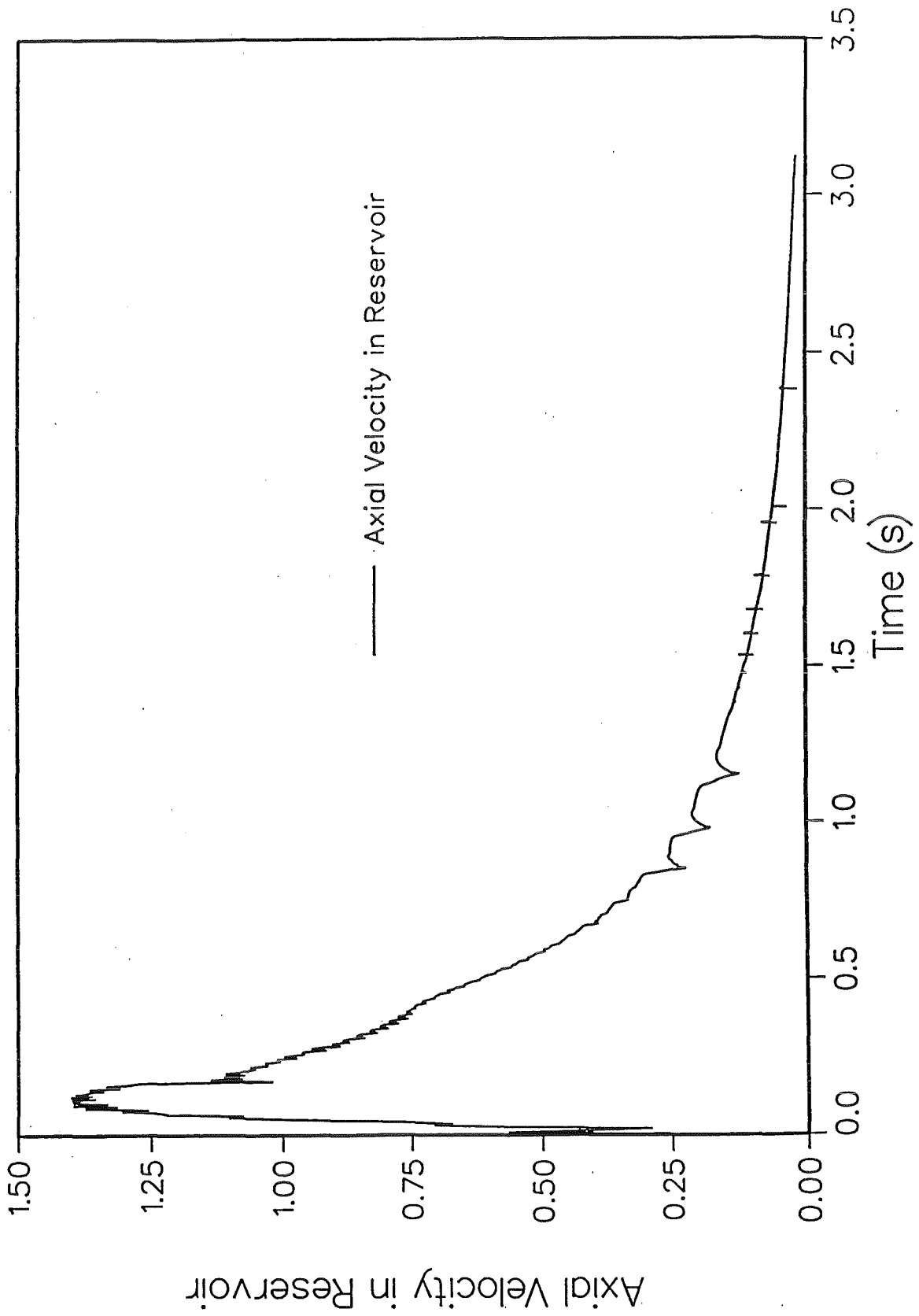
Fig. 5: Axial Velocity in Reservoir

10

Summary Report on an Application for the SIMMER-III Code Assessment, Phase 1

Impact of Liquid Slugs on Rigid Surfaces

by

W. Maschek, G. Arnecke, S. Kleinheins, M. Flad*

Forschungszentrum Karlsruhe
Postfach 3640, 76021 Karlsruhe, Germany

*D.T.I . GmbH Karlsruhe

September 1995

Outline of the Case

The purpose of this application of SIMMER-III is the simulation of continuous liquid slugs moving through gas/air and their impact behavior on rigid surfaces. In the case of a vapor explosion in the vessel of a PWR a molten corium slug might be accelerated upwards which then impinges on the upper vessel structure. This phenomenon is described with codes like PLEXUS /1/. In the present application of SIMMER-III some specific calculations of PLEXUS are recalculated and compared with SIMMER-III results. The simulation of a falling liquid slug through air driven by gravity or pressure is of interest as in SIMMER-III no free fluid surface with its related instabilities is modelled.

Key words

Two dimensional two-phase flow, liquid slug impact, momentum transfer, jet propagation

1. Objectives of the Application

This application of SIMMER-III should investigate the motion of liquid slugs in air, the impact behavior of these slugs on rigid surfaces and obstacles and the momentum transfer during impact. In addition, the modelling of virtual walls in SIMMER-III is tested. The results can also serve as a check for results of the PLEXUS code /1/ for the specific case of slug impact on a rigid surface. In PLEXUS the fuel slug is modelled by an ensemble of small compressible spheres (particles). With decreasing sphere-radius the PLEXUS model should converge against the continuum model of fluids, which is however not fulfilled /2/. When the particle slug impacts on a rigid surface the whole slug disintegrates and disperses (Fig. 1.1). SIMMER-III shows a different behavior with the fluid slug flowing and spreading after impact on a rigid wall or an obstacle. The comparison with experiments and other code calculations back the SIMMER-III results. The momentum transfer calculated by SIMMER-III is less than the one calculated by PLEXUS. The motion of the falling liquid slug through air driven by gravity or pressure is of interest as no free fluid surface is modelled in SIMMER-III with its related Taylor-or Helmholtz-instabilities.

2. Description of Experiments

Two types of experiments are needed for comparison with the calculations. Firstly, experimental information about falling slugs through air is necessary and secondly, experiments on the impact of liquids on a rigid surface or an obstacle is needed.

In /3/ a liquid slug is released from a container and falls approximately as a cylinder towards a lower water surface. Surface disturbances of various wavelengths can be observed. The lower slug surface shows some 'mushrooming'.

For the impact phenomena of liquid slugs, in literature, experiments with impinging solids (projectiles) and liquid jets on rigid surfaces are reported. Experiments for soft pellets are e.g. reported in /4/. A pellet of rocket propellant is accelerated towards a rigid surface and is deformed. The generated shock wave finally ignites the pellet and destroys it. Before this, the pellet is deformed and shows a flow-like behavior (Fig.2.1). The numerical simulation of the deformation and flowing process is simulated with the SALE /5/ and HELP /6/ code (fluiddynamic codes). The pellet is simulated as a nonviscous, compressible fluid. The results of the simulation compared to experiment are described as excellent.

In /7/ the results of impact phenomena of waterdrops on rigid structures are displayed (Fig.2.2). The impact velocity is approx. 150 m/s. Compressible and incompressible code calculations are used for the simulation. The results show the typical deformation and flowing process. Additional experimental and theoretical information can also be gained from /2,8/. No disintegration process of the bulk slug is observed in all these analyses and experiments.

3. Analytical Solution

Analytical solution for impact processes of a liquid on a rigid surface based on continuum-theoretical approaches imply a flow redistribution at impact and no disintegration of the slugs /2/.

4. Understanding of Phenomena

Experimental information on the impact of liquid droplets and slugs is available.

5. SIMMER-III Representation

Three different cases have been analyzed with liquid slugs accelerated either by gravity or vapor pressure and finally hitting a rigid surface or a rigid target. The liquid slugs analyzed had a height / diameter ratio of 0.42. An additional case with a long liquid slug with a H/D ratio of 16.7 has been investigated to further study the liquid /gas flow phenomena and surface phenomena modelled by SIMMER-III. The different cases are displayed in Tab. 5.1 and the geometrical arrangements are schematically displayed in Fig. 5.1.
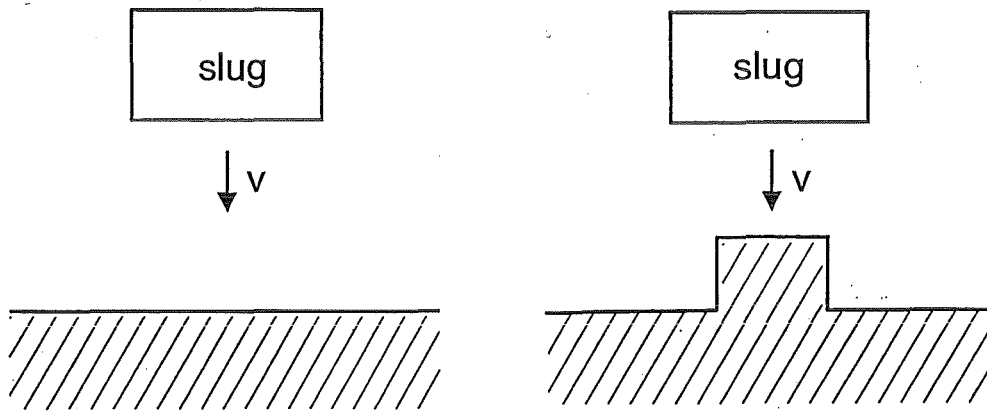
Fig. 5.1.   Geometrical arrangement of liquid slugs and impact-structure.

Case	Acceleration	Fall-distance (cm) pressure (MPa)	Geometry H/D ratio	Impact conditions
S1	gravitation	200	0.42	surface
J1	pressure	5	0.42	surface
J2	pressure	5	0.38	obstacle
S2	gravitation	580	16.7	surface

Tab. 5.1   SIMMER-III calculational cases

5.1 Geometry, Initial and Boundary conditions

A 2-D mesh with (50x100 cells) has been used for the calculations. In the gravity driven cases the liquid water slug is used. The initial conditions for the pressure driven slugs are, that a hot two phase fuel region with 5 MPa is layered above and accelerates a cold liquid fuel slug. The slug moves within a tube modelled by virtual walls. In the case J2 the obstacle has both been modelled by virtual walls and a solid structure (structure model).

5.2 Code Version and Computer Used

The calculations are based on SIMMER-III Version 1.G. The computations were performed on a mainframe IBM3670.

5.3 Code Modifications

No code modifications have been performed.

5.4 Parametric Cases

see Tab. 5.1

6. Results

Case S1

In case S1 (Fig. 5.2) the liquid water slug drops onto the horizontal surface with a velocity of 6.2 m/s. The peak pressures obtained are $3.2 \cdot 10^5$ Pa, far below acoustic pressures. (Note the ambient pressure in Fig. 5.3, which is modelled to obtain similar conditions with the cases J1 and J2.) For the calculation the 2nd order numerical scheme has been used. The pressure distribution is given in Fig. 5.3.

The momentum transfer is determined by fluid forces and at the maximum about 60 percent of the initial momentum (evaluation of momentum at central impact location) is imparted in $\Delta t = h_{slug}/v_{slug}$. This magnitude of momentum transfer is backed by experiments /10/. After impact, the liquid slug spreads and flows along the surface. An additional calculation with a first order scheme (case S1D) shows a strong numerical smearing and damping. The impact pressures and the momentum transfer are reduced by a factor of 2. Thus the application of the first order method gives inadequate results.

In Fig. 5.2 one can observe some surface perturbations at the lower and radial outer surface. They are not related to a Taylor or Kelvin-Helmholtz instability as in SIMMER-III no free surface of the liquid slug is modelled (see case S2).

Case J1

In case J1 a liquid fuel slug is accelerated by a high temperature two phase fuel cushion. The liquid slug moves between virtual walls and impacts the lower boundary with $v \sim 33$ m/s /Fig. 5.4). The peak pressure in the central impact location (point of momentum evaluation) goes up to $7 \cdot 10^8$ Pa (Fig. 5.5). After impact the reflected pressure wave leads to some cavitation processes. The momentum transfer is dominated by shock waves and about 85% of the initial momentum is transferred in the first pressure peak ($\Delta t = h_{slug}/c_{sound}$). Again the slug starts a flowing process after impact.

Case J2

In case J2 the pressure accelerated fuel slug hits an obstacle before impinging on the lower rigid surface (Fig. 5.6). The peak velocities obtained are 32 m/s and the peak pressures are $6 \cdot 10^8$ Pa (Fig. 5.7). After the impact the flowing processes

around the obstacle can be identified which finally turns into a drippling process when the pressure is reliefed. About 70% of the initial momentum is transferred in the first pressure peak.

The obstacle was modelled both by the ordinary structure model and by virtual walls. Problems occurred with the virtual wall model when the slug impacted on the horizontal wall. The timesteps became increasingly small and levelled of at 10^{-8} s (condition OPTPIT, number of pressure iteration limit exceeded).

Case S2

In case S2 the falling of a long cylindrical slug is modelled to investigate the liquid / gas interaction at the slug surface. The results are compared qualitatively to the experimental result from /3/. Three calculations have been performed with a variation of the drag coefficients CDD (10^{-4},1,10^4) displayed in Fig. 5.8, and Fig. 5.9. It can be seen from the results that the bulging out of the liquid is strongly controlled by the drag coefficient CDD and can be suppressed by a large CDD value. For a good adjustment of the CDD values further experimental results seem to be necessary.

7. Conclusions

SIMMER-III is able both to describe the movement of liquid slugs through gas and the impact of such slugs on rigid structures. The results of other codes and experimental results back the SIMMER-III impact calculations. When using a first order numerical scheme, strong numerical diffusion effects can be observed and the impact pressues and the momentum transfer is underestimated.

8. Recommendations

To better simulate surface instabilities of liquid slugs a modelling of free surfaces is required. Similar techniques as realized in SOLA-VOF /11/ could be used but seem to be difficult to implement in the environment of a multiphase, multicomponent, multifield code.
Simple experiments with falling slugs could provide better data for the simulation of surface effects.

9. References

/1/ H. Bung, P. Galon, M. Lepareux, A. Combescure
A New Method for the Treatment of Impact and Penetration Problems.
SMIRT 12, (1993), Paper B02/1.

/2/ B. Göller
IRS, Jan. 1995 (Internal FZK report)

/3/ H.N. Oguz, A. Prosperetti, A. Kolaini
Air Entrainment of a Falling Water Mass,
J. Fluid Mech., Vol. 294, 181 (1995)

/4/ Robert R. Karpp
A Model for Computing Late Detonations Initiated in Propellants by Impact
LA 10270-MS (1984)

/5/ L.J. Hageman, D.E. Wilkins, R.T. Sedgwik, and J.L. Waddell
"HELP: A Multi-Material Eulerian Program for Compressible Fluid and
Elastic-Plastic Flows in Two Space Dimensions and Time",
Systems, Science and Software report SSS-R-75-2654 (July 1975)

/6/ A.A. Amsden, H.M. Ruppel, and C.W. Hirt
"SALE: A Simplified ALE Computer Program for Fluid Flow at All Speeds,"
Los Alamos Scientifc Laboratory Report LA-8095 (June 1980)

/7/ N. Nishikawa, S. Amatatu, T. Suzuki
Simulation of Impact Phenomena by Impinging Droplets, p 569
Computational Fluid Dynamics,
G. de Vahl Davis and C. Fletcher (Ed.)
Elsevier Science Publishers B.V. (North-Holland) (1988)

/8/ J.B.G.Hwang, F.G. Hammitt
High-Speed Impact Between Curved Liquid Surface and Rigid Flat Surface
Trans. of the ASME, Journal of Fluids Engineering, 396, June 1977

/9/ C. Mundo, M. Sommerfeld, C. Tropea
Droplet-Wall Collisions: Experimental Studies of the Deformation and
Breakup Process,
Int. J. Multiphase Flow, Vol. 21, No.2, 151 (1995)

/10/ Th. Stach
IRS, Jan. 1995 (Internal FZK report)

/11/ B.D. Nichols, C.W. Hirt, R.S. Hotchkiss
SOLA-VOF: A Solution Algorithm for Transient Fluid Flow with Multiple Free
Boundaries
LA-8355 (1980)

/12/ L.A. Glenn
On the Dynamics of Hypervelocity Liquid Jet Impact on a Flat Surface
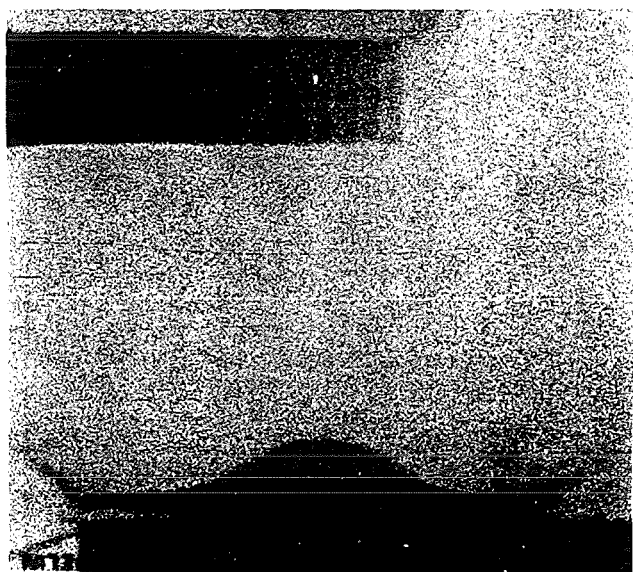Journal of Appl. and Physics (ZAMP), Vol. 25, 383, 1974
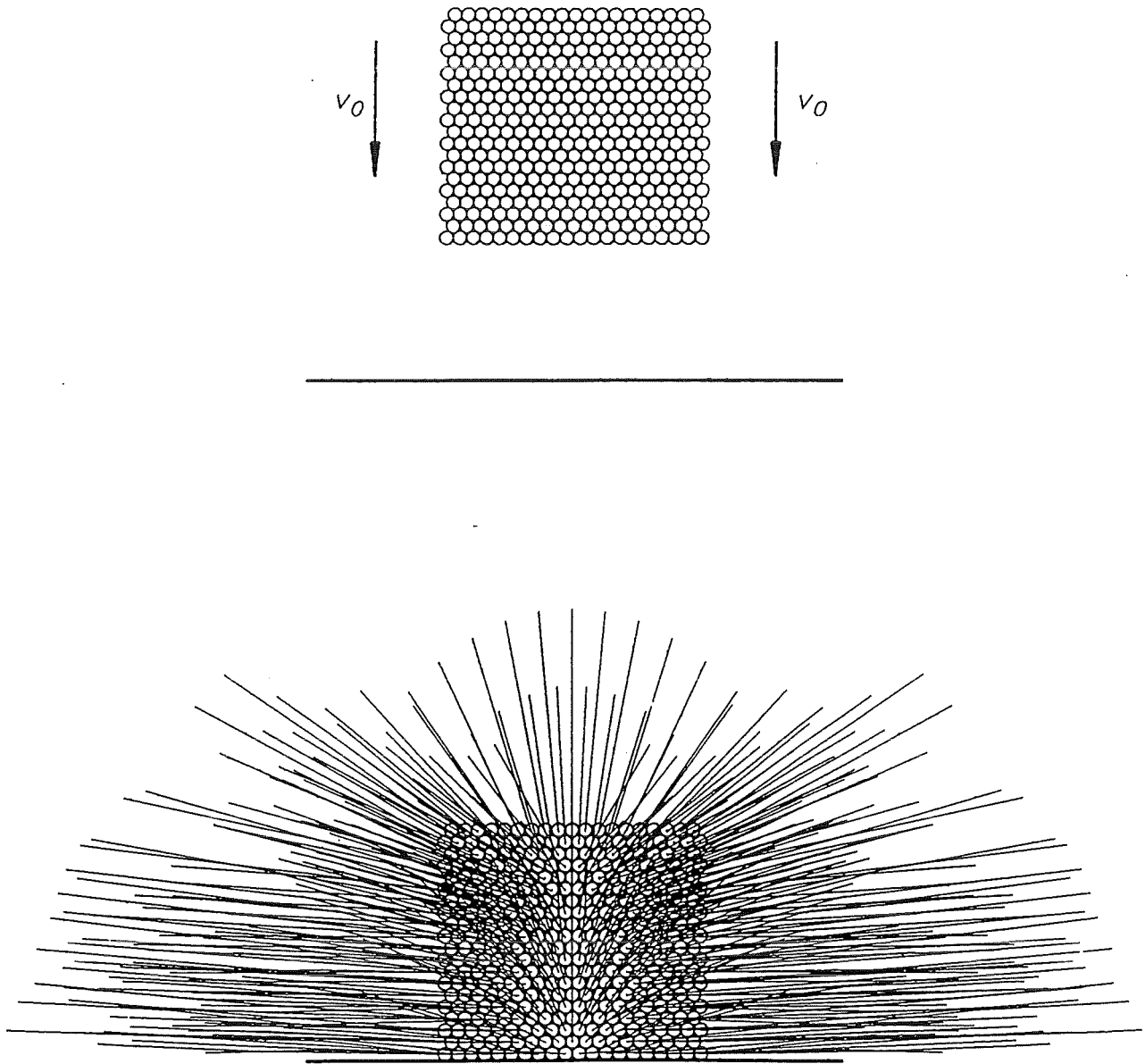
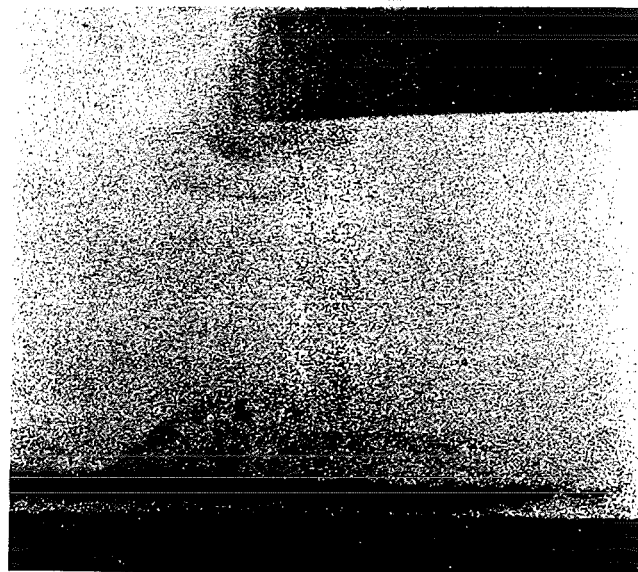Fig. 1.1   Impact of a plane compressible water slug on a rigid surface simulated
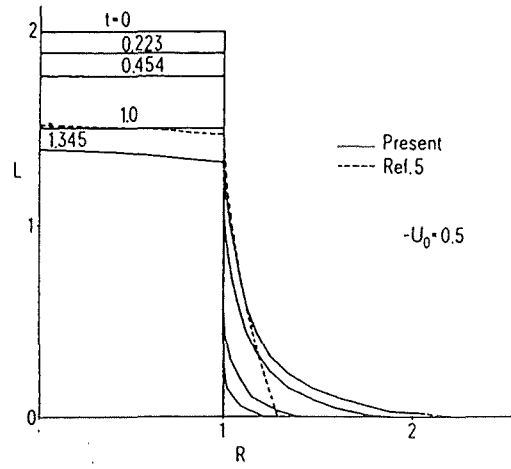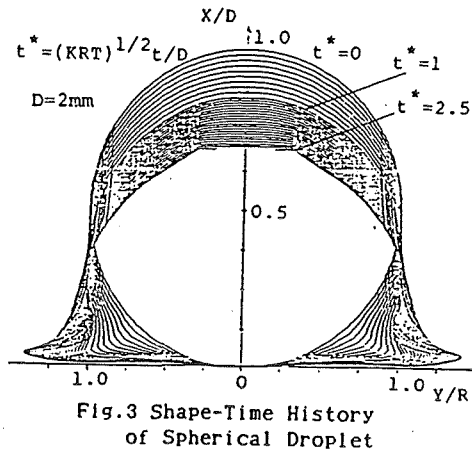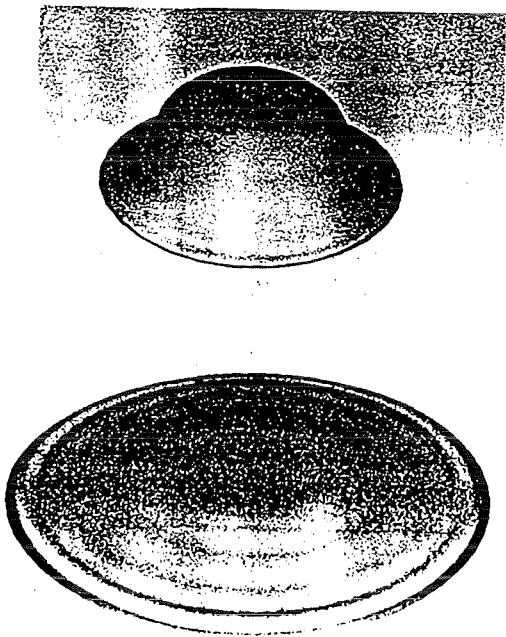by PLEXUS /2/

1.9 μ SEC

15.9 μ SEC

30.8 μ SEC
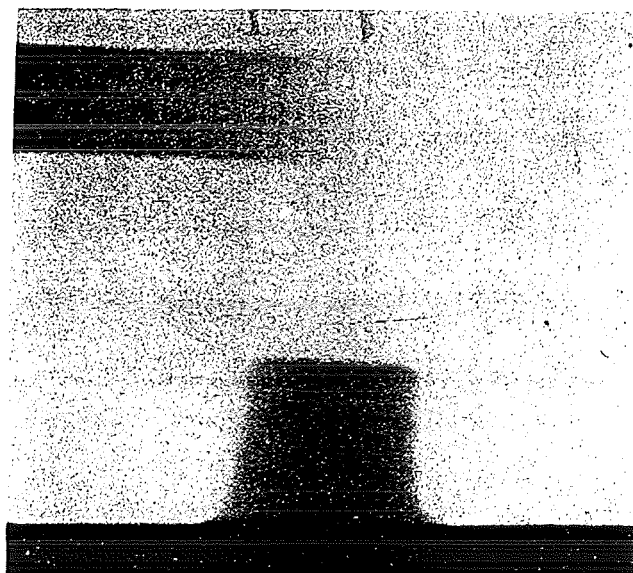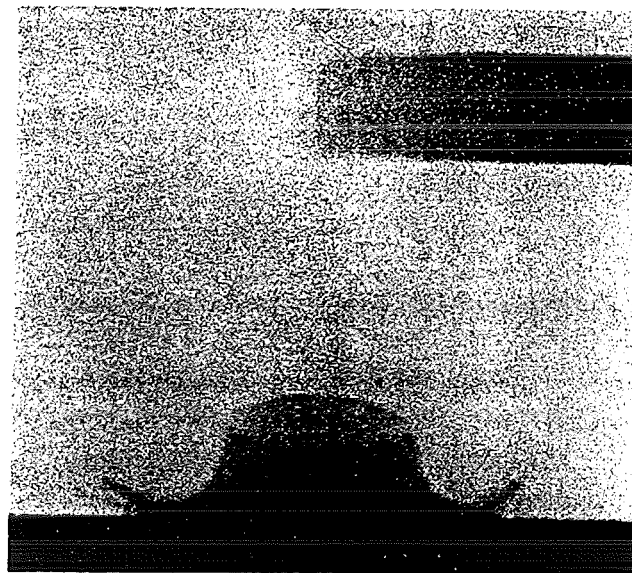
50.6 μ SEC

Fig. 2.1   Radiograph of pellet impact on a rigid surface /4/

X/D

$t^* = (KRT)^{1/2} t/D$

D=2mm

$t^*=0$ $t^*=1$ $t^*=2.5$

1.0

0.5

1.0   0   1.0   Y/R

Fig.3 Shape-Time History
of Spherical Droplet

t=0

0.223

0.454

1.0

1.345

L

——— Present
----- Ref.5

$-U_0 = 0.5$

1   2

R

Shape history; interface motion as a
function of time
(a) subsonic impact

(b) supersonic impact

t=0

0.158

0.256

0.504

0.717

L

$-U_0 = 2$

1   2   3

R
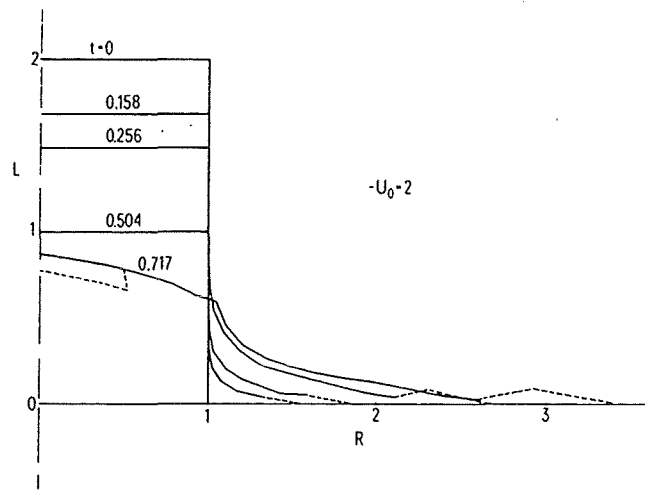
Fig. 2.2   Shape-time history of a sperical droplet /7/ and a liquid slug /12/ im-
pacting on a rigid surface
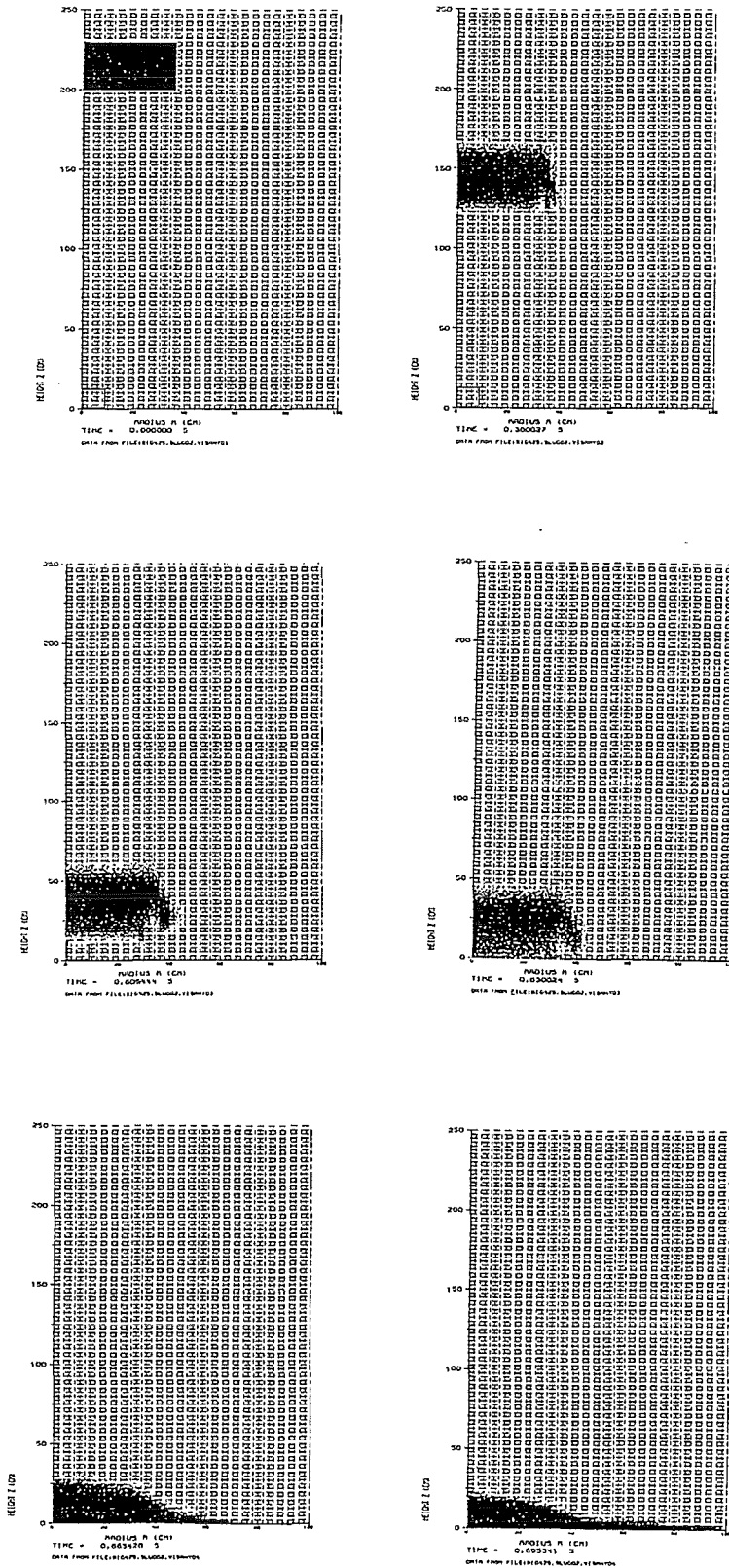
Fig. 5.2　Motion and impact of liquid slug (case S1)
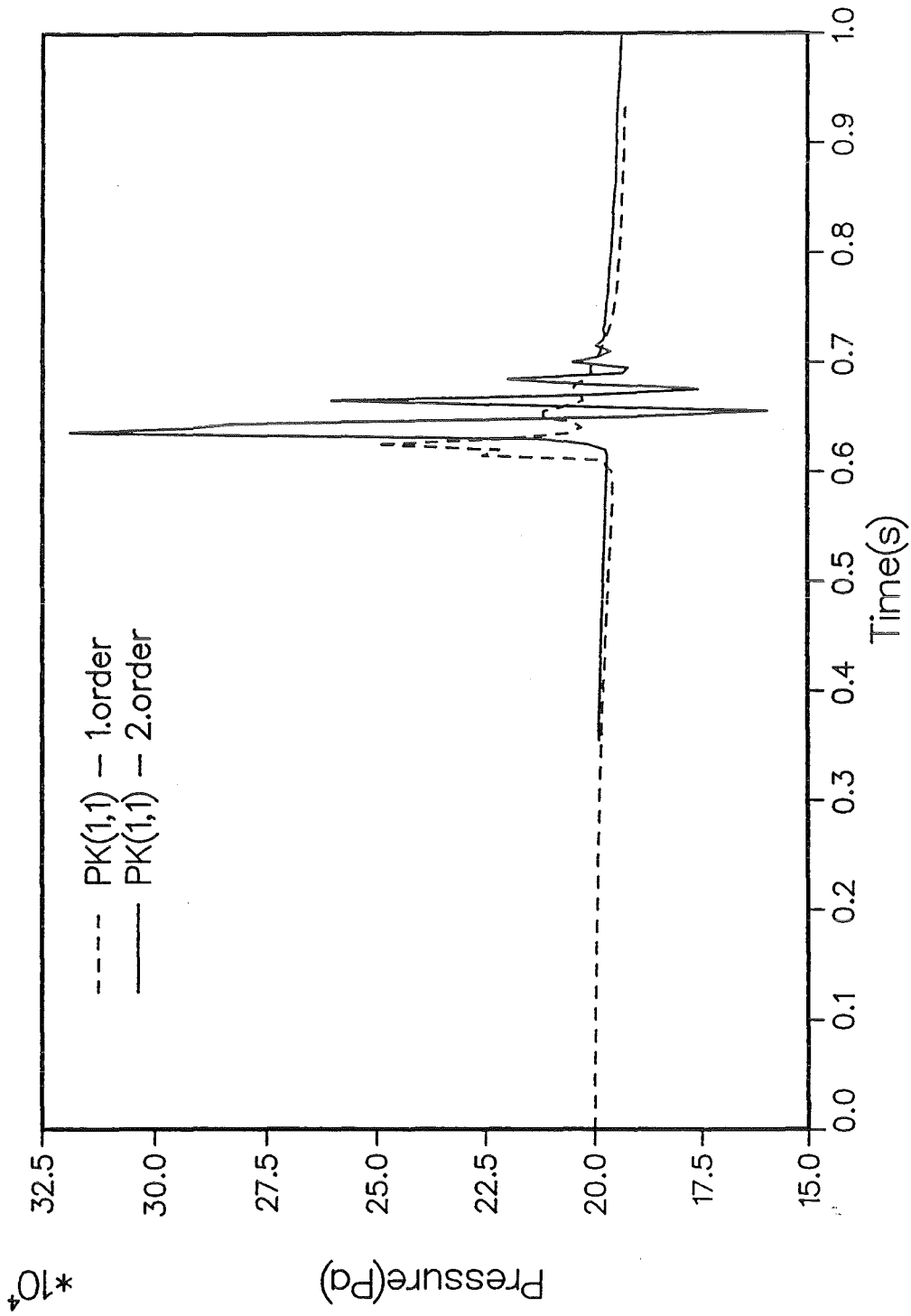
Fig. 5.3   Pressure trace of cases S1 (second order numerial scheme) and S1D
(first order)
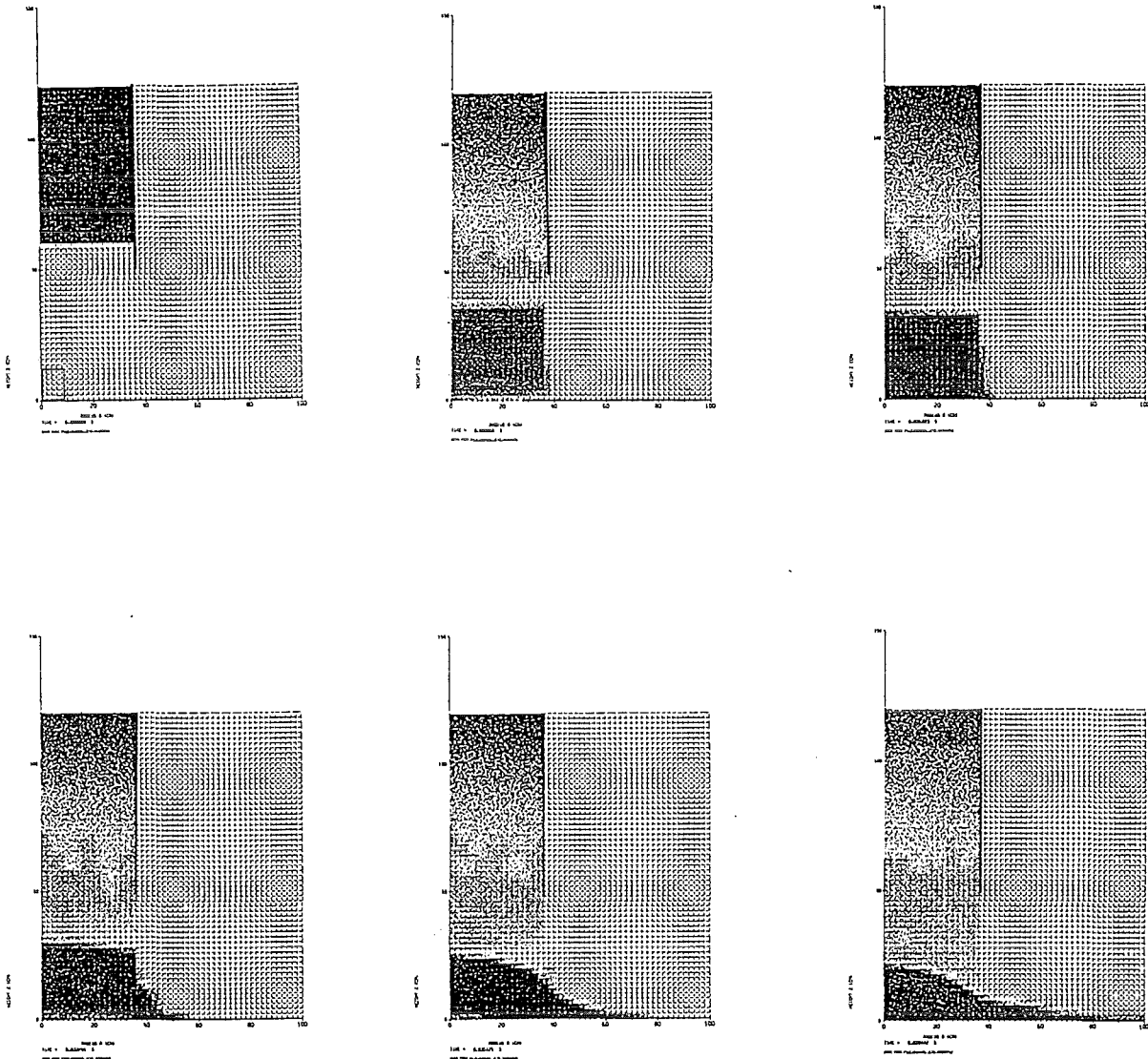
Fig. 5.4   Motion and impact of a liquid slug (case J1)
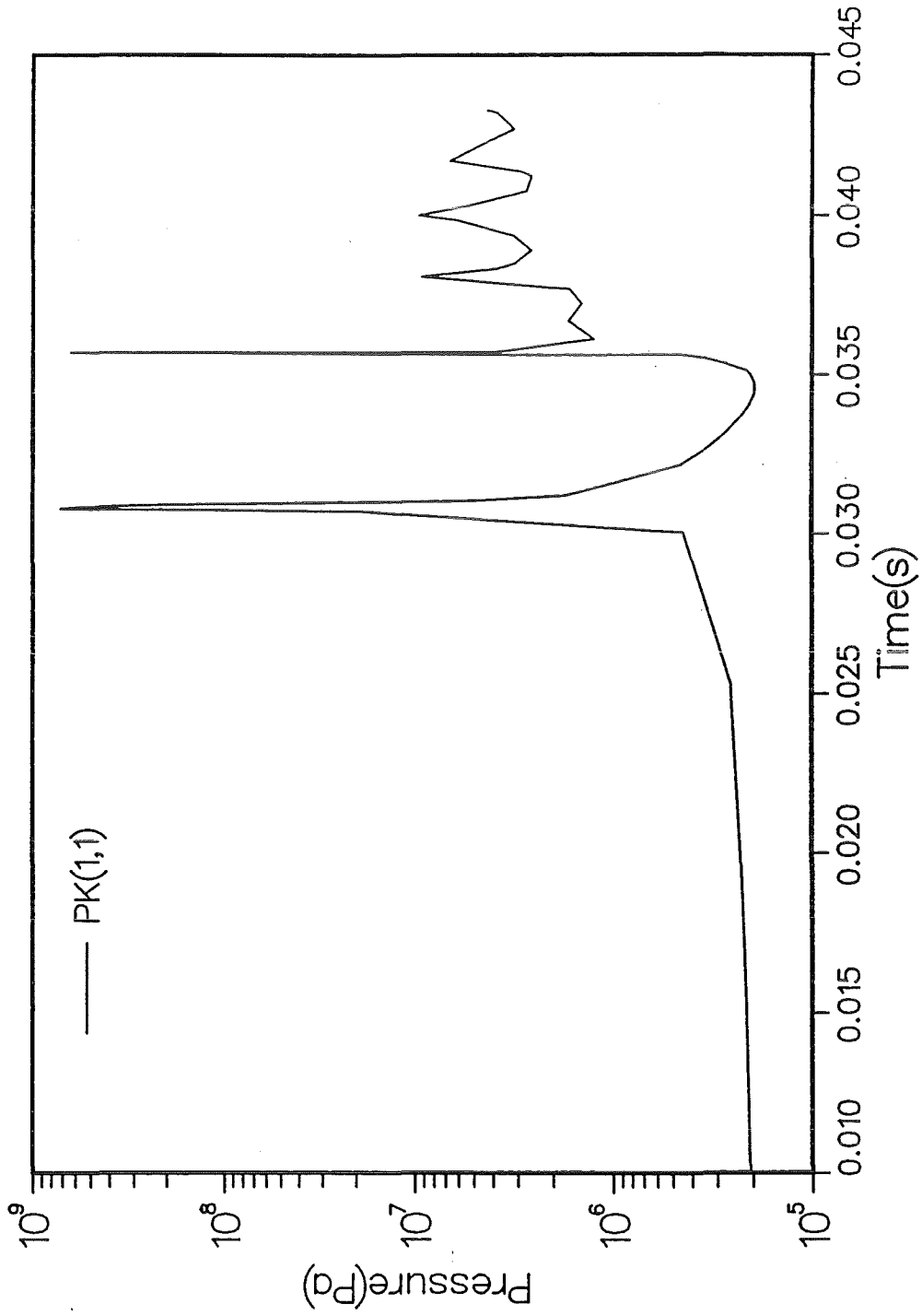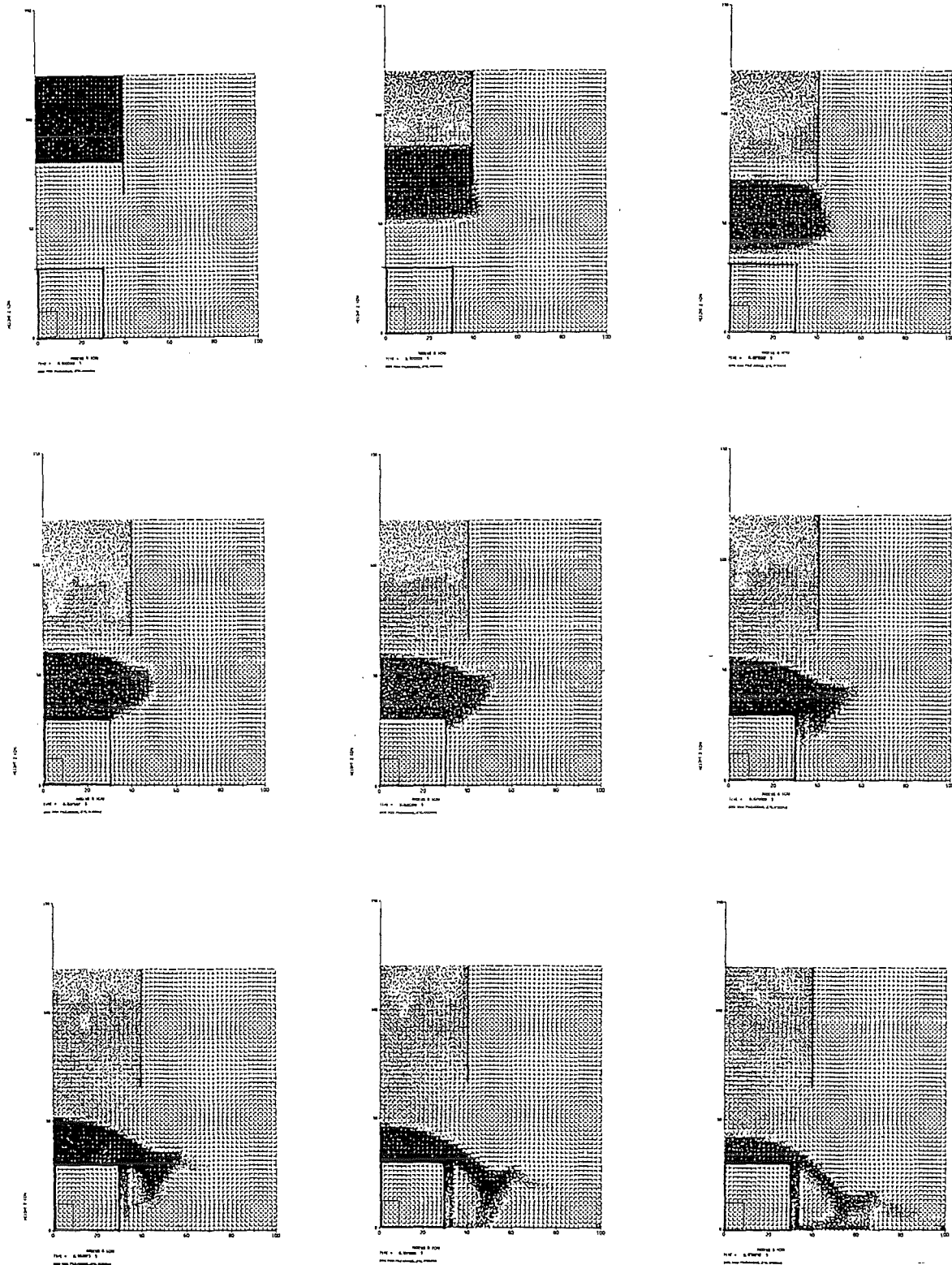
Fig. 5.5   Pressure trace of case J1

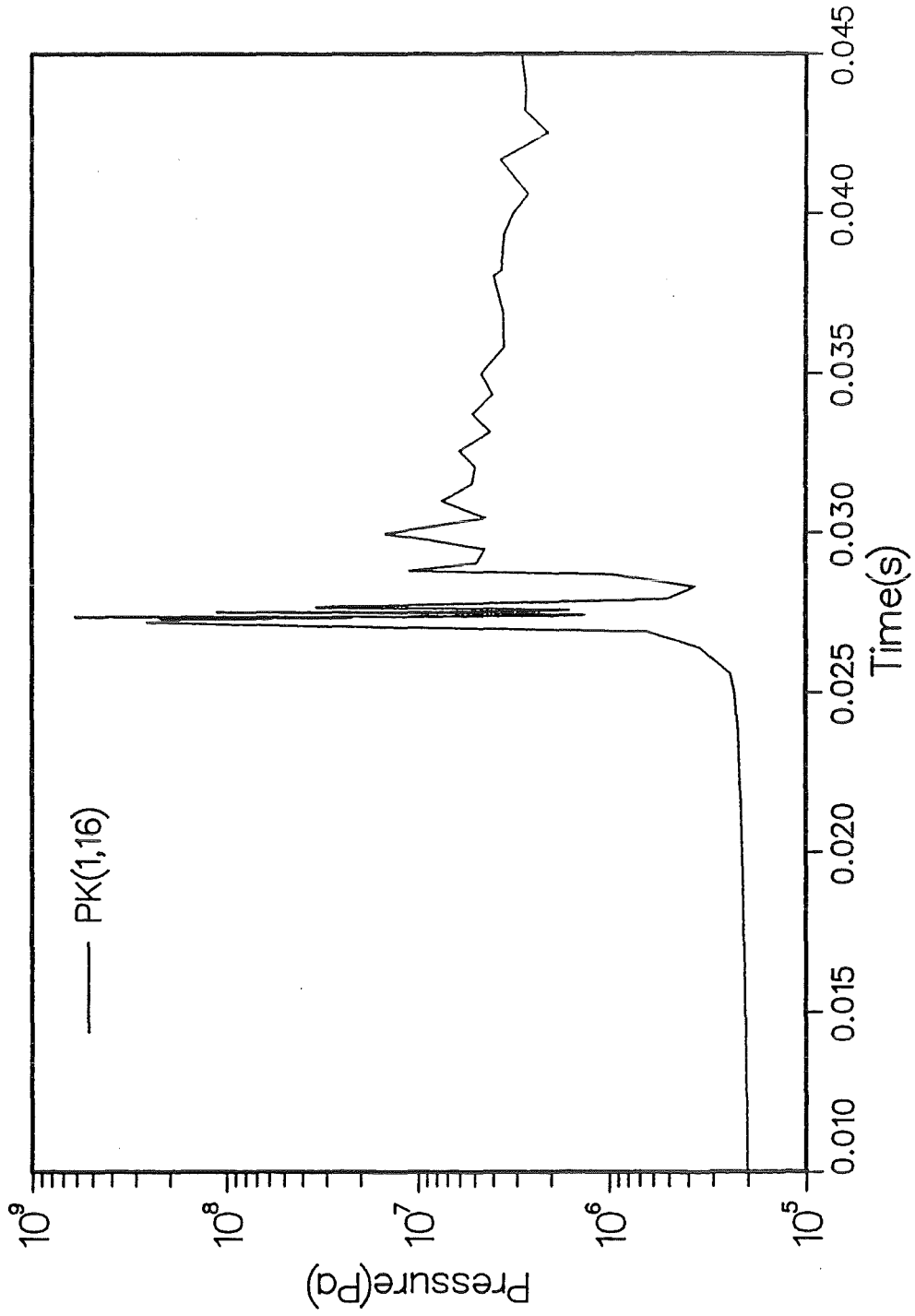Fig. 5.6   Motion and impact of a liquid slug on an obstacle (case J2)
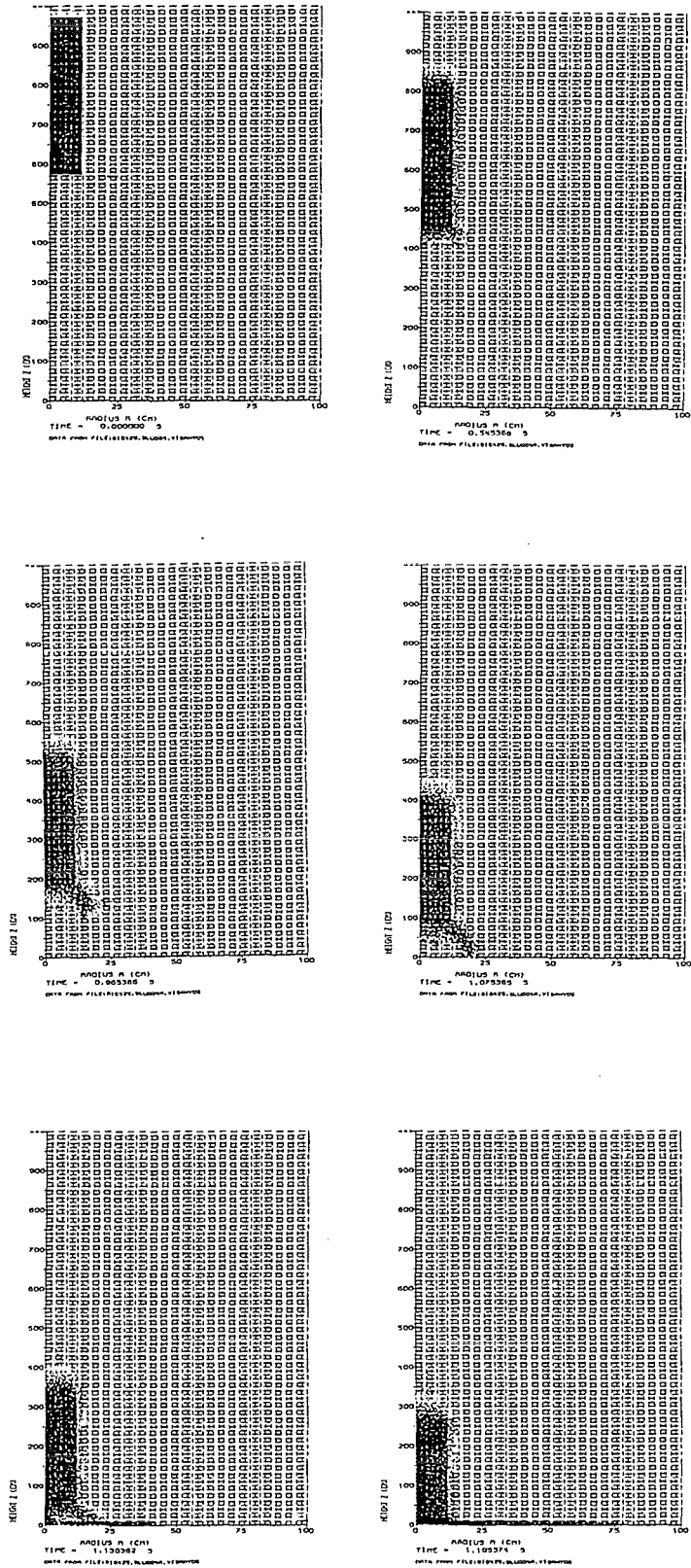
Fig. 5.7   Pressure trace of case J2
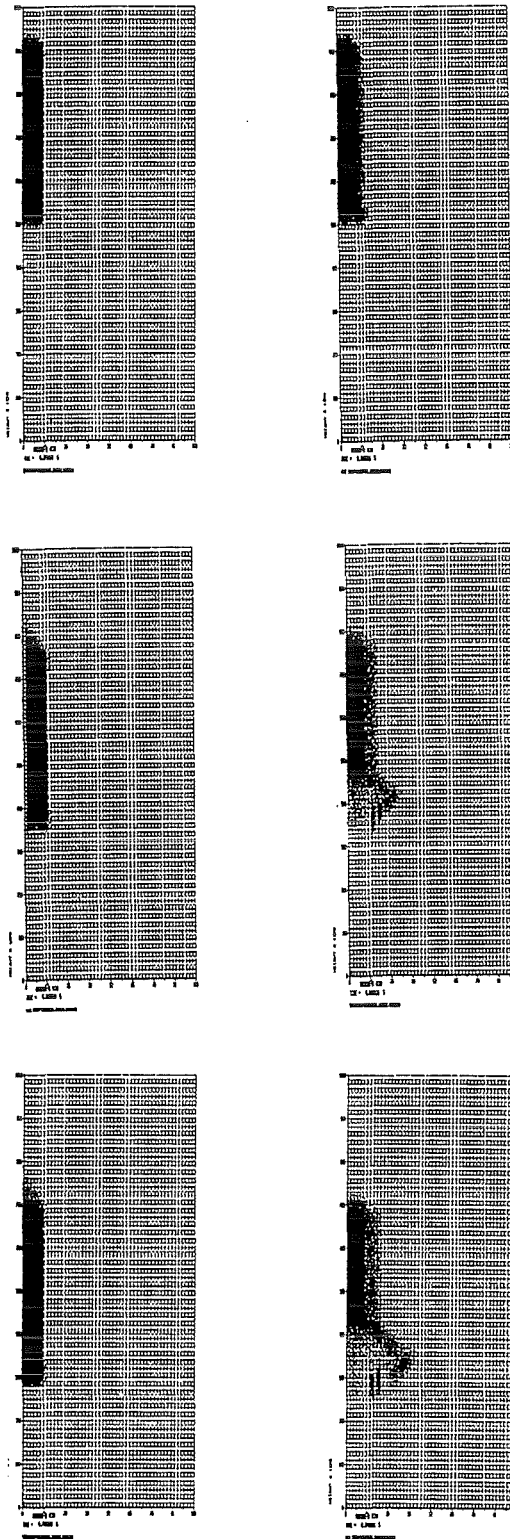
Fig. 5.8   Motion and impact of liquid slug (case S2)

Fig. 5.9   Influence of the CDD drag parameter on surface instabilities of the slug (case S2)   -CDD = 10⁴ and CDD = 10⁻⁴